A NEW CLASS OF IONIC POLYMERS CONTAINING AMINO ACID RESIDUES OF METHIONINE AS GREEN CORROSION INHIBITORS

BY

LIPIAR KHAN MOHAMMAD OSMAN GONI

A Thesis Presented to the
DEANSHIP OF GRADUATE STUDIES

KING FAHD UNIVERSITY OF PETROLEUM & MINERALS

DHAHRAN, SAUDI ARABIA

In Partial Fulfillment of the
Requirements for the Degree of

MASTER OF SCIENCE

In

CHEMISTRY

APRIL 2018

KING FAHD UNIVERSITY OF PETROLEUM & MINERALS

DHAHRAN- 31261, SAUDI ARABIA

DEANSHIP OF GRADUATE STUDIES

This thesis, written by **Lipiar Khan Mohammad Osman Goni** under the direction of his thesis advisor and approved by his thesis committee, has been presented and accepted by the Dean of Graduate Studies, in partial fulfillment of the requirements for the degree of **Master of Science in Chemistry.**

Dr. Mohammad Abu Jafar Mazumder
(Advisor)

9/7/2018

Dr. Abdulaziz A. Al-Saadi
Department Chairman

Dr. Shaikh Asrof Ali
(Member)

Dr. Salam A. Zummo
Dean of Graduate Studies

عمادة الدراسات العليا
DEANSHIP OF GRADUATE STUDIES

Dr. Hasan Al-Muallem
(Member)

DEDICATION

To my beloved parents Mohammad Faruque and Rehana Faruque, my lovely sister Titli, my grandparents, relatives and friends, and my mentors whose loves and supports know no bounds.

ACKNOWLEDGMENTS

I am grateful to almighty Lord for without his guidance I would not have been able to carry out this task and finish it in due time. I am thankful to Him for giving me this excellent opportunity of working with some professionals in the area of polymer chemistry and corrosion inhibition and learn a lot from them.

I want to express my heartfelt gratitude to my MS thesis supervisor Dr. Mohammad Abu Jafar Mazumder, Associate Professor of Chemistry at KFUPM. I believe that achieving my thesis objectives would have been an impossible task had Dr. Mazumder not supported and inspired me throughout this entire phase. I would like to thank my thesis committee members Distinguished Professor Dr. Shaikh Asrof Ali and Associate Professor Dr. Hasan Al-Muallem for their never-ending support and caring attitude. I consider myself extremely privileged to have had this wonderful opportunity of working with all of them.

I am indebted to all of my instructors at KFUPM who taught me different courses and contributed extensively to my intellectual growth. I am thankful to Dr. Mazen K. Nazal, Research Scientist at KFUPM, for his guidance on electrochemical corrosion experiments. I am grateful to my colleagues Mr. Ibrahim, Dr. Alhaffar, Dr. Zakariyah, Dr. Mansha, and Mr. Waheed for all the supports they have provided me with. I want to take this opportunity to say thanks to my friends and staffs in the chemistry department at KFUPM.

It has been a wonderful journey with my compatriots at KFUPM. I cannot thank them enough for they have been my family away from my home. I am grateful to my KFUPM friends who make the cultural and academic environment at KFUPM incredibly diverse. I will cherish the wonderful memories I have with them for the rest of my life.

I am forever grateful to the Chemistry Department and King Fahd University of Petroleum & Minerals for giving me this generous opportunity to pursue a master degree in chemistry. The first-rate education that I have gotten here will guide me to shape a prosperous career in chemistry.

TABLE OF CONTENTS

LIST OF TABLES

LIST OF FIGURES

LIST OF ABBREVIATIONS

AIBN	: Azobisisobutyronitrile
CoC	: Cost of Corrosion
CMC	: Critical Micelle Concentration
CPE	: Cationic Polyelectrolyte
CPE	: Constant Phase Element
DP	: Degree of Polymerization
DQA	: Diallyl Quaternary Ammonium
EDX	: Energy Dispersive X-ray
EIS	: Electrochemical Impedance Spectroscopy
FTIR	: Fourier Transform Infrared Spectroscopy
GNP	: Gross National Product
GDP	: Gross Domestic Product
GCC	: Gulf Cooperation Council
GPC	: Gel Permeation Chromatography
LPR	: Linear Polarization Resistance
NACE	: National Association of Corrosion Engineers
NMR	: Nuclear Magnetic Resonance Spectroscopy
OCP	: Open Circuit Potential
RU	: Repeating Unit
SCE	: Saturated Calomel Electrode
SEM	: Scanning Electron Microscopy
TGA	: Thermogravimetric Analysis
XPS	: X-ray Photoelectron Spectroscopy

ABSTRACT

Full Name : Lipiar Khan Mohammad Osman Goni

Thesis Title : A New Class of Ionic Polymers Containing Amino Acid Residues of Methionine as Green Corrosion Inhibitors

Major Field : Chemistry

Date of Degree: April 2018

In solvent acetone, ethyl ester hydrochloride of *N*,*N*-diallylmethionine having sulfide motifs underwent alternate cyclopolymerization with SO_2 to give an alternating copolymer with SO_2, while in DMSO ($Me_2S{=}O$), it gave a terpolymer containing sulfide and sulfoxide motifs in a 1:1 ratio as a result of oxygen transfer from Me_2SO. Likewise; copolymerization of hydrochloride salt of *N*,*N*-diallylmethionine with SO_2 in DMSO gave copolymer containing sulfide/sulfoxide motifs in a ≈1:1 ratio. The sulfide moiety of these polymers have been transformed to sulfoxide and sulfone respectively. The chemical, physical and solution properties of these polymers were studied in detail. The critical micelle concentration of the polymers was determined to be ≈ 7 ppm. The inhibition efficiency obtained from different techniques are in good agreement. The corrosion efficiencies increased with increasing the concentration of the polymers. At a concentration of 175 μM at 60 °C, all of the polymers imparted inhibition efficiencies of more than 90% with a terpolymer imparting efficiency as high as more than 99%. Adsorption of polymer compounds onto the mild surface follows both chemisorption and physisorption processes, and obeyed Langmuir, Temkin and Freundlich adsorption isotherms. The XPS and SEM-EDX further confirmed that the synthesized compounds form a protective film onto the metal surface and resist from further corrosion attack.

ملخص الرسالة

الاسم الكامل: ليبيار خان محمد عثمان غني

عنوان الرسالة: فئة جديدة من البوليمرات الأيونية التي تحتوي على بقايا أحماض أمينية من الميثيونين كمثبطات للتآكل الأخضر

التخصص: كيمياء

تاريخ الدرجة العلمية: أبريل 2018

في مذيب الأسيتون ، إيثيل إستر هيدروكلوريد ل N, N-diallylmethionine الذي له زخارف كبريتية خضع لسلسلة من البوليمرات المتناوبة مع ثنائي اكسيد الكبريت (SO2) لإعطاء كوبوليمر بديل مع ثنائي اكسيد الكبريت (SO2)، بينما في ثنائي ميثيل سلفوكسيد {(DMSO (Me2S=O}، أعطي بوليمر ثلاثي (a terpolymer) يحتوي على زخارف كبريتيد وسلفوكسيد بنسبة 1:1 كنتيجة لنقل الأكسجين من Me2SO. بطريقة مماثلة؛ البلمرة لملح هيدروكلوريد لل N,N-diallylmethionine مع ثنائي اكسيد الكبريت (SO2) في ثنائي ميثيل سلفوكسيد (DMSO) أعطت بوليمرات ثنائية (copolymer) المحتوية علي زخارف كبريتيد / سلفوكسيد بنسب ≈1:1. تم تحويل جزء كبريتيد هذه البوليمرات إلى سلفوكسيد (sulfoxide) وسلفون (sulfone) على التوالي. تمت دراسة الخواص الكيميائية والفيزيائية والمحلول لهذه البوليمرات بالتفصيل. تم تحديد تركيز micelle الحرجة للبوليمرات لتكون ≈ 7 جزء في المليون. كفاءة التثبيط تم الحصول عليها من تقنيات مختلفة في اتفاق جيد. زادت كفاءة التآكل مع زيادة تركيز البوليمرات. عند تركيز 175 ميكرومتر عند 60 درجة مئوية، فإن جميع البوليمرات أعطت كفاءة تثبيط أكثر من 90٪ مع كفاءة تيربوليمر تصل إلى أكثر من 99٪. يتبع إدمصاص مركبات البوليمر على السطح المعتدل كلا من عمليات امتصاص كيميائي و فيزيائي، و أطاعت الأيسوثرم الامتزاز Langmuir و Temkin و Freundlich. كما أكدت XPS و SEM-EDX أن المركبات المركبة تشكل طبقة واقية على السطح المعدني وتكف عن التعرض لمزيد من التآكل.

CHAPTER 1

INTRODUCTION

1.1 Corrosion and its Global Impact

Corrosion is referred to the deterioration of materials by the chemical reactions between its reactive ambiance [1]. It is a hazardous phenomenon having a devastating impact on gas and oil manufactures and their subsequent transportation, triggered more or less by almost any aqueous environment and happens by means of redox reactions in gas and oil production, handling and pipeline systems [2]. Technically, corrosion is considered as a bounded electrochemical reduction-oxidation (redox) reaction taking place on a surface of the materials, typically metals, prompting the release of electrons by the dissolution of metal and their successive transfer to another position on the surface causing the oxygenated water or hydrogen ions to be reduced and resulting in gradual deterioration and consequent failure of the host material. This corrosion process consists of a cathode, an anode and an electrolyte. The anode is the location where the corrosion of metals takes place to generate free electrons, which travel through the corrosive electrolytic medium to the cathode, where hydrogen ions (from an acidic corrodent) get reduced to hydrogen gas. Natural gas and crude oil usually contain several highly contaminated products which are innately corrosive. Free water, carbon dioxide (CO_2) and hydrogen sulfide (H_2S) are well-established examples of extremely corrosive media in case of oil and gas wells and pipelines [3]. Furthermore, oxygen contaminations in basic or neutral conditions lead to the production of hydroxyl ions through the reduction of oxygenated water by the current produced at the anodic site due to oxidation process [4]. In general,

upon exposure to metals, the chemical species, such as moisture/water (H_2O), acids (HNO_3, HCl, H_2SO_4), bases ($NaHCO_3$, $CaCO_3$, NaOH), salts (NaCl), aggressive metal polishes and gases (ammonia, formaldehyde and sulfur-containing gases), liquid chemicals perpetuate the degradation of the metals [5].

The effects of corrosion in our daily lives are both direct and indirect. It is direct in the sense that corrosion has impact on the useful service lives of our possessions, and indirect, in that producers and suppliers of goods and services incur corrosion costs, which they pass on to consumers. At home, corrosion can easily be recognized on metal tools, automobile body panels, charcoal grills, and outdoor furniture. Painting is one of the major preventative maintenances that safeguards such items from corrosion. Corrosion protection is built into all major household appliances such as furnaces, dryers, washers, ranges, and water heaters [6].

How corrosion affects us during our travel from home to work is of far more serious consequence. The corrosion of steel reinforced bar in concrete can occur without being noticed and can cause the failure of a section of highway, damage to buildings, bridges, parking structures, and collapse of electrical towers, etc., resulting in great economical loss and jeopardizing public safety. Corrosion that occurs in major industrial plants, such as chemical processing plants or electrical power plants is perhaps the most dangerous of all. Such type of corrosion could result in plant shutdowns. Some corrosion consequences are economic, and result in the following:

- Replacing the corroded equipment.
- Taking preventive measures, such as painting.
- Equipment shutdown due to corrosion failure.

- Overdesigning to allow for corrosion.
- Efficiency loss.
- Damage of equipment adjacent to one in which corrosion failure occurs.

Some consequences are social and can cause the following issues:

- Health, for instance, escaping product from a corroded equipment or the corrosion product itself can cause pollution.
- Safety, as an example, sudden failure can cause explosion, fire, release of toxic product, and construction collapse.
- Unpleasant appearance of the corroded materials to the eye.
- Depletion of natural resources, including the metals and fuels used to manufacture them.

Corrosion damage can sometimes be greatly exaggerated by the circumstances. Throughout the course of the history, many corrosion accidents have gone unnoticed for reasons of liability or simply because the evidence disappeared in the catastrophic event, others have made the headlines. Some devastating corrosion accidents that have claimed lives and incurred huge economic losses are included below in Table 1.1.

Table 1.1 Some Corrosion Accidents

Name of the Accident	Year	Place	Reason and Damage
Silver Bridge Collapse [7]	1967	Ohio, USA	Stress corrosion cracking and corrosion fatigue cause the bridge to collapse and kill 46 people.
Bhopal Accident [8]	1984	Bhopal, India	Corrosive pipelines, valves and other safety equipment caused the release of toxic methyl isocyanate (MIC) that claimed 3000 lives and injured an estimated 500,000 people.
Swimming Pool Roof Collapse [9]	1985	Uster, Switzerland	Stress corrosion cracking caused a swimming pool roof to collapse and kill 12 people.
Sinking of the Erika [10]	1999	Brittany, France	Corrosion caused holes in the main deck coaming, the port side and starboard inert gas system risers that eventually broke the oil tanker Erika in two to cause huge oil spillage.
Rupture of a Natural Gas Transmission Pipeline [11]	2016	Pennsylvania, USA	Corrosion along two of the circumferential welds in a natural gas transmission pipeline caused it to rupture and damage some homes nearby.
Ohio State Accident [12]	2017	Ohio, USA	An uniform corrosion caused a thrill ride's Gondola support beam to reduce in thickness and fail during the operation to kill one person and injure seven others.

Corrosion is considered to be one of the major challenging problems for most of the industrialized countries. Before designing any industry, the effect of corrosion on the equipment and its surrounding always deserve to be a considerable issue. A lot of money has been expended by the oil companies all over the world to mitigate these corrosion problems. Nevertheless, disasters such as, casualties, economic losses and environmental side effects triggered by corrosion, still happen quite often [13].

Corrosion can cause severe failures in boiler tanks, pressure basins, blades of motors/turbines, harmful/aggressive chemical containers, aeroplane parts, automotive routing devices and bridges. Furthermore, the losses caused by corrosion are not only limited to the metals but also extend to water, energy and the manufacturing phase of the metal frames [5]. It has been reported that the maintenance cost of the corrosion related issues in industries/establishments for any country is in the range of 1-5 % of their gross national product (GNP) [14].

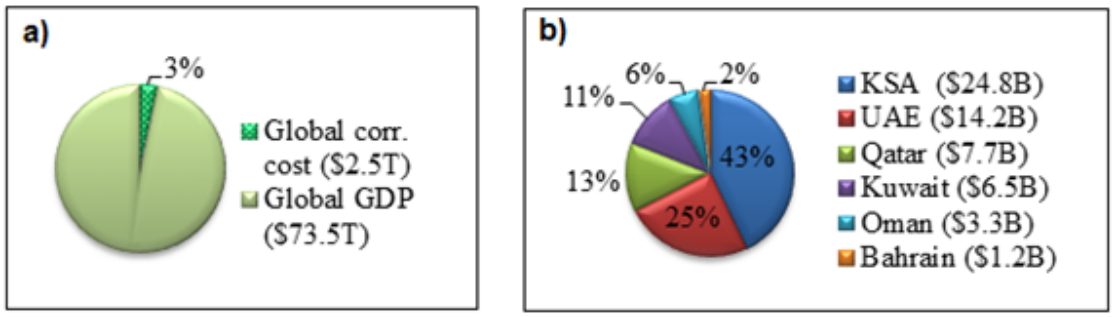

Figure 1.1 (a) Global Cost of Corrosion (2013), (b) Cost of Corrosion in GCC Countries (2011)

A study revealed by NACE in 2013 has shown that the global cost of corrosion was estimated to be US$2.5 trillion which was equivalent to 3.4% of the global GDP of that year (Fig. 1.1a) [15]. This study utilized the World Bank economic sector and GDP data

to relate the cost of corrosion studies to a global cost of corrosion. In order to address the economic sectors for different parts of the world, the global economy was divided into economic regions with similar economies (according to World Bank). These were: United States, European Region, India, Arab World (as defined by the World Bank), Russia, China, Japan, Four Asian Tigers plus Macau, and Rest of the World.

Table 1.2 Global Cost of Corrosion by Region and Sector [15]

Economic Regions	Agriculture CoC USD Billion	Industry CoC USD Billion	Services CoC USD Billion	Total CoC USD Billion	Total GDP USD Billion	CoC % GDP
United States	2.0	303.2	146.0	451.3	16,270	2.7%
India	17.7	20.3	32.3	70.3	1,670	4.2%
European Region	3.5	401	297	701.5	18,331	3.8%
Arab World	13.3	34.2	92.6	140.1	2,789	5.0%
China	56.2	192.5	146.2	394.9	9,330	4.2%
Russia	5.4	37.2	41.9	84.5	2,113	4.0%
Japan	0.6	45.9	5.1	51.6	5,002	1.0%
Four Asian Tigers Plus Macau	1.5	29.9	27.3	58.6	2,302	2.5%
Rest of the World	52.4	382.5	117.6	552.5	16,057	3.4%
Global	152.7	1446.7	906.0	2505.4	74,314	3.4%

However, the costs estimated in Table 1.2 typically do not include environmental consequences or individual safety. It is noteworthy that as additional cost of corrosion

studies become available, or studies are updated, more detailed and accurate global costs can be assessed.

The total cost of corrosion in the Gulf Co-operational Council (GCC) states was estimated to be US$57.96 billion (Fig. 1.1b) [16]. Among the GCC states, Kingdom of Saudi Arabia (KSA) incurred the highest annual cost of corrosion. UK suffered a corrosion cost of £13.65 billion in 1969 [17]. Corrosion has a severe impact on between a quarter and a half of all drinkable water mains in France, particularly old ones that are made of cast iron or uncoated steel [13]. A 2-year study conducted by the U.S. Federal Highway Administration (FHWA) and National Association of Corrosion Engineers (NACE) in 2002 disclosed that the estimated annual cost of corrosion in the country was $276 billion, which was 3.1% of the US GDP. Nearly half of the amount was allotted to establish corrosion mitigation methods such as selection of mechanically resistant plastics and corrosion-resistant alloys, development of protective coatings, corrosion inhibitors and cathodic protectors [4]. Gas and oil production, being one of the leading energy sectors, contributes a huge portion of the direct costs for corrosion [18,19]. The total cost of oil and gas production and exploration is approximately $1.4 billion; while chemical/petrochemical manufacturing contributes $1.7 billion and petroleum refining adds $3.7 billion [20].

1.2 Concept of Corrosion and its Types

Corrosion are of many kinds but they can be subdivided into two main types, internal and external. External corrosion is regarded as the corrosive effect of high temperature, high humidity, high salt and highly acidic environments on the metallic part of the alloy [4]. On the contrary, internal corrosion, is associated with stored or transported gases or

liquids [21]. A continuous exposure of the metal to fluids can cause this type of corrosion either in anaerobic or aerobic condition [22]. Water is believed to be the most common liquid that has contact with extremely corroded metallic planes, while oil, in spite of being not corrosive, contains hydrocarbon phases most of which are complex emulsions containing oxygen, water and other dissolved corrosive gases.

A metal after being exposed to an electrolyte (a corrosive solution), loses electrons at the anodic sites (Eq. 1), which are consumed by the hydrogen ions or oxygenated water at the cathodic sites. Metal cations are then released into the electrolyte able to bond with negative atoms or ions. The loss of metal occurs as an anodic reaction.

$$Fe\ (s) \rightarrow Fe^{2+}\ (aq) + 2e^{-} \qquad (1)$$

The electrons released from the anode are consumed in cathode. The most common cathode reactions are shown by Eqs. (2)-(5) [23]:

i. Hydrogen evolution from acidic solution

$$2H^{+}\ (aq) + 2e^{-} \rightarrow H_2\ (g) \qquad (2)$$

ii. Hydrogen evolution from neutral water

$$2H_2O\ (l) + 2e^{-} \rightarrow H_2\ (g) + 2OH^{-}\ (aq) \qquad (3)$$

iii. Oxygen (O_2) reduction in acidic solution

$$O_2\ (g) + 4H^{+}\ (aq) + 4e^{-} \rightarrow 2H_2O\ (l) \qquad (4)$$

iv. Oxygen reduction in neutral or basic solution

$$\tfrac{1}{2}\ O_2\ (g) + H_2O\ (l) + 2e^{-} \rightarrow 2OH^{-}\ (aq) \qquad (5)$$

The four broad groups of electrochemical, chemical, biological and mechanically assisted corrosions are presented in Table 1.3.

Table 1.3 Different Corrosive Environments

Natures of Corrosion	Types of Corrosion	Causes of Corrosion	Affected Areas/Materials
Electrochemical corrosion	Galvanic corrosion [24]	Difference in electrode potentials	Metal with more negative potential
	Crevice corrosion [24]	Metal within narrow clearances being devoid of oxygen	Crevices
	Pitting corrosion [24]	Chloride ions	Passive metals
	Stray current corrosion [25]	Extraneous DC current from electrified railroads, mining operations etc.	Underground pipelines
Chemical corrosion	Sweet corrosion [26]	carbon dioxide producing carbonic acid in water	Transmission pipelines, main downhole tubing
	Oxygen corrosion [24]	Depolarization and electron acceptance capability of oxygen	Drill pipes
	Sour corrosion [26]	hydrogen sulfide working as an acid in water	Deep wells
	Concentrated brines corrosion [27]	Dense halide brines of calcium, zinc and magnesium	Stainless steels, sites susceptible to pitting and crevice corrosion
	Strong acids corrosion [28]	Hydrochloric acid, hydrofluoric acid etc. pumped into the wells increase formation permeability	Deep wells
Biological corrosion	Microbiologically induced corrosion [25]	Organic acids, carbon dioxide, hydrogen sulfide produced by fungi and bacteria	Underground pipelines
Mechanically assisted corrosion	Cavitation [28]	Gas bubbles' implosion on metal surfaces	High-speed blade propellers and pumps
	Erosion [28]	Cutting action of high-velocity abrasive particles	Drill pipes
	Erosion corrosion [24]	Removal of protective film of corrosion products by erosion	propellers, impellers, pumps, heat exchanger tubes, valves
	Corrosion Fatigue [28]	Alternating stresses in a corrosive environment	Welded connections on drillships, drilling and production rigs and platforms
	Sulfide stress corrosion [29]	Dispersion of molecular hydrogen into the metals' matrices	valve trim, blowout preventer hard parts and tool joints
	Chloride stress cracking [30]	Tensile stress in the presence of oxygen, chloride ions and high temperature	austenitic stainless steels, pipe-wells and tubing bundles
	Stress corrosion cracking [24]	Combined effect of corrosive environment and non-cyclic tensile stress	Bridge cables, landing gear on aircraft

1.3 Corrosion Inhibitors

Resisting corrosion in the oil and gas industries is of paramount importance because of the economic losses due to corrosion [31]. Employing corrosion inhibitors is one of the most economically viable corrosion combatting methods [32,33]. Corrosion inhibitors are referred to as mixtures or substances that applied in low concentration to inhibit, eliminate or minimize the corrosion in aggressive environment [34]. Inhibitors slow down the corrosion process either by (i) increasing the anodic or cathodic polarization behavior (Tafel slopes), (ii) reducing the movement or diffusion of ions to the metallic surface, or (iii) increasing the electrical resistance of the metallic surface [35]. The mechanisms involved in the corrosion inhibition processes are (i) adsorption; formation of a film that is adsorbed on the metal surface (ii) formation of corrosion products, such as iron sulfide (FeS) which is passivizing species (iii) production of precipitates which can protect and eliminate or inactivate an aggressive constituent [36].

Based on the chemical nature of the inhibitors, they can be classified into organic and inorganic [31]. These organic and inorganic substances can also be categorized as neutralizing, scavenging, barrier or film-forming and other miscellaneous inhibitors depending on their mechanism of actions or compositions [37].

1.3.1 Neutralizing Inhibitors

The main purpose of using a neutralizing inhibitor is to abate H^+ concentrations to control the corrosion in the refinery industries. The presence of concentrated acids such as carbonic acid (H_2CO_3), sulfuric acid (H_2SO_4), hydrochloric acid (HCl), sulfurous acid (H_2SO_3), thiosulfuric acid ($H_2S_2O_3$) etc. are the main reasons of corrosion in the refinery

processes [37,38]. Although these acids pertain in dilute concentrations across the process stream, these acids become more concentrated in condensates to cause severe corrosion to the systems i.e., distillation equipment and heat exchanger [39]. A range of neutralizers are exploited in many applications of the refinery including ammonia (NH_3), sodium hydroxide (NaOH), morpholine and various amines, polyamines and alkylamines. The applications of each of these neutralizers are dictated by its physical characteristics. The condensation profile of the neutralizers should be close to that of acids so that it can deliver its job as soon as the acid forms in the system. Sodium hydroxide (NaOH), a strong alkali, functions as an effective neutralizer if injected to the desalted crude but not effective in overhead heat exchangers. Whereas ammonia (NH_3) is a cheap overhead neutralizer but it is not soluble in the initial condensate, and quick evaporation causes to lose its efficiency [4,37].

1.3.2 Scavengers

In oil and gas industries, corrosive agents can be removed by the utilization of scavenger systems. Dissolved oxygen, one of the primary causes of corrosion in oilfield water. Both chemical and mechanical means have been exploited to get rid of dissolved oxygen in oil field waters. The mechanical means include vacuum deaeration and counter current gas stripping, whereas the chemical means can be considered as hydrazine, sodium sulfite, ammonium bisulfite, and sulfur dioxide etc. The scavenging action of sodium sulfite and hydrazine are well-recognized and are depicted through the Eqs. 6 and 7.

$$Na_2SO_3 + ½\ O_2 \rightarrow Na_2SO_4 \quad (6)$$

$$2H_2NNH_2 + ½\ O_2 \rightarrow 2NH_3 + H_2O + N_2 \quad (7)$$

The preference of one method to other is dictated by the economic and environmental factors. When it requires to remove large quantities of dissolved oxygen, mechanical means are preferred. Chemical means are used to remove small quantities of dissolved oxygen, and to remove residual oxygen after the application of steam stripping system. Any organic chemicals such as scale inhibitors, corrosion inhibitors, and biocides can possibly intervene the oxygen-scavenger reaction and should be selected meticulously [4,37].

1.3.3 Barrier or Film-Forming Inhibitors

Film-forming corrosion inhibitors, alternatively known as barrier or interface inhibitors, as compared to neutralizers and even scavengers, are more proactive because these inhibitors do not need to react with acids or corrosive agents to be operative [40]. These inhibitors construct a protective barrier on the metal surface. The formation of this protective barrier happens through strong interactions such as π-orbital adsorption, chemisorption and electrostatic adsorption that significantly prevent the corrosive substances from penetrating into the metal surface [41]. The term adsorption means the attachment of an inhibitor molecule to a metal surface, basically only one molecular layer thick, and not penetrating into the bulk of the metal itself [42]. However, it has been reported that steric factors, aromaticity, functional groups, electronic structure of the molecules, π-orbital character of donating electrons and electron density at the donor atoms are some of the specific physico-chemical properties of the inhibitor molecules that

dictate the adsorption process [43,44]. Thus, the corrosion inhibition efficiency of an organic inhibitor is dictated by its adsorption ability and the mechanical, structural, and chemical characteristics of the adsorption layers formed under particular condition [45].

The organic inhibitor molecules are usually composed of a hydrophobic group that extends away from the surface and a polar head, which is responsible for interacting with the metal surface. An additional protective layer is also formed by the hydrophobic part so that the aqueous species can't come in contact with the metal surface. It is recommended that these molecules are combined well with hydrocarbon stream to facilitate their access to all parts of the process stream for a wider contact and a subsequent coverage [4]. When these inhibitors can't reach to any point in the process, addition of neutralizers to the formulation will compensate. Depending on the type of electrochemical reaction being blocked, these film-forming or interface inhibitors can be further classified into anodic, cathodic or mixed-type [46,47].

1.3.3.1 Anodic Inhibitors

Anodic inhibitors, also known as passivation inhibitors, reduces the rate of anodic reaction by forming sparingly soluble deposits including hydroxides, oxides, or salts in close to neutral conditions. Because these deposits can alternatively be referred to as passivating films that is why anodic inhibitors are also known as passivators. The corrosion potential of the metal is shifted to more positive values, and the value of the current in the curve decreases with the presence of the corrosion inhibitors [47]. It is worth mentioning that the concentration of an anodic inhibitor should be high enough to show a considerable amount of anodic effect. Otherwise, the formation of the film on the metal surface will be affected significantly leading to partial film formation keeping sites

of the metal exposed to corrosive solution and thus causing localized corrosion. This effect is more pronounced when the concentration of the inhibitors used is below its critical concentration, and could be worse than not using the inhibitors at all [48].

1.3.3.2 Cathodic Inhibitors

Meanwhile, cathodic inhibitors work by decelerating the reduction reactions by forming a protective layer on cathodic areas against oxygen in alkaline solutions and hydrogen in acidic conditions. This protective layer restricts the diffusion of reducible species and increases the impedance of the surface. When the cathodic reaction is affected, the corrosion potential is shifted to more negative values [47]. These cathodic inhibitors cause sulfide-stress cracking or hydrogen blistering. Therefore, hydrogen permeation tests are carried out once the material has been categorized as cathodic inhibitor to evaluate its efficiency [49].

1.3.3.3 Mixed Inhibitors

Approximately 80% of organic inhibitors belong to the mixed-type inhibitor. A protective layer can be formed either via physisorption (due to ionic or electrostatic interaction) or via more specific chemisorption. The physisorption occurs when ionic corrosion inhibitors attach to metal surface, particularly anions attach to positively charged metal substrates. The formation of these interactions take place quickly but prone to breakage at higher temperature. Chemisorption, on the contrary, forms slower than physisorption and increases with increasing temperature [4]. Chemisorption or chemical adsorption process produces an electronic bond between the surface and the adsorbate. It generally involves charge transfer or charge sharing between a solid metal substrate and an adsorbent, such

as the corrosion inhibitor molecule. Chemisorption in irreversible and involves more heat than physical adsorption [50].

1.4 Statement of the Problem

Since corrosion causes loss of economic and natural resources and human lives in case of infrastructure collapses, it is of paramount importance to look into smart and developed corrosion mitigation techniques. The prevention of corrosion in a corrosive environment is a huge challenge [43]. Anodic protection [51], cathodic protection [52,53], coating [54] alloying are some of the approaches toward mitigating corrosion. Exploitation of chemical inhibitors [55,56] is the most effective and practical method of corrosion prevention owing to its ease of use. Organic compounds having O, N and S atoms appeared as corrosion inhibitors in the eighteenth century. An organic inhibitor is said to be efficient if it is capable of getting adsorbed on the metal surface [43]. Several authors have reported the uses of organic [18,57–59] and inorganic compounds [60–62] as corrosion inhibitors and classified them depending on their mode of action.

Even after having an abundance of corrosion inhibitors to reduce the dilemma, the search for cost-effective, environment-friendly and more efficient inhibitors is still on. Organic and inorganic inhibitors, albeit efficient corrosion inhibitors at times, pose a dangerous threat to health and ecology. This has driven researchers toward the invention of nontoxic inhibitors that imparts efficiency to the maximum intent and least impact on nature and mankind [43]. Different eco-friendly green corrosion inhibitors have been reported by several authors [63–65]. Nevertheless, novel approaches and current trends in corrosion inhibitors are in favor of the use of polymers. Polymers, owing to the presence of a large number of binding sites, adsorb very well on the metal surface and impart superior

corrosion inhibition efficiency. Furthermore, multi-functionality, solubility, flexible viscosity and increased number of attachment points render polymers superior to their organic and inorganic counterparts.

1.5 Objectives

Amino acids and polyamino acids have been tested as corrosion inhibitors because of their environmentally benign nature. Abd-El-Nabey et al., [66] studied cysteine and methionine for their corrosion inhibition of mild steel in 1N H_2SO_4. Amin et al., [67] tested the inhibition efficiency of alanine (Ala), cysteine (Cys) and S-methyl cysteine (S-MCys) for iron in aerated stagnant 1.0M HCl solutions. Barouni et al., [68] studied the inhibitive effect of valine (Val), glycine (Gly), arginine (Arg), Lysine (Lys) and Cysteine (Cys). The influence of sulfur-containing amino acids, namely methionine, cysteine and N-acetylcysteine (ACC) on the corrosion behavior of mild in a highly concentrated solution of phosphoric acid in absence and presence of Cl^-, F^- and Fe^{3+} ions have been investigated by Morad et al [69]. The inhibitive effect of cysteine on copper metal in 0.6 M NaCl and 1.0 M HCl has been investigated by Ismail using electrochemical studies [70]. Synergistic inhibitive effect of cysteine and Cu(II) ions on iron in 0.5M sulfuric acid has been investigated by El-Deab [71].

El-Hafez and Badawy [72] studied the corrosion inhibition efficiency of cysteine, N-acetylcysteine and methionine as environmentally safe inhibitors for the corrosion of Cu-10Al-5Ni alloy in 3.5% NaCl solution. Corrosion inhibition efficiency of 87% was recorded with glutamic acid at a concentration of 0.025 M [73]. Saifi et al., [74] investigated the inhibitive action of cysteine on Cu-30Ni alloy in aerated 0.5 M H_2SO_4. Badawy et al. [75] demonstrated that glycine at a concentration of as low as 0.1 mM can

impart an inhibition efficiency of about 85% on Cu-Ni alloy in neutral chloride solution. For low Ni content alloy (Cu-5Ni), a remarkably high efficiency of 96% was achieved at a low concentration of 2.0 mM cysteine. Helal and Badawy [76] studied the inhibitive action of some amino acids including phenylalanine and cysteine on Mg-Zn-Al alloy in stagnant naturally aerated chloride free neutral solutions.

The aim of the present investigation is to synthesize a series of novel pH-responsive polymers containing residues of the amino acid methionine. The pH-responsive polymers containing trivalent nitrogen, carboxylate functionalities and above all the sulfide motifs of amino acid residues of methionine will then be subjected to corrosion inhibition of mild steel widely used in the oil and gas industries.

The long-term goal of this research is thus two-fold: (i) synthesis of an interesting novel class of ionic polymers, and (ii) their applications in the fields of corrosion inhibition. The use of essential amino acid methionine is anticipated to generate green inhibitors. The sulfide motif of the amino acids is expected to have powerful chelating ability because of its polarizability. The presence of multiple cationic and anionic sites within a polymer chain along with the sulfides is anticipated to undergo strong adsorption on the metal surface to prevent corrosion.

To achieve this, the thesis will have the following objectives:

To have academic significance:

1. Synthesis of a novel diallyl quaternary ammonium (DQA) monomer containing essential amino acid methionine residue.

2. Cyclopolymerization of the new DQA monomer with SO_2 to cationic polyelectrolytes (CPEs).
3. Converting the new DQA monomer to zwitterionic monomer and cyclopolymerization to zwitterionic polyelectrolytes.
4. Transformation of the sulfide moiety of polymers to sulfoxide and sulfone.
5. Physical characterization and solution properties of these polyelectrolytes will be studied in detail.

To have industrial significance:

6. Evaluation (screening) of the synthesized monomers and polymers as corrosion inhibitors to prevent acidic corrosion of 1 M HCl.

CHAPTER 2

Synthesis of Diallylamine salts/sulfur dioxide Alternate Polymers Containing Amino Acid Residues

2.1 Introduction

Cyclopolymerization [77–79] of diallylammonium salts or their alternate copolymerization [80–83] with SO_2 have etched an important place in the synthesis of a plethora of industrially significant ionic polymers. Utilization of one such alternate copolymerization, a methionine-based diallylamine salt monomer **3** was synthesized, and copolymerized with SO_2 in solvent ethanol or acetone to give water-insoluble copolymer containing sulfide **4** (Scheme 2.1). Surprisingly, the copolymerization in solvent dimethyl sulfoxide (DMSO) led to the formation of water-soluble polymer as a mixture of sulfide/sulfoxide **5.** During the polymerization ≈50% of the sulfide motifs has been oxidized to sulfoxide as a result of oxide exchange from DMSO. The polymer's water-solubility paved the way to study its inhibitive behavior against corrosion of mild steel in the hostile environment of 1 M HCl. Polymer **5** having so many centers of lone pair of electrons and the unquenched nitrogen and sulfur valences imparted remarkable inhibition of mild steel corrosion in 1 M HCl, as evinced by the preliminary study [84]. At a concentration of 5 ppm, L-Methionine ethyl ester hydrochloride (**1**), methionine-based monomer **3** and polymer **5** imparted inhibition of mild steel corrosion to the extent of 57, 58 and 96%, respectively. A polymer backbone containing numerous chelation centers associated with the pendants are expected to undergo stronger adsorption onto the metal surface, thereby achieving greater corrosion control than their monomeric analogs [85–87]. The effect of sulfoxide motifs in **5** on the corrosion inhibition could not be

quantified and compared with that of the sulfide motifs because of water-insolubility of polymer **4**. It is worth mentioning that repeated attempts to hydrolyze the ester functionalities in **4** under basic or acidic conditions resulted in failure.

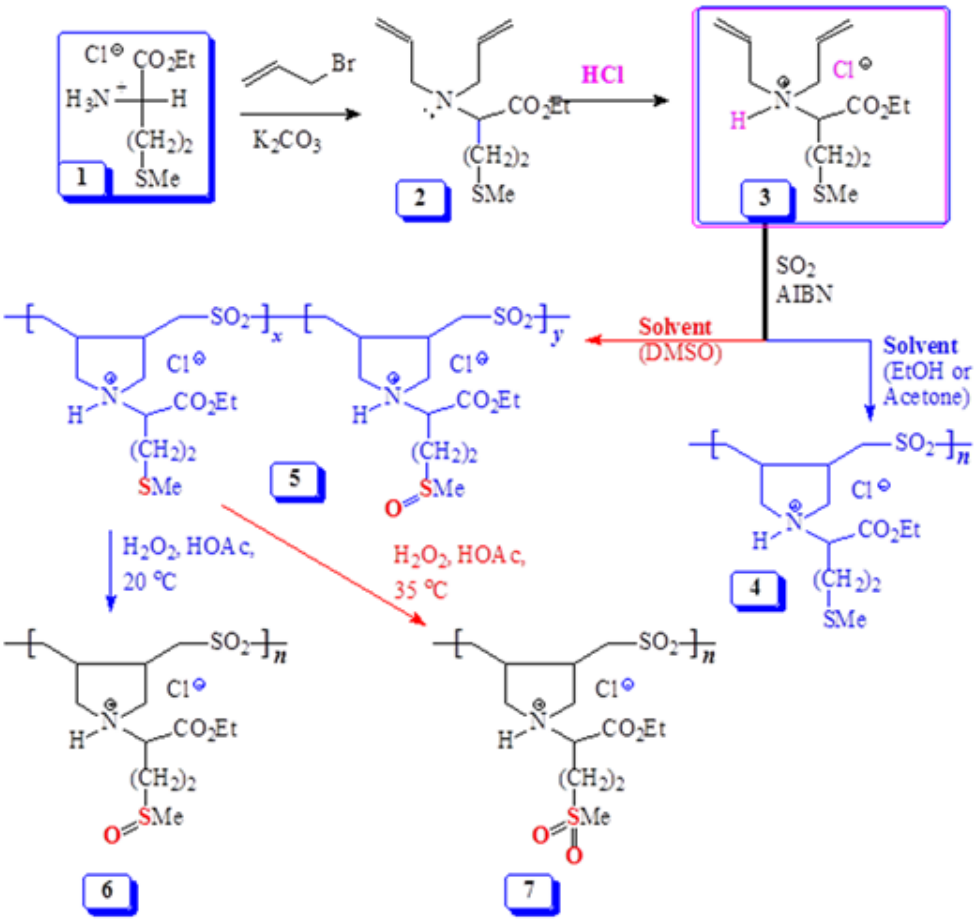

Scheme 2.1 Synthesis of methionine ester hydrochloride-based diallylamine salt/sulfur dioxide alternate copolymers.

In the current work, the ester functionality in monomer precursor **2** was hydrolyzed to zwitterionic and cationic monomers **8** and **9**, respectively with the anticipation that the corresponding polymers **10** and **11**, obtained via Butler's cyclopolymerization protocol [52-58], would be water-soluble (Scheme 2.2). The obtainment of the polymers and

changing their functional motifs would allow us to study their solution properties, and a preliminary study to compare the corrosion inhibition efficiencies of these polymers imparted by carboxylic acid, ester, sulfide, sulfoxide, and sulfone functional motifs.

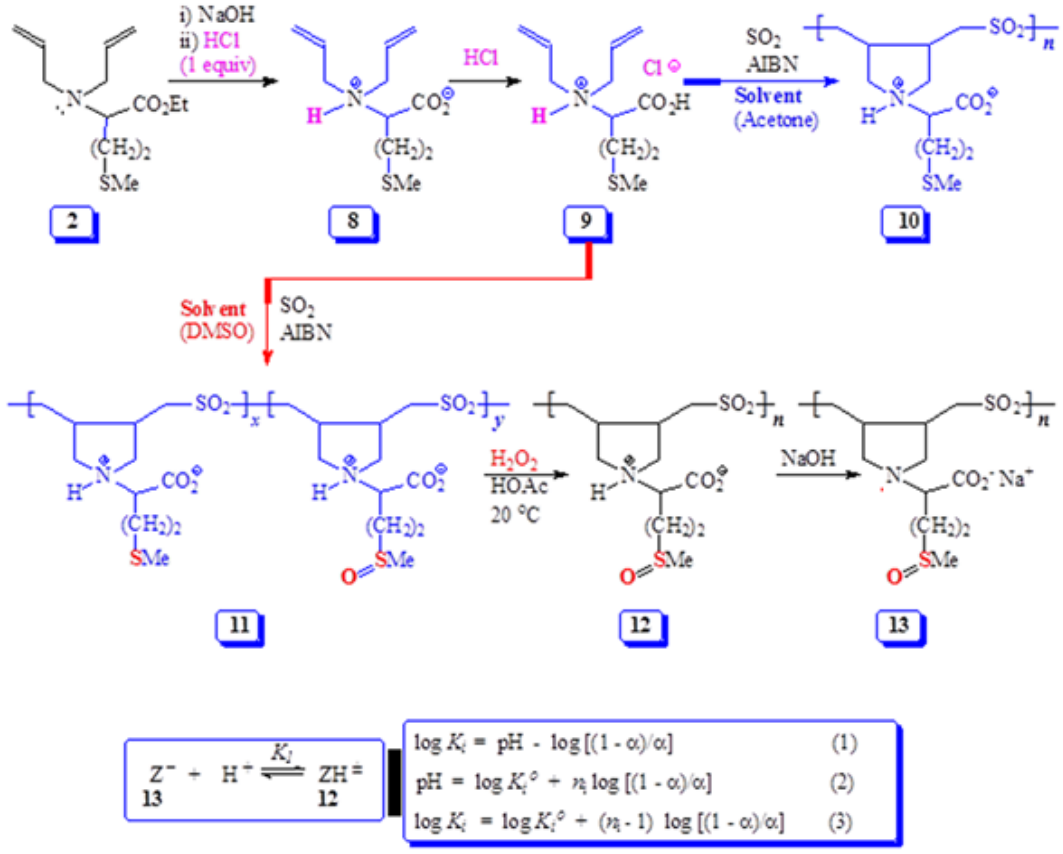

$$Z^- + H^+ \underset{}{\overset{K_i}{\rightleftharpoons}} ZH^+$$
13 12

$$\log K_i = pH - \log[(1-\alpha)/\alpha] \quad (1)$$

$$pH = \log K_i^{\circ} + n_i \log[(1-\alpha)/\alpha] \quad (2)$$

$$\log K_i = \log K_i^{\circ} + (n_i - 1) \log[(1-\alpha)/\alpha] \quad (3)$$

Scheme 2.2 Synthesis of methionine-based diallylamine salt/sulfur dioxide alternate copolymers.

2.2 Experimental

2.2.1 Physical Methods

Perkin Elmer 16F PC FTIR was used to record IR spectra, while ^{1}H and ^{13}C NMR were collected in a JEOL LA 500 MHz spectrometer for the determination of the chemical composition of the synthesized compounds. A Perkin Elmer Elemental analyzer (Carlo-

Erba: 2400) was utilized for elemental analysis. The viscosity values of synthesized compounds were determined in CO_2-free water using an Ubbelohde viscometer (Viscometer Constant 0.005317 mm^2 s^{-2}) under N_2. Thermogravimetric analysis (TGA) was performed under N_2 (flow rate 50 mL/min) using an SDT thermogravimetric analyzer (Q600: TA Instruments, New Castle, DE, USA). Surface tension was measured using a surface tensiometer (PHYWE, Germany).

2.2.2 Materials

Ethyl ester hydrochloride of L-Methionine (**1**) was obtained from Fluka Chemie AG. Hydrogen peroxide (35 w/v %) and potassium carbonate (K_2CO_3) were purchased from BDH Chemical Ltd (Pool, England). Azobisisobutyronitrile (AIBN) (Fluka Chemie AG) was recrystallized from $CHCl_3$-EtOH. All solvents were of HPLC grade. Dimethylsulfoxide (DMSO), dried over CaH_2 overnight, was distilled (bp $_{4\ mmHg}$ 64–65 °C). Diallyl derivative of methionine **2** and its hydrochloride salt **3** were prepared from L-methionine ethyl ester hydrochloride **1** as described [84].

2.2.3 Synthesis of monomers and polymers

2.2.3.1 Cyclocopolymerization of monomer 3 with SO_2

Polymer **5** was prepared as described [84]. Briefly, a mixture of **3** (2.70 g, 9.19 mmol) and sulfur dioxide (SO_2) (0.588 g, 9.19 mmol) in DMSO (2.02 g) was polymerized using an initiator (AIBN, 0.066 g, 0.4 mmol) at 60 ^oC for 24 h. The mole ratio of monomers (**3** and SO_2) to initiator was thus kept at 46:1. After dialysis against deionized water, the polymer was freeze dried. The isolated polymer sulfide/sulfoxide **5** was obtained as a white powder (2.23 g, 66%). Polymer **4** was synthesized following the same procedure

except that ethanol (2.02 g) or acetone (2.02 g) was used as a solvent.

Table 2.1 Cyclocopolymerizationa of monomer **9**/SO_2

Entry No.	Monomer (mmol)	SO_2 (mmol)	Solvent (g)	AIBN (mg)	(**Polymer**) Yield (%)	$[\eta]^b$ (dL g^{-1})
1	15	15	Acetone (8)	150	**(10)** 71	0.0928
2	15	15	Acetone (8)	200	**(10)** 63	0.0895
3	15	15	DMSO (3.5)	150	**(11)** 62	0.0552
4	15	15	DMSO (3.5)	200	**(11)** 51	0.0532

[a] Polymerization reactions were carried out at appropriate concentrations of monomer **9** and SO_2 in the presence of azobisisobutyronitrile (AIBN) at 60 °C for 48 h to give polymer **10** in solvent acetone and **11** in DMSO.

[b] Viscosity of 1-0.25 % solution of **10** (or **11)** treated with 1 equivalent of NaOH in 0.1 M NaCl at 30.0 ± 0.1 ^oC was measured with Ubbelohde Viscometer (K=0.005317 mm^2 s^{-2}).

2.2.3.2 Conversion of polymer sulfide/sulfoxide 5 to polymer sulfoxide 6

Hydrogen peroxide (35 w/v %) (0.888 g, 9.14 mmol) was slowly added to a solution of **5** (0.802 g; 2.20 mmol) in glacial acetic acid (2.37 g) at 20 °C. The reaction mixture was stirred at 20 °C for 5 h or until the completion of oxidation of the sulfide to sulfoxide as indicated by the ^1H NMR spectrum. The resultant solution was dialyzed against de-ionized water for 3 h followed by 30 min in 0.2 M HCl then 30 min again in de-ionized water. The freeze-drying of the dialyzed solution afforded polymer **6** as a white solid (0.720 g, 88%). Elemental analysis of $C_{13}H_{24}ClNO_5S_2$ found: C, 41.4; H, 6.6; N, 3.6; S, 16.8; requires: C, 41.76; H, 6.47; N, 3.75; S, 17.15%; ν_{max} (KBr) 3427, 2924, 2609 (br), 1741, 1634, 1408, 1378, 1305, 1214, 1129, 1016, 946, 854, 782, 670 and 514 cm^{-1}.

2.2.3.3 Conversion of polymer sulfide/sulfoxide 5 to polymer sulfone 7

The sulfide to sulfone oxidation was carried out using a slightly modified procedure [88]. Hydrogen peroxide (35 w/v%) (0.586 g, 6.03 mmol) was slowly added to a solution of polymer **5** (0.537 g; 1.47 mmol) in glacial acetic acid (1.50 g) at room temperature. After stirring the reaction mixture at 35 °C for 4 h or until the ^{1}H NMR indicated the completion of oxidation to sulfone **7**, the polymer solution was dialyzed against de-ionized water for 4 h followed by 30 min in 0.2 M HCl to reduce the cloudiness of the solution then 30 min again in de-ionized water. The solution was then freeze-dried to obtain polymer **7** as a white solid (0.470 g, 82%). Elemental analysis of $C_{13}H_{24}ClNO_6S_2$ found: C, 39.7; H, 6.4; N, 3.4; S, 16.1; requires C, 40.05; H, 6.20; N, 3.59; S, 16.44%; ν_{max} (KBr) 3414, 2926, 2609 (br), 2361, 1742, 1633, 1451, 1409, 1377, 1304, 1216, 1128, 1038, 966, 851, 771, 669 and 510 cm^{-1}.

2.2.3.4 Synthesis of cationic monomer 9 and its zwitterionic counterpart 8

A heterogeneous mixture of monomer precursor **2** (20.6 g, 80 mmol), CH_3OH (50 mL), H_2O (20 mL), and sodium hydroxide (3.60 g, 90 mmol) was stirred for 4 h at 40 °C. After concentrating the homogeneous mixture, the residue was diluted with water (15 mL), acidified with concentrated HCl (37%) (8.87 g; 170 mmol) (i.e. two equivalents of HCl), and then freeze-dried to obtain a mixture of cationic acid hydrochloride monomer **9** and NaCl. After trituration with acetone (100 mL) and filtering off the insoluble NaCl, the filtrate was concentrated to obtain monomer **9** as a colorless thick liquid (20.2 g, 95%). Elemental analysis of $C_{11}H_{20}ClNO_2S$ found: C, 49.4; H, 7.7; N, 5.2; S, 11.8; requires C, 49.71; H, 7.58; N, 5.27; S, 12.06%; ν_{max}. (neat) 3348, 3088, 2921, 2848, 2360, 2331, 1735, 1635, 1448, 1425, 1388, 1325, 1201, 1157, 1078, 995, 946, 872, 770 and 736 cm-

1; ^{1}H (D2O) 1.98 (3H, s), 2.06 (1H, m), 2.52 (1H, m), 2.65 (1H, m), 3.70 (2H, m), 3.81 (2H, m), 4.09 (1H, d, J 9.2), 5.48 (4H, m), 5.79 (2H, m), (residual H in D2O at 4.65 ppm); ^{13}C (D2O): 15.00 (1C, SCH3), 26.0 (1C, CH2CH2S), 30.4 (1 C, CH2CH2S), 55.1 (2C, NCH2), 62.9 (1C, NCH), 126.44 (2C, CH=CH2), 127.79 (2C, CH=CH2), 171.3(1C, CO2), (67.4, dioxane). The 13C spectral assignments were confirmed by DEPT- 135 NMR analysis.

In a separate experiment, the above procedure was followed in one-tenth scale. Here, instead of two equivalents, one equivalent HCl (9.00 mmol; based on NaOH used) was used to neutralize the $CO_2^-Na^+$ salt to generate zwitterionic monomer **8** as a white solid (1.74 g; 93%). Mp. 55-59 °C. Elemental analysis of $C_{11}H_{19}NO_2S$ found: C, 57.4; H, 8.4; N, 6.0; S, 13.7.; requires C, 57.61; H, 8.35; N, 6.11; S, 13.98%; $\upsilon_{max.}$ (KBr) 3415, 3082, 3024, 2976, 2964, 2918, 2838, 1627,1455, 1426, 1357, 1339, 1302, 1275, 1219, 1154, 1121, 1080, 1060, 1012, 994, 951, 773, 760, 718, 694, 666, 628, and 575 cm^{-1}; ^{1}H (D_2O) 1.98 (3H, s), 2.02 (2H, m), 2.46 (1H, m), 2.57 (1H, m), 3.65-3.75 (5H, m), 5.45 (4H, m), 5.79 (2H, m); ^{13}C (D_2O): 15.1 (1C, S$\underline{C}H_3$), 27.0 (1C, $CH_2\underline{C}H_2S$), 30.6 (1 C, $\underline{C}H_2CH_2S$), 54.4 (2C, N$\underline{C}H_2$), 65.6 (1C, N$\underline{C}$H), 126.7 (2C, $\underline{C}$H=CH_2), 127.2 (2C, CH=$\underline{C}H_2$), 172.9 (1C, $\underline{C}O_2$), (67.4, dioxane). The ^{13}C spectral assignments were confirmed by DEPT- 135 NMR analysis.

2.2.3.5 Cyclopolymerization of monomer 9 and SO_2 in acetone

As described in Table 2.1, sulfur dioxide (0.962 g, 15 mmol) was adsorbed onto a solution of monomer **9** (4.0 g; 15 mmol) in acetone (8.0 g) at 0 °C in a 25-mL round bottom flask. After addition of the specified amount of AIBN [150 mg (0.91 mmol) or 200 mg (1.22 mmol)], the closed flask was heated at 60 °C for 48 h. The mole ratio of

monomers (**9** and SO_2) to initiator was thus kept at 33:1 or 24.6:1. Within 2 h, the polymer started to separate as a white precipitate. After the time elapsed, the polymer was filtered, dissolved in $NaHCO_3$ solution, and dialyzed against deionized water for 3 h, 0.1 M HCl for 3 h, followed by de-ionized water for additional 24 h. Phase separation occurs within the dialysis tube. The resultant polymer **10** was thereafter isolated and dried under vacuum at 60 °C. Elemental analysis of $C_{11}H_{19}NO_4S_2$ found: C, 44.8; H, 6.7; N, 4.6; S, 21.6; requires C, 45.03; H, 6.53; N, 4.77; S, 21.85%.ν_{max}. (KBr) 3570, 2971, 2921, 2852, 2553 (br), 1622, 1456, 1397, 1303, 1126, 1017, 954, 877, 768, 654, and 514 cm^{-1}.

2.2.3.6 Cyclopolymerization of monomer 9 and SO_2 in DMSO

As described in Table 2.1, sulfur dioxide (0.962 g, 15 mmol) was adsorbed onto a homogeneous mixture of monomer **9** (4.0 g; 15 mmol) in DMSO (3.5 g) in a 25 mL round bottom flask. After the addition of the specified amount of AIBN, the closed flask was heated at 60 °C for 48 h. Noted that few times the reaction flask was cooled and opened to release N_2 gas obtained from the decomposition of the initiator. The resultant reaction mixture was dialyzed against deionized water for 10 h, then freeze-dried to obtain polymer **11**. Elemental analysis of polymer **11** having an approximate 1:1 ratio of sulfide ($C_{11}H_{19}NO_4S_2$) and sulfoxide motifs ($C_{11}H_{19}NO_5S_2$) found: C, 43.4; H, 6.2; N, 4.4; S, 20.8; requires C, 43.87; H, 6.36; N, 4.65; S, 21.29%; ν_{max}. (KBr) 3425, 2922, 1626, 1452, 1400, 1305, 1128, 1021, 947, 876, 766, 653 and 515 cm^{-1}.

2.2.3.7 Conversion of polymer sulfide-sulfoxide 11 to corresponding sulfoxide 12

Hydrogen peroxide (35 w/v %) (0.237 g; 2.44 mmol) was slowly added to a solution of polymer **11** (0.675 g; 2.24 mmol) in glacial acetic acid (2.24 g) at 20 °C. The reaction

mixture was then stirred at 20 °C for 5 h or until the completion of oxidation as indicated by ^{1}H NMR spectrum. After the time elapsed, the resultant mixture was dialyzed against de-ionized water for 8 h, and then freeze-dried to obtain polymer **12** (0.496 g, 72%). Elemental analysis of $C_{11}H_{19}NO_5S_2$ found: C, 42.4; H, 6.3; N, 4.4; S, 20.4; requires C, 42.70; H, 6.19; N, 4.53; S, 20.72%; ν_{max} (KBr) 3481, 2923, 2678 (br), 1632, 1456, 1401, 1305, 1128, 1021, 787, 677 and 507 cm^{-1}.

2.2.4 Potentiometric Titrations

The protonation constant (*K*) of basic nitrogen was calculated by potentiometric titration at 23 °C in salt-free water following the published literature procedure described elsewhere [89,90]. As described in Table 2.2, a certain amount of zwitterionic polymer **12** ($ZH^{\pm}$) in CO_2-free water (200 mL) was titrated using step-wise addition of 0.0959 M NaOH solution (0.05-0.15 mL). After each addition, the solution was stirred briefly using a magnetic stir bar under N_2 and the pH values were recorded, and the log *K*s were calculated using the Henderson-Hasselbalch Eq. (2) (Scheme 2.2). Where degree of protonation (α) is defined as the ratio $[ZH^{\pm}]_{eq}/[Z]_o$. The $[Z]_o$ and $[ZH^{\pm}]_{eq}$ are the respective initial analytical concentration of the monomeric units in **12** ($ZH^{\pm}$) and its concentration at the equilibrium as given by: $[ZH]_{eq} = [Z]_o - C_{OH^-} - [H^+] + [OH^-]$. The C_{OH^-} is the concentration of the added NaOH, while $[H^+]$ and $[OH^-]$ at equilibrium were calculated from the pH value.

Table 2.2 Protonation of polymer **13** (Z–) at 23 °C in salt-free water

run	$ZH^{\pm}$ [a] (mmol)	C_T [b] mol dm^{-3}	α-range	pH-range	Points [c]	Log K_1^o [d]	n_1 [d]	R^2, [e]
1	0.2586 ($ZH^{\pm}$)	-0.09594	0.85-0.12	5.37-9.27	19	7.28	2.52	0.9963
2	0.2893 ($ZH^{\pm}$)	-0.09594	0.87-0.10	5.32-9.35	22	7.27	2.54	0.9975
3	0.3232 ($ZH^{\pm}$)	-0.09594	0.88-0.12	5.27-9.30	24	7.34	2.46	0.9982
Average						7.30 (4)	2.51 (4)	

Log K_1 [f] = 7.30 + 1.51 log [(1-α)/α] For the reaction: $Z^- + H^+ \overset{K_1}{\rightleftharpoons} ZH^{\pm}$

[a] $ZH^{\pm}$ represents polymer 12

[b] (-ve) values describes titration with NaOH

[c] Number of data points

[d] Standard deviations in the last digit are given under parentheses

[e] R^2 = Correlation coefficient

[f] log K_i = log K_i^o + (n_i -1) log [(1-α)/α]

The Equation 2 (Scheme 2.2) describes the apparent basicity constants of typical polyelectrolytes; in the case of sharp basicity constants log K^o = pH at α = 0.5 and n = 1. The pH *vs*. log [(1- α/α)] plot gave log K^o and '*n*' as the intercept and slope, respectively.

The modified Henderson-Hasselbalch equation (3) (Scheme 2.2) is obtained by inserting the value of pH from Eq. 2 into Eq. 1 whereby (n – 1) gives a measure of the deviation of the studied polymers from the behavior of small molecules which show sharp basicity constants with an n value of 1.

2.2.5 Surface tension

A surface tensiometer (PHYWE, Germany) as described [91] equipped with torsion dynamometer (0.01 N) and platinum-iridium ring (diameter =1.88 cm) was utilized to

determine the surface tension of 1 M HCl containing various concentrations of the synthesized polymers at 60 °C.

2.2.6 The standard free energy of micelle formation ($\Delta G°_{mic}$)

The $\Delta G°_{mic}$ of the synthesized polymers were determined by Eq. (4) [92]:

$$\Delta G°_{mic} = RT \ln(C_{cmc}) \qquad (4)$$

where C_{cmc} represents the polymer concentration at the CMC.

2.3 Results and Discussion

2.3.1 Monomer and polymer syntheses

Cationic monomer **3** underwent cyclopolymerization with SO_2 in ethanol or acetone solvent to afford cyclocopolymer **4**, while in DMSO solvent to give alternate copolymer **5** in which the sulfide and sulfoxide were formed in an approximate ratio of 1:1 (Scheme 2.1) [83]. Copolymer **5** upon oxidation using H_2O_2/HOAc at 20 and 35 °C afforded polymer sulfoxide **6** and polymer sulfone **7**, respectively, in excellent yields.

Hydrolysis of the ester group in trivalent amine **2** [84] with NaOH followed by acidification with one and two equivalents of HCl led to zwitterionic **8** and cationic acid hydrochloride monomer **9**, respectively (Scheme 2.2). Monomer **9** underwent AIBN-initiated copolymerization with SO_2: while in acetone medium it gave copolymer **10** after depletion of HCl during dialysis, the polymerization in DMSO afforded polymer **11**. The formation of polymer **11** with a ≈ 1:1 ratio of the sulfide/sulfoxide moieties is a result of oxygen exchange between the sulfide in the polymer and sulfoxide in DMSO ($Me_2S=O$) [93]. The polymers are obtained in moderate to good yields (Table 2.1) despite possible degradative chain transfer owing to the presence of allylic motifs [94] and the ability of

sulfide functionality to act as chain transfer agent. The sulfide groups in copolymer **11** was oxidized to polymer **12** having fully oxidized sulfoxide motifs.

2.3.2 Solubility behavior

Like polymer sulfide **4** containing ester functionalities (CO_2Et), copolymer (±) **10** having zwitterionic motifs [$–NH^+$ $–CO_2^-$] was found to be insoluble in water. However, (+) **6**, (+) **7**, (+) **9**, (±) **11** and (±) **12** were water-soluble owing to the greater polarity of the sulfoxide motifs which dominates over the zwitterionic motifs in dictating the solubility behavior. While overall hydrophobicity of polymer sulfide (+) **4** makes it water-insoluble, the electroneutral polymer sulfide/sulfoxide (±) **11** and sulfoxide (±) **12**, like the majority of known as polyzwitterions [95–97], was expected to be insoluble in water owing to intragroup, intra- and interchain attractive interactions leading to the formation of ionic crosslinks. Their water solubility, therefore, is attributed mainly to the presence of polar sulfoxide motifs. The presence of salts of smaller masses is known to impart water-solubility causing disruption of the attractive forces [98]; however polyzwitterion (±) **10** having sulfide groups remained insoluble in the presence of NaCl (0-5 M) or HCl (1-12 M). A 1 wt.% solution of copolymer **10** in 2 M NaI was found to be partially soluble. Being softer (more polarizable), iodide ions effectively neutralizes the ionic crosslinks so as to disrupt attractive interactions [98]. Note that the treatment of polymer (±) **10** with 1.0 equivalent NaOH changes the zwitterionic motifs [$–NH^+\cdots\cdots CO_2^-$] to anionic motifs [$–N\cdots\cdots CO_2^-Na^+$] thereby imparting water-solubility.

2.3.3 TGA Curves, FT-IR, NMR Spectra, and Molar mass by end group analysis

The TGA curves of **6**, **7**, **10**, and **12** are shown in Figure 2.1; a loss of ≈2-7% up to 180-200 °C was accounted for the removal of moisture. An accelerated loss of ≈ 40% for the polymers in the range ≈ 200-250 °C resulted from the release of CO_2 and SO_2 whose combined masses are calculated to be ≈ 36%. A further loss of ≈ 30% may be linked to the removal of the methionine pendants occurred in the range 250-400 °C. Overall, all these polymers were asserted to be stable up to ≈200 °C.

The IR spectrum of monomer (+) **9** revealed a strong absorption band at 1735 cm^{-1} attributed to C=O stretch of CO_2H group, while the band was absent in the spectrum of zwitterionic monomer (±) **8**. Likewise, this band was absent in the spectra of polymers (±) **10-12**; instead peaks at ≈1400 (symmetric stretching) and ≈1427 cm^{-1} (anti-symmetric stretching) were assigned to the COO^- motifs in the dipolar zwitterionic form of the polymers [98]. The strong bands at ≈ 1305 cm^{-1} and ≈1128 cm^{-1} in the IR spectra of all the as-synthesized polymers are due to the SO_2 stretching vibrations, while a band at 1021 cm^{-1} can be assigned to the S=O stretching absorption in **5, 6, 11** and **12**.

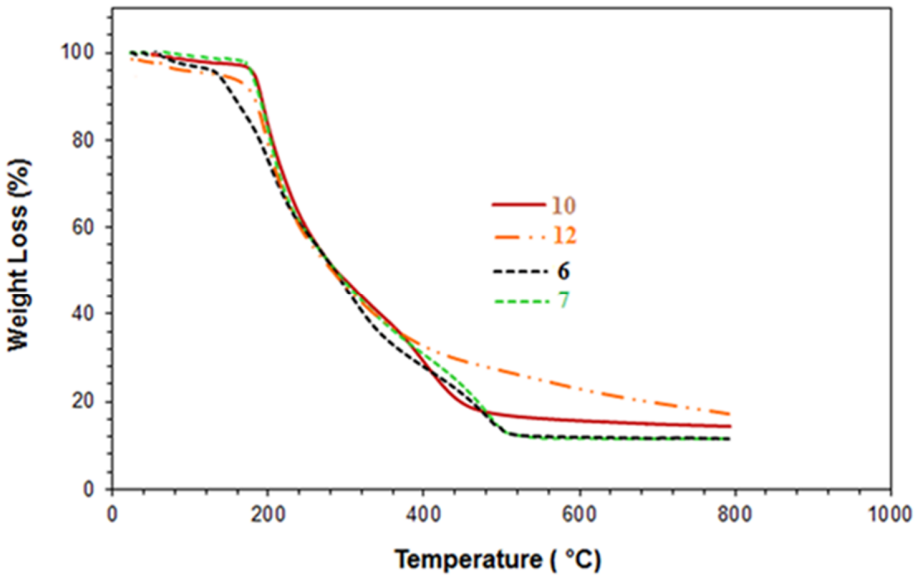

Figure 2.1 TGA Curves for **6**,**7**, **10** and **12**

Elemental analysis of $C_{13}H_{24}ClNO_6S_2$ found: C, 39.7; H, 6.4; N, 3.4; S, 16.1; requires C, 40.05; H, 6.20; N, 3.59; S, 16.44%; ν_{max} (KBr) 3414, 2926, 2609 (br), 2361, 1742, 1633, 1451, 1409, 1377, 1304, 1216, 1128, 1038, 966, 851, 771, 669 and 510 cm^{-1}.

Figures 2.2-2.4 display some representative ^{1}H and ^{13}C NMR spectra of monomer **9** and several polymers. As can be seen, the methyl protons marked ‘c’ and ‘c’’ of **5** appeared at δ2.0 and 2.6 ppm, respectively (Figure 2.2a). The downfield signal at δ2.6 was attributed to the sulfoxide motifs as a result of greater electron withdrawing ability of S=O as compared to sulfide group. Upon oxidation, the sulfide group in **5** is converted into sulfoxide **6** as evident by disappearance of the signal marked ‘c’ (Figure 2.2b). Further oxidation resulted in the formation of sulfone motifs in **7**; the methyl protons marked ‘c’’ appeared at a downfield shift of δ3.0 ppm because of greater electronegativity of sulfone groups in **7** (Figure 2.2c).

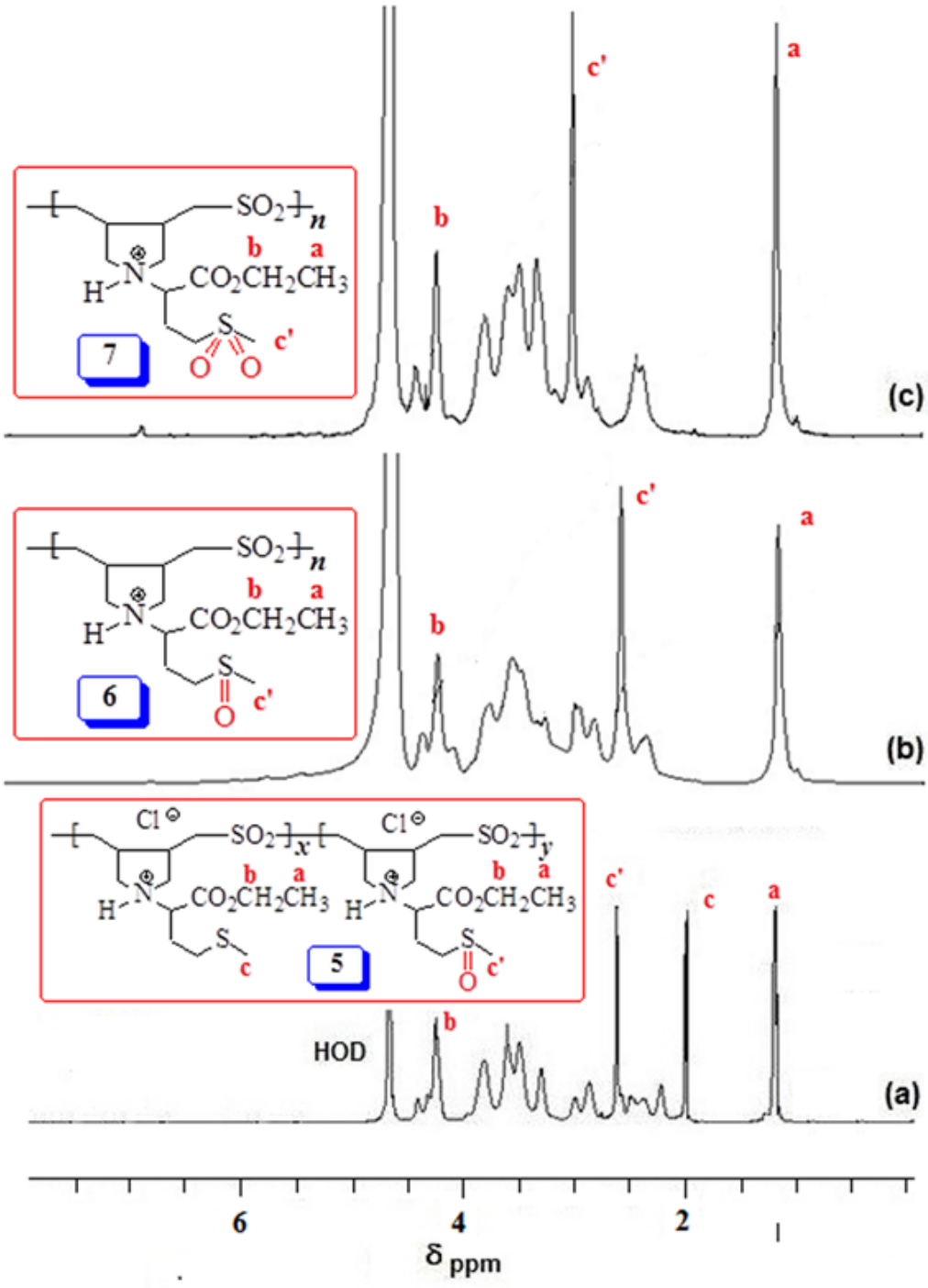

Figure 2.2 ^{1}H NMR Spectra of (a) **5**, (b) **6** and (c) **7** in D_2O

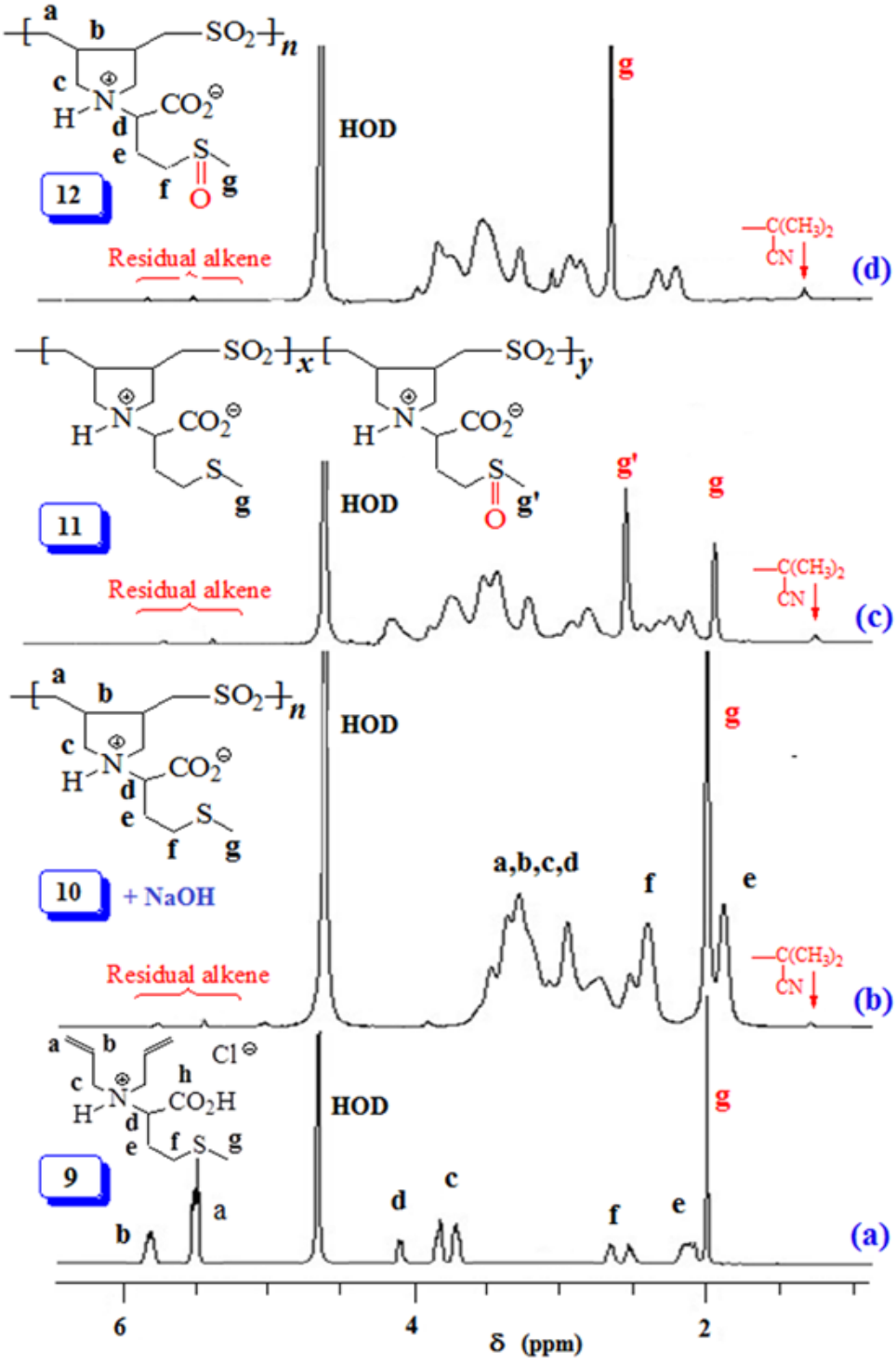

Figure 2.1 ^{1}H NMR Spectra of (a) **9**, (b) **10** (+1 equiv NaOH), (c) **11** and (d) **12** in D_2O

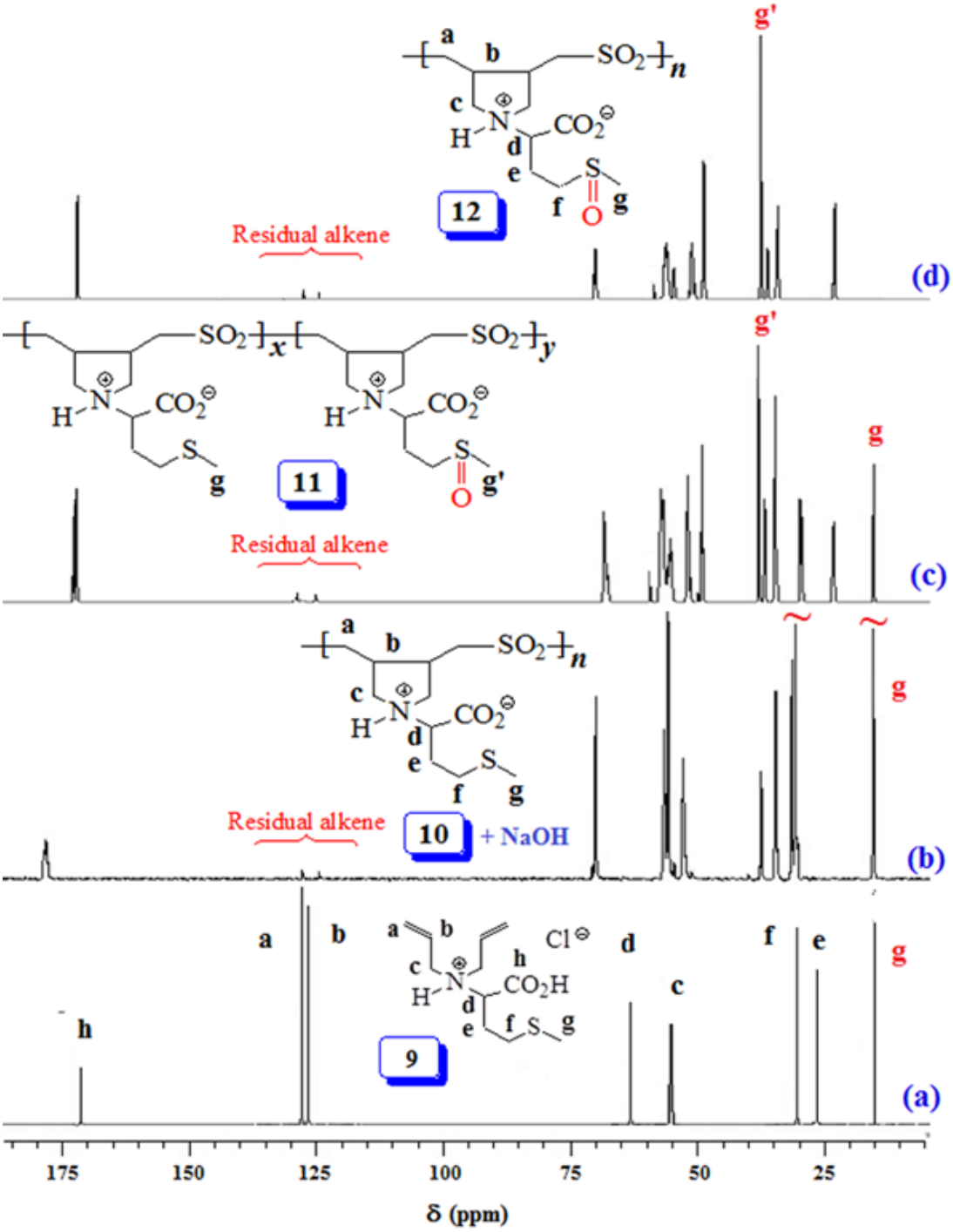

Figure 2.4 ^{13}C NMR Spectra of (a) **9**, (b) **10** (+1 equiv NaOH), (c) **11** and (d) **12** in D_2O

Polymers **10-12** even after extended dialysis contain ≈ 3-4 % residual alkene as revealed by alkene protons and carbons in the range δ5.4-5.8 (Figure 2.3) and ≈125 ppm (Figure 2.4), respectively. The presence of pendant double bonds [90] could be resulting either from chain propagation without cyclization or transfer to the monomer [80]. The SMe protons of polymer **10** marked '**g**' appeared at δ 2.0 ppm (Figure 2.3b), while partial oxidation of SMe to O=SMe is confirmed by the presence of additional signal of methyl protons of polymer **11** marked '**g′**' at ≈ δ2.6 ppm (Figure 2.3c). Complete oxidation of sulfide to sulfoxide polymer **12** is assured by the missing SMe signal both in the ^{1}H and ^{13}C spectra of polymer **12**; carbon signal of SMe (marked **g**) and O=SMe (marked **g′**) appeared at ≈ δ15 and 37 ppm, respectively.

As reported earlier [99] and found in the current work, the molar masses of the polymers could not be obtained by GPC presumably owing to the strong adsorption of amine and carboxyl motifs to the column materials. End group analysis, however, helped [100] us to calculate the approximate number average molar masses (M_n) of some of the polymers **10-12**. The $(CH_3)_2C(CN)$ group (originating from the AIBN initiator) attached to the chain end is displayed as a broad singlet at δ1.31 ppm and was not interfered with any competing signal (Figure 2.3). However, the calculation is complicated by the lack of understanding of the mode of chain termination. In the absence of chain transfer, while the coupling mechanism would lead to two initiator fragments at two chain ends, termination by disproportionation on the other hand would have only one terminal with the initiator fragment. Low molar masses (*vide infra*) are suggestive of the chain termination by a degradative chain transfer process [94] involving transfer of an allylic hydrogen from monomer **9** to a chain radical. The resultant stable allylic radical cannot

reinitiate polymerization and as such the transfer would amount to a termination process. However, chain transfer to the sulfide motifs may give a radical which may able to reinitiate a new chain which may not have the initiator fragment $(CH_3)_2C(CN)$ at either end of the dead polymer. Even though sulfide group may act as a chain transfer agent, its chain transfer constant, C_s (i.e. the ratio of rate constant of the chain transfer of a propagating radical to the rate constant for propagation of the radical) value of ≈ 0.0022 does make it an insignificant process. Keeping in view the degradative chain transfer as the main process, it can be assumed that each polymer chain on average will have one initiator fragment. The integrated area (**A**) at δ1.31 is attributed to the 6 H of the end group $(CH_3)_2C(CN)$, while the area **B** covering signals in the range δ1.5-4.3 ppm belongs to all the 18 H of each repeating unit (RU). The degree of polymerization (DP), calculated by taking the area ratio of 1 H of the RU and the end group, thus equals to (**B**/18)/(**A**/6). The average DP is thus found to be 40.9 and 42.1 for polymer **11** and **12**, respectively. The similar values are expected since polymer **11** was transformed to **12**. The DP value of 40.9 was translated into a number average molar mass of 12,300 g mol^{-1} for polymer **11**. Likewise, the DP of polymer **10** was calculated to be 95 with a molar mass of 27,900 g mol^{-1} suggesting that polymerization in solvent acetone led to polymer **10** having higher molar mass than polymer **11** obtained in DMSO solvent. End group analysis cannot be carried out for polymers **5-7** since the signal for the initiator fragment $(CH_3)_2C(CN)$ is expected to overlap with that of the methyl protons marked ‘a’ (Figure 2.2).

2.3.4 Viscosity measurements

The viscosity plots for polymers **5**-**7** are shown in Figure 2.5. In salt-free water, reduced viscosity increases with decrease in concentrations of **6** as expected of a polyelectrolyte. In 0.1 M NaCl, the viscosity plots become normal. The polymers have very low intrinsic viscosity [η] values thereby suggesting low molar masses for the polymers.

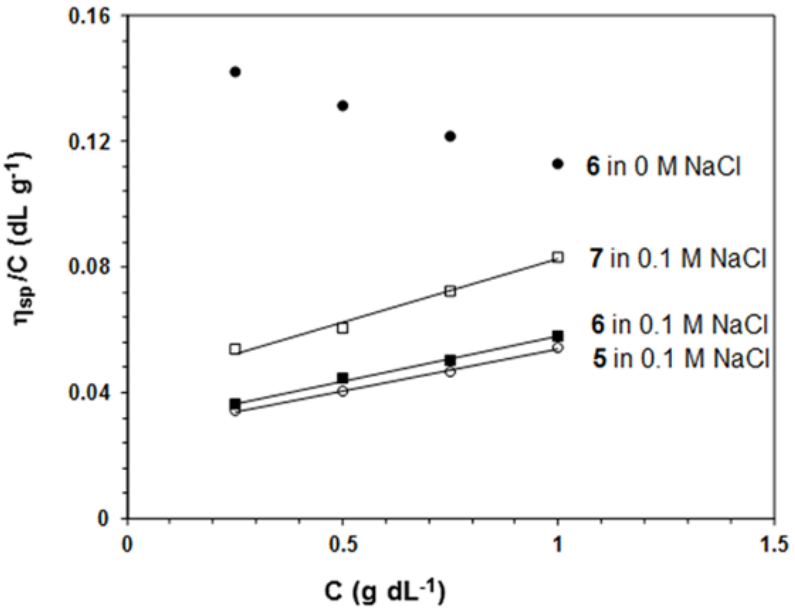

Figure 2.5 Using an Ubbelohde Viscometer at 30 °C: the Viscosity Behavior of (a) ●**6** in salt-free water, (b) □ **7** in 0.1 M NaCl, (c) ■ **6** in 0.1 M NaCl, (d) ○ **5** in 0.1 M NaCl

The viscosity plots (Figure 2.6) of **10** and **11** (both treated with 1 equivalent of NaOH) in 0.1 M NaCl revealed that the former, obtained from polymerization carried out in acetone, has higher [η] (0.0928 *vs.* 0.0552 dL g^{-1}) (*cf.* Figure 2.6: a *vs.* f). The data are in line with the end group analysis (*vide supra*) which revealed higher molar mass for polymer **10** as compared to that of polymer **11**. As expected, polymers **11** and **12** have similar [η] since the latter was derived from the former by oxidation (*cf.* Figure 2.6: f vs. g).

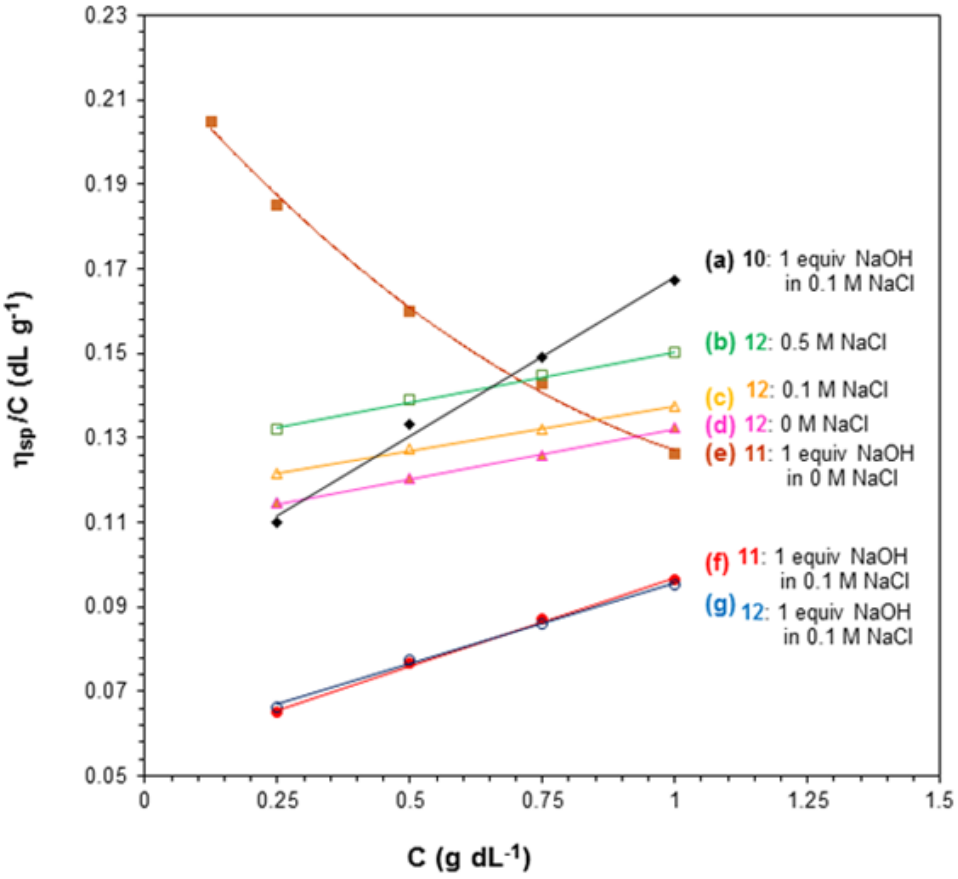

Figure 2.6 Using an Ubbelohde Viscometer at 30 ºC: the Viscosity Behavior of (a) ♦**10** in 0.1M NaCl (+ 1 equiv NaOH), (b) □ **12** in 0.5 M NaCl, (c) Δ **12** in 0.1 M NaCl, (d) **12** in salt-free water, (e) ■ **11** in salt-free water (+ 1 equiv NaOH), (f) ● **11** in 0.1 M NaCl (+ 1 equiv NaOH)

The anti-polyelectrolyte behavior of the zwitterionic motifs in (±) **12** is demonstrated by the increasing viscosity values with increasing salt concentrations (*cf.* Figure 2.6: b,c,d) [101]. The Cl^- ions bind more strongly to the positive nitrogens as compared to the binding of Na^+ to the CO_2^- thereby leaving an excess of negative charge on the zwitterionic dipoles of polymer **12**, the repulsion among which leads to an increase in the hydrodynamic volume hence viscosity with increasing NaCl concentration [96,102,103].

Polyzwitterion, PZ (±) **11** on treatment with 1 equivalent NaOH is converted to an anionic polyelectrolyte as a result of the change of the zwitterionic motifs ($NH^+...CO_2^-$) to anionic motifs ($N...CO_2^-$). As such the viscosity curve of PZ (±) **11** in the presence of NaOH became concave upwards in salt-free water (Figure 2.6e). The viscosity values of PZ (±) **12** in the presence of NaOH is found to be like that of (±) **11** and almost overlaps with the plot in Figure 2.6e; as such it is not shown in the Figure. In 0.1 M NaCl, the viscosity decreases and the plot becomes linear demonstrating its polyelectrolyte behavior (Figure 2.6f).

Lower viscosity values as revealed in Figure 2.6 are indicative of lower molar masses of the polymers. This is expected since monomer **9** has degradative chain transfer allylic groups [94], as well as the sulfide functionality capable of initiating chain transfer.

2.3.5 Basicity Constant

The apparent basicity constant of amine nitrogens in polymer **13** is described by Eq. (3) (Scheme 2.2) where log K^o = pH at $\alpha = 0.5$ and $n = 1$ observed for basicity constant of small molecules. The slope and intercept of the straight line plot of pH *vs*. log $[(1-\alpha)/\alpha)]$ gave the values of '*n*' and log K^o, respectively (Figure 2.7a). In salt-free water, basicity constant log K^o was determined to be 7.30 (Table 2.2), which is found to be less than the log K^o value of 9.93 for a similar polymer having a glutamic acid residue [104]. Lower basicity constant of nitrogens in polymer **13** may be attributed to the higher electronegativity of the sulfoxide motifs. Since log K of a base (B^-) is the pK_a of its conjugate acid (HB), the presence of sulfoxide motifs in polymer **12** makes it a stronger acid.

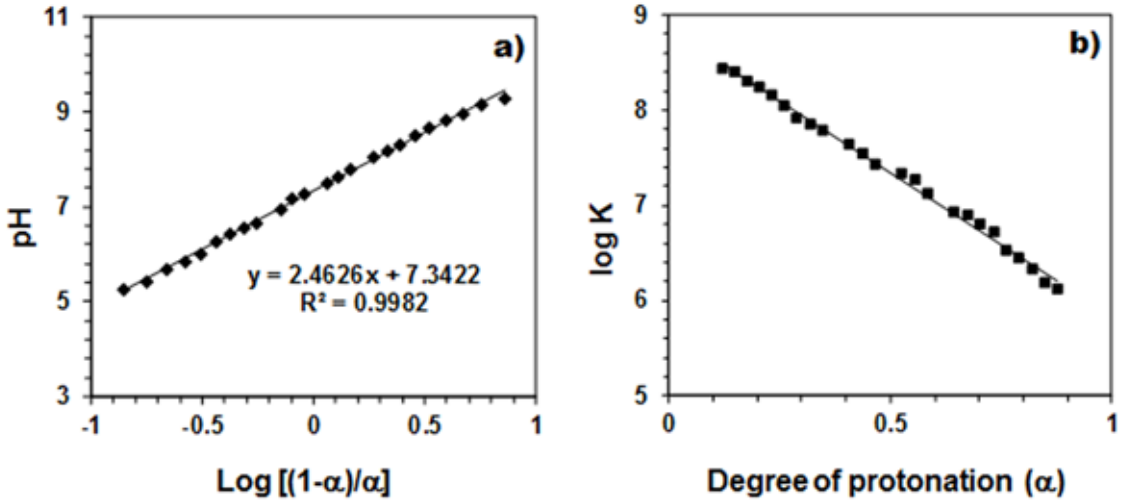

Figure 2.7 Variation of (a) pH versus log[(1-α)/ α] and (b) log K versus Degree of Protonation (α) for the Determination of Protonation Constant (K) of Polymer **13**

The *n* value of 2.51 reflects the "apparent" [105] nature of the basicity constant. A measure of the polyelectrolyte index *n* is shown in Figure 2.7b displaying a greater variation of *K* with α signifying a strong polyelectrolyte effect (because of *n* being greater than 1). With increasing α, a gradual decrease of log *K* [involving (Z^-) **13** + $H^+ \leftrightharpoons$ ($ZH^{\pm}$) **12]** is a result of decreasing overall negative charges that induces protonation. The greater *n* value confirms the consequence of entropy effects [105,106]. Since anionic polymer (-) **13** is expected to be more hydrated than the zwitterionic (±) polymer **12**, water molecules from the repeating unit of anionic polymer **13** is released as it is transformed to zwitterionic polymer **12**. With each protonation, the excess average negative charge in the polymer backbone of polymer **12** or **13** decreases as does the average number of water molecules associated with each repeating unit. Therefore, there will be lesser and lesser number of water molecules to be released from the polymer backbone of polymer **12** or

13 with increasing α, and associated entropy change dictates the decrease of K with increasing α.

2.3.6 Surface tension

The plots of surface tension γversus concentration of the polymers to determine the CMC of **5-7** and **11** were measured in 0.1 M HCl at 60 °C are shown in Figure 2.8.

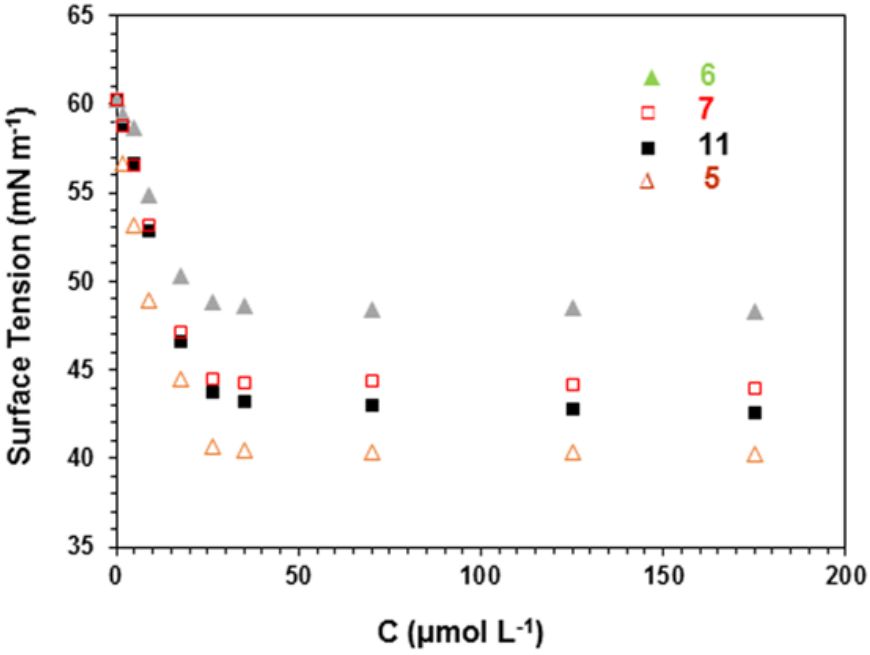

Figure 2.8 Surface tension versus concentration of inhibitor compounds **5-7** and **11** in 1 M HCl solution at 60 °C

The polymers may be considered as cationic surfactants because of the presence of ionic hydrophilic head and moderate hydrophobic pendants of $(CH_2)_2SMe$. The polymer backbone consisting of $-CH_2-CH-CH-CH_2-$ may as well be considered as hydrophobic. Polymers are found to show moderate surface active property having CMC values in the range 18.1-22.0 µM (i.e. 6.3-8.58 ppm) (Table 2.3). The molarity of polymers is

calculated on the basis of molar mass of the repeating unit having a unit each of the monomer (average of S and S=O) and SO_2. ΔG^{o}_{mic} of micellization was calculated to be ≈ - 30 kJ mol^{-1}.

Table 2.3 Surface properties of compounds **5**, **6**, **7**, and **11** in 1 M HCl solutions at 60 °C

Compound	Surface tension (mN m^{-1})	C_{cmc} (μmol L^{-1})	C_{cmc} (ppm)	$\Delta G°_{mic}$ (kJ mol^{-1})
1M HCl	60.2	-	-	-
5	40.3	18.1	6.62	–30.2
11	43.0	20.9	6.30	–29.8
6	48.3	20.1	7.52	–29.9
7	44.1	22.0	8.58	–29.7

2.3.7 Inhibition of mild steel corrosion

Gravimetric weight loss method [91,107], the most reliable protocol, was utilized to determine the inhibition efficiency (IE) of the synthesized polymers on mitigating mild steel corrosion in a hostile environment of 1 M HCl for 6 h at 60 ºC. The IEs were determined as described [107] after immersing steel coupons into 1 M HCl (250 mL) in the absence (blank) and presence of the synthesized polymers. The %IE was then calculated using Eq. (5):

$$\%\,IE = \frac{W_b - W_i}{W_b} \times 100 \qquad (5)$$

where W_b and W_i represent weight loss in the absence and presence of the polymers, respectively. At a meager concentration of 17.5 μM (in terms of repeating unit) (≈ 6 ppm) of polymers **5**, **6**, **7**, **11**, and **12**, IEs of 89, 94, 87, 96, and 94% are achieved, respectively.

Usually, the %IEs are expected to increase with increasing inhibitor concentration. In the ester (-CO_2Et) series, the increase of IE of the polymers in the order: **6** > **5** > **7** suggests the greater effectiveness of the sulfoxide (S=O) motifs as compared to sulfide (S) and sulfone (O=S=O) in mitigating the mild steel corrosion. Polymers **11** and **12** having carboxy groups (CO_2^-) performed even better, presumably owing to the protection of the metal surface via the formation of coordinate type of bond involving the chelating motifs of amino carboxylate ($N^{\cdots\cdots} CO_2^-$) with the vacant d-orbitals of iron [108–110]. Note that amino ester motifs ($N^{\cdots\cdots} CO_2Et$) in **5-7** cannot provide such a chelating motifs to cover and safeguard the metal surface.

2.4 Conclusion

Cationic and zwitterionic polymers **4-7** and **10-12** based on amino acid methionine and its derivative methionine sulfoxide and sulfone have been synthesized via cyclopolymerization of diallylamine salts. The TGA indicated that the synthesized polyelectrolytes were stable up to 200 ^oC. The solubility of the polymers is greatly influenced by the oxidation state of the sulfur; while the sulfide pendant imparts water-insolubility, polymers bearing polar sulfoxide and sulfone pendants were found to be water-soluble. Water-soluble polyzwitterion (±) **12** bearing sulfoxide pendants showed anti-polyelectrolyte behavior as demonstrated by increasing viscosity with increasing NaCl concentrations. Surface tension measurement indicated the polymers (+) **5**, (+) **6**, (+) **7**, and (±) **11** as moderately surface active agents to aid the formation of surface film on the metal surface to assist in the inhibition of metal corrosion in hostile environments. A preliminary investigation has demonstrated that the synthesized polymers containing unquenched nitrogen and sulfur valences acted superbly in mitigating mild steel

corrosion in 1 M HCl. The presence of nonbonding electrons in nitrogen as well as in the more polarizable sulfur motifs, leads to the formation of coordinate type of bond with the vacant d-orbitals of iron or accumulated Fe^{2+} especially on anodic sites of the metal surface thereby imparting corrosion inhibition. The molar masses, surface tension and protonation constant of the nitrogens in these polymers are expected to affect corrosion inhibition efficiency. We are currently examining the corrosion inhibition of these amazing and apparently green polymers in detail using various electrochemical techniques. The study would focus on the long-term inhibition activity especially near CMC of the polymers.

CHAPTER 3

Biogenic Amino Acid Methionine-Based New Corrosion Inhibitors of Mild Steel in Acidic Media

3.1 Introduction

The organic inhibitor molecules owe their inhibition of mild steel corrosion to the presence of heteroatoms whose effectiveness are known to increase in the order O < N < S < P [111]. Our objective was to exploit the presence of S, N and O in amino acid methionine **1** in mitigating mild steel corrosion in hostile environments. Third-period elements like S and P being more polarizable can utilize their lone pair of electrons in the formation of coordinate type bonds with the vacant *d*-orbitals of Fe or Fe^{2+} on the metal surface [112] thereby interfering with anodic or cathodic reactions responsible for corrosion [113,114]. For mild steel corrosion, methionine **1** (Scheme 3.1), having three different heteroatoms, at concentrations of 25, 149 and 746 ppm, has been reported to impart inhibition efficiency (IE) of 47% in 0.1 M HCl [5] at 25 °C, 89% in 1 M HCl [115] at 30 °C, and 54.8% in 0.5 M H_2SO_4 [116] at 30 °C, respectively. Methionine methyl ester hydrochloride at a concentration of 923 ppm has been shown to achieve an IE of 81.2% in 1 M HCl [117] at 30 °C. The IEs of methionine **1**, methionine sulfoxide **2** and methionine sulfone **3** at respective concentrations of 149, 165 and 181 ppm have been determined to be 79, 85 and 88%, respectively, against copper corrosion in 1 M HNO_3 at 30 °C [118].

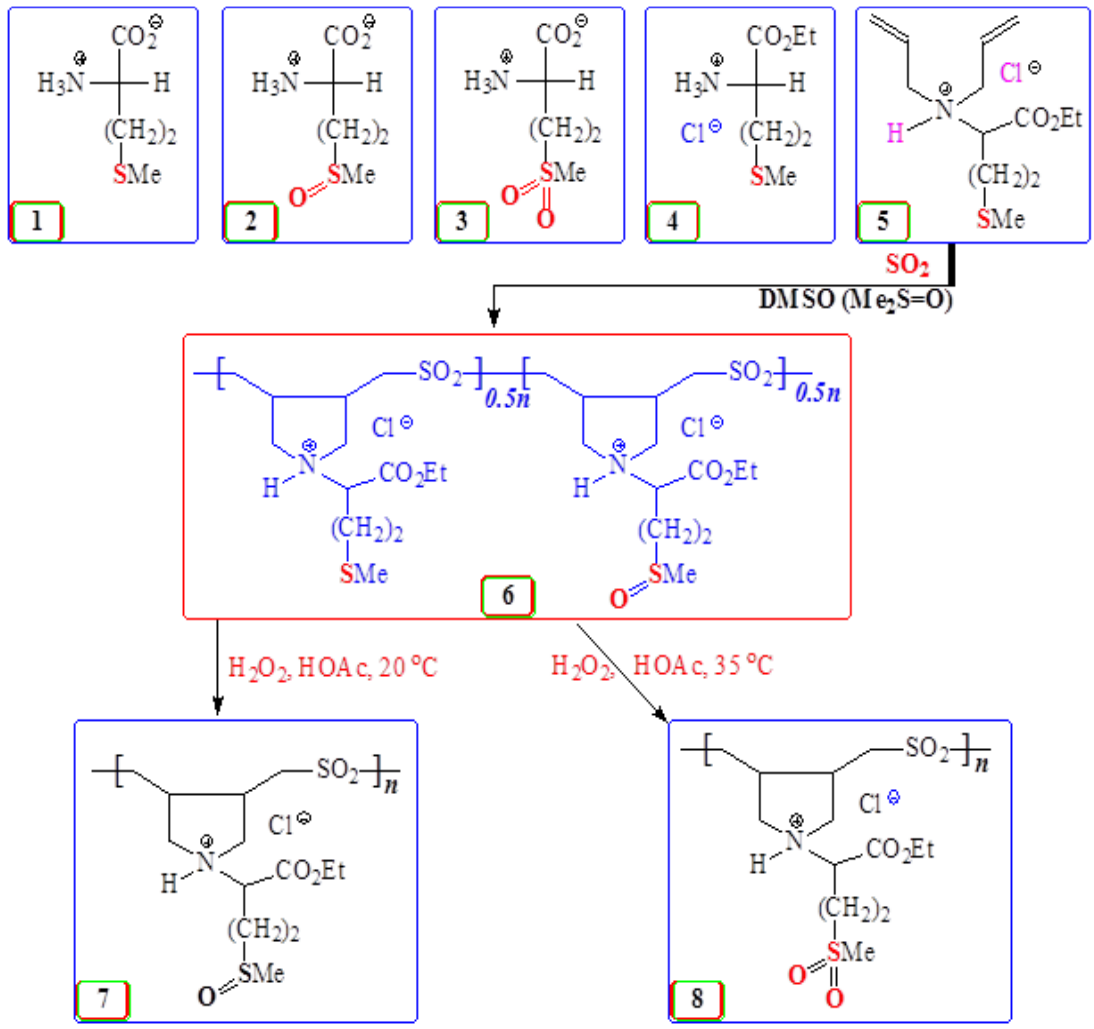

Scheme 3.1 Amino acid methionine-based cyclopolymer corrosion inhibitors containing sulfide, sulfoxide and sulfone motifs.

The above discussion evinced that the use of low cost, non-toxic methionine as an attractive green corrosion inhibitor has at best achieved modest successes. However, we anticipate that the inclusion of methionine residues in a polymeric backbone might lead to its ability for a better surface coverage and protection from corrosive media. In fact, there are reports which demonstrated that polymers having multiple adsorption sites provide better IE than their monomeric analogs [85–87]. In this context, we explored the

possible utilization of Butler's cyclopolymerization protocol [77,79,80] in the synthesis of polymers containing the residues of biogenic amino acid methionine (**1**). The protocol involving diallylammonium salts has etched an important place in the synthesis of a plethora of industrially significant ionic polymers [77,79,80]. Poly(diallyldimethylammonium chloride), the simplest cyclopolymer synthesized using this protocol, has been the subject matter in over one thousand publications and patents; over 35 million pounds of this product alone are sold per year for water purification and personal care formulations [79]. The macromolecule having five-membered ring skeleton of pyrrolidine motifs embedded in the backbone is considered the eighth major polymer architecture of synthetic high polymers [119,120]. Diallylammonium salts have also been subjected to undergo copolymerization with sulfur dioxide to obtain a wide variety of alternate copolymers [81–83]. In one such copolymerization, methionine (a biogenic amino acid)-derived diallylamine salt **5**/SO_2 copolymerization in solvent dimethyl sulfoxide (DMSO) afforded alternate copolymer **6** in which almost half of the sulfide is oxidized sulfoxide *via* O exchange with DMSO. Copolymer **6** was then transformed into polymer sulfoxide **7** and polymer sulfone **8** by treatment with H_2O_2 at 20 and 35 °C, respectively (Scheme 3.1) [84]. Note that polymers **6-8** have the residues of methionine, methionine sulfoxide and methionine sulfone keeping intact the original motifs of nitrogen with unquenched valency.

In this chapter, we will discuss the inhibition of mild steel corrosion in 1 M HCl by polymers **6-8** having methionine residues in each repeating unit. In addition to their efficacy as inhibitors, the study would reveal the comparative efficacies of the sulfide, sulfoxide and sulfone motifs.

3.2 Experimental

3.2.1 Materials

Ethyl ester hydrochloride of L-Methionine **1,** allyl bromide and Azobisisobutyronitrile (AIBN) were purchased from Fluka Chemie AG. AIBN was recrystallized from $CHCl_3$-EtOH. Hydrogen peroxide (35% w/v), hydrochloric acid (37% w/v), acetic acid and potassium carbonate (K_2CO_3) were purchased from BDH Chemical Ltd (Pool, England), and used as received. Dimethylsulfoxide (DMSO), dried over CaH_2 overnight, was distilled (bp $_{4\ mmHg}$ 64–65 °C). All these chemicals were used for the synthesis of the polymers.

3.2.2 Physical Methods

The structural composition was determined by FT-IR (Perkin Elmer 16F PC FTIR), and NMR (JEOL LA 500 MHz). The elemental composition was determined by Elemental Analyzer (Perkin Elmer, Model 2400). The viscosity values of synthesized compounds were determined by Ubbelohde viscometer (Viscometer Constant 0.005317 $mm^2\ s^{-2}$). Thermogravimetric analysis (TGA) was performed using Platinum/Platinum–Rhodium (Type R) thermocouples under N_2 (flow rate 50 mL min^{-1}) using an SDT thermogravimetric analyzer (Q600: TA Instruments, New Castle, DE, USA) by stepping up the temperature (10 °C min^{-1}) over 20–800 °C. The electrochemical measurements were performed on a computer-controlled potentiostat-galvanostat (Auto Lab, Booster 10A-BST707A).

3.2.3 Synthesis

L-Methionine **1**-derived monomer of hydrochloride salts **5**, and its SO_2-copolymer **6** were synthesized as described in an earlier report [84]. The SO_2-sulfide/sulfoxide copolymers **6** were converted to sulfoxide **7** and sulfone **8** following the procedure mentioned in the literature [121].

3.2.4 Specimens

The inhibition efficiency of the synthesized polymers were tested by electrochemical and gravimetric measurements in 1 M HCl solution using coupons prepared from mild steel having the following compositions: C (0.089), Mn (0.34), Cr (0.037), Ni (0.022), Mo (0.007), Cu (0.005), V (0.005), P (0.010), Fe (99.47). The flag shaped mild steel coupons (thickness: 1 mm) were used in electrochemical measurements. The stem of the flag, which measured approximately 3 cm, was insulated by an Araldite paint (RS, Saudi Arabia). The remaining area was about 1 cm^2 and provided exposed area of 2 cm^2. The mild steel specimens were abraded with different grades emery papers (100–1500 grit size), then degassed with acetone, washed with deionized water, and dried in a hot air at room temperature, and stored in a desiccator before their use.

3.2.5 Solutions

Solution of 1 M HCl was prepared from concentrated HCl (37%) using double distilled de-ionized water. The polymer compounds at required concentrations were used to perform the corrosion inhibition test in 1M HCl solution. The inhibition test carried out in absence of polymer compound was considered as blank.

3.2.6 Gravimetric measurements

Gravimetric weight loss measurements to determine the efficiency of the inhibitors were performed using mild steel coupons of almost equal masses and sizes. The mild steel coupons measuring (2.5 cm×2.0 cm×0.1 cm) were submerged in 250 mL of 1 M HCl for 6 h in the presence or absence of the polymer compounds at 60 °C. After the time elapsed, the steel coupons were cleaned wiping the coupons with tissue paper, washed with distilled de-ionized water, and dried in a vacuum oven to a constant weight.

The percent inhibition efficiencies ($\eta\%$) were then calculated by Eq. (1) :

$$\eta\% = \frac{W_b - W_i}{W_b} \times 100 \quad (1)$$

where, W_i and W_b represent weight loss in the presence or absence of polymer compound, respectively.

The average relative weight loss of the mild steel coupons was determined from three individual measurements. The average weight losses in percentage was deviated within a range of 0.5-2.0%.

3.2.7 Electrochemical measurements

3.2.7.1 Open circuit potential (OCP) versus time

The effect of immersing time of mild steel coupon on its OCP has been studied in 1 M HCl as blank and two different concentrations (1.00 and 175 μM) of three different polymer compounds **6-8** prepared in 1 M HCl solution. The measurement was at various immersing times (0 to 60 min) as shown in Fig. 3.1. It has been found that the steady OCP was achieved after around 30 min.

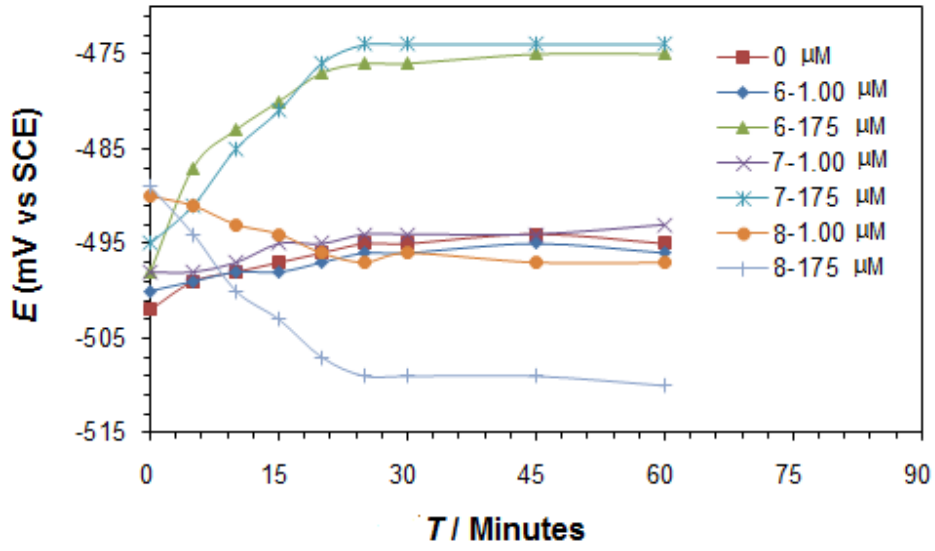

Figure 3.1 Variation of OCP of mild steel with time of immersion in 1 M HCl solution containing different concentrations (1.00 and 175 µM) of **6-8** at 60 ºC

3.2.7.2 Tafel extrapolations

The Tafel experiments were performed in a three electrodes containing electrochemical cell system. The saturated calomel electrode (SCE) was used as reference electrode, a 5 mm diameter graphite rod was used as an auxiliary electrode and the mild steel coupon was the working electrode. The stable OCP of working electrode was obtained after immersing the mild steel coupon for 30 min. All the three electrodes were immersed in absence or presence of polymer compounds **6-8** in 1 M HCl (250 mL) solution at 60 ºC, which was considered as a test solution. Potentiostat - galvanostat (Auto Lab, Booster 10A-BST707A, Eco Chemie, Netherlands) coupled with a computer controlled NOVA (version 1.8) software was used to record the polarization curves with a current of 1 A. The scan was performed in potential window ± 250 mV around the corresponding OCP maintaining a scan rate of 0.5 mV s^{-1}. Equation 2 was used to calculate the inhibition efficiencies based on the corrosion current density.

$$\eta(\%) = \left(\frac{I_{\text{corr Blank}} - I_{\text{corr Inhibitor}}}{I_{\text{corr Blank}}}\right) \times 100 \quad (2)$$

Where, $I_{\text{corr Blank}}$ is the current of corrosion in absence of polymer compound, and $I_{\text{corr Inhibitor}}$ is the current of corrosion in presence of polymer.

3.2.7.3 Linear Polarization Resistance (LPR) Method

By recording the current versus potential in range of ±10 mV around E_{corr} under the same conditions described in previous section (Tafel extrapolations), the LPR for the three types of polymer compounds **6-8** at different concentrations (0, 1.75, 4.85, 8.75, 17.5, 26.2, 35.2 and 175 μM) was measured. The surface coverage (θ) was calculated from the polarization resistance in absence (R'_{p}) and presence ($\overline{\boldsymbol{R'_{\text{p}}}}$) of polymer compounds using Eq. 3.

$$(\eta\%) = (\theta\%) = \left(\frac{\overline{R'_{\text{p}}} - R'_{\text{p}}}{R'_{\text{p}}}\right) \times 100 \quad (3)$$

3.2.7.4 Electrochemical Impedance Spectroscopy (EIS)

The same three electrodes system described in earlier section (Tafel extrapolations) was used to perform the electrochemical impedance experiments. A freshly prepared solution (250 mL) containing different concentrations of polymer compounds in 1 M HCl at 60 ºC was used. An amplitude of 10 mV and a frequency in the range between 100 KHz and 50 mHz were employed to record the Nyquist and Bode plots at the corresponding OCP, then the resulted data were fitted with the lowest deviated electrochemical equivalent circuit with experimental values.

3.2.8 Surface Morphology

3.2.8.1 XPS

The XPS analysis was performed by X-ray photoelectron spectrometer (Thermos Scientific, Model # Escalab 250 Xi). Avantage software was used to process the data. The C 1s peak at 285.4 eV was considered as reference peak. A non-linear least squares algorithm with a Gaussian–Lorentzian combination and a Shirley base line were used to deconvolute the XPS spectra.

3.2.8.2 SEM and EDX

The surface morphology of the inhibited (presence of polymer) and corroded (blank) metal surface was performed using a field-emission scanning electron microscope (FESEM, Lyra 3, Tescan, Czech Republic) with accelerating voltages of 20-30 kV. In addition, an energy dispersive X-ray (EDX) spectroscope (Oxford Inc., UK) fitted with an X-Max detector was used to determine the chemical compositions and for mapping the level of homogeneity of these metal surfaces. The SEM images were captured after immersing the steel samples at 60 °C for 6 h in absence (0 μM) or presence of polymer (175 μM).

3.3 Results and Discussion

3.3.1 Polymer Synthesis

The polymer SO_2-sulfide/sulfoxide (1:1) copolymers **6** [84], and its sulfoxide **7** and sulfone **8** were synthesized following the published literature procedure [121]. The intrinsic viscosity [η] values of the cyclocopolymers **6**, **7** and **8** were obtained from viscosities of 1-0.125% solutions in 0.1 M NaCl at 30 °C using Mark-Huggins viscosity

relationship, and were determined to be 0.137, 0.151 and 0.143 dL g^{-1}, respectively. These low values of [η] indicate the low molar masses of the polymers. The TGA curves of the copolymers **6-8** indicated that these copolymers are stable up to 200 ^{o}C.

3.3.2 Corrosion gravimetric measurements

The results of the experiments obtained from gravimetric weight loss measurements after 6 h immersion of the mild steel coupons in absence or presence of polymers **6-8** in 1 M HCl (250 mL) at 60 ^{o}C are presented in Table 3.1.

Table 3.1 The η%[a] for inhibitors **6**, **7** and **8** obtained by gravimetric weight loss method for the inhibition of corrosion of mild steel at 60 ^{o}C in 1 M HCl for 6 h.

Sample	η(%) at concentration of inhibitors (in μM)							
	1.75	4.85	8.75	17.5	26.2	35.1	70.2	175
6	50.6	57.7	74.3	82.1	90.5	90.8	92.4	93.0
7	53.4	66.9	77.0	83.2	90.7	93.1	94.6	96.8
8	42.9	54.3	64.8	75.6	82.7	85.0	94.3	95.7

[a] IE (i.e., η) = surface coverage θ.

Each set of experiments were carried out three times to get the average weight loss results. The gravimetric weight loss study indicated that the inhibition efficiency (η%) values were found to be 93.0, 96.8 and 95.7% at a concentration of 175 μM of ester functionalized cyclocopolymers **6**, **7** and **8**, respectively, while at a concentration of ≈13 ppm (35.1 μM), the η% values were determined to be 90.8, 93.1 and 85.0%, respectively. The experimental results obtained from gravimetric studies also revealed that an increase in the concentrations of the cylocopolymers increase the inhibition

efficiency, reaching maximum values that can be ascribed to the formation of polymer layer onto the mild steel surface. At the range of concentrations studied for these cyclocopolymers, the ester functionalized cyclocopolymer with sulfoxide motifs **7** showed slightly better performance resisting the corrosion of the mild steel. The better performance of the cyclocopolymer **7** for inhibiting the corrosion of mild steel could be due to the presence of sulfoxide motifs in the polymer structure.

3.3.3 Polarization measurements

The stable OCP values were obtained from the experiment of OCP versus time. Fig. 3.1 showed that the OCP in absence or presence of the polymer molecules **6** or **7** slightly moved towards positive direction and became stable within a short time, producing the free corrosion potential E_{corr} of the mild steel coupon. In the presence of polymer molecule **8** (1.00 μM), the OCP values had a slow rate of change towards more negative values, while at high concentration (175 μM) the rate of change was slower with higher magnitude and reached the steady state after ≈ 30 min. An increase in the polymer concentration increased the magnitude of the E_{corr} shifts towards a positive direction. Shifting of E_{corr} towards the positive direction indicates that the inhibitors are inhibiting the anodic destruction by being adsorbed on those sites.

Fig. 3.2 shows the Tafel potentiodynamic polarization curves for the mild steel in absence and presence of different concentrations (1.00 to 175 μM) of cyclocopolymers **6-8** in 1 M HCl solution at 60 ºC. The extrapolation of linear segments of anodic and cathodic sides in Tafel plots was used to obtain various electrochemical parameters such as the produced current density of corrosion (i_{corr}) and corrosion potential (E_{corr}) of mild steel coupons, which are summarized in Table 3.2.

As shown in Table 3.2, the significant decrease in the i_{corr} is an evidence of the inhibitive nature of the synthesized polymer compounds. The shifting of E_{corr} values to positive or negative direction with a magnitude lower than 85 mV suggests that they are mixed type inhibitors, which mainly block the anodic and cathodic sites [122]. This bears the testimony that the inhibitors do not accelerate the corrosion reactions rather block them by creating a thin film on the metal surface. It was also observed that there is no significant change or clear trends in cathodic (β_c) and anodic (β_a) slopes, which suggests no change in the inhibition mechanism with increasing the concentrations of the inhibitors.

The corrosion inhibition efficiencies of the synthesized polymer compounds for mild steel coupon in 1 M HCl solution at 60 ºC obtained from Tafel and LPR experiments, are summarized in Tables 3.2 and 3.3, respectively. To our great satisfaction, the cyclocopolymer containing sulfoxide motifs **7** showed relatively better inhibition efficiency than **6** or **8**. In addition, it has been found that they are in well agreement with the inhibition efficiencies calculated based on the weight loss method (Table 3.1).

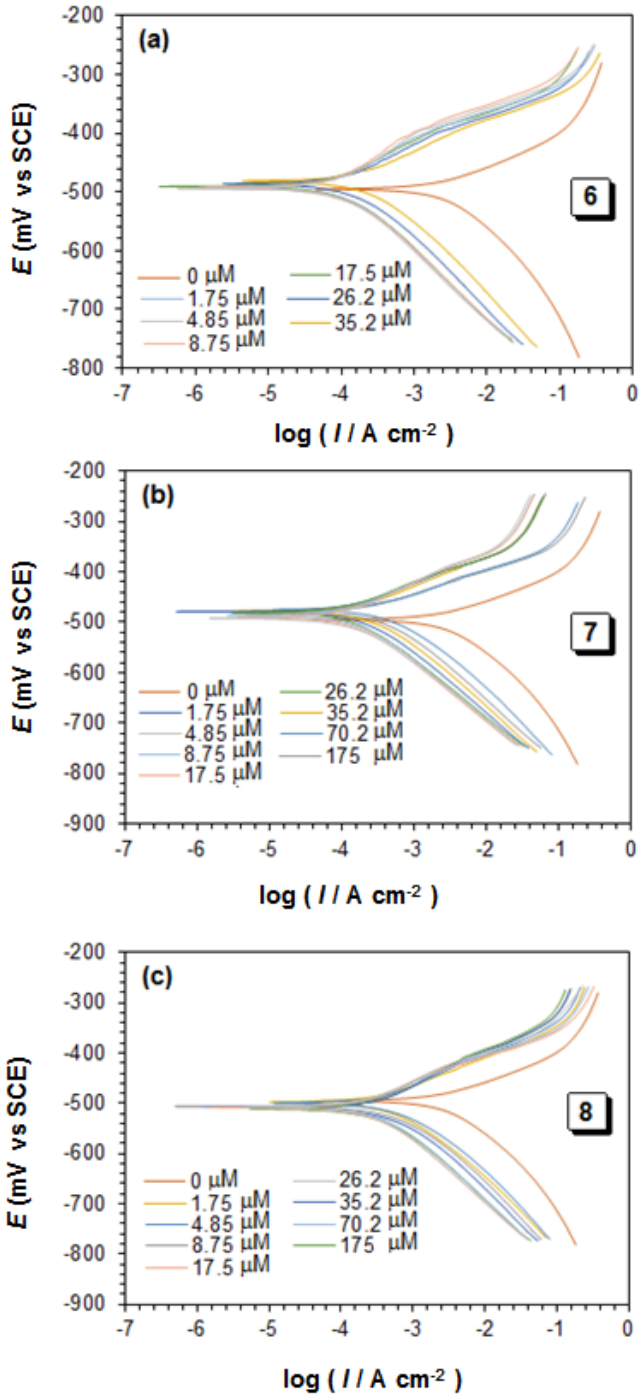

Figure 3.2 Potentiodynamic polarization curves at 60 °C for mild steel in 1 M HCl containing various concentrations of (a) **6**, (b) **7** and (c) **8**

Table 3.2 Results of Tafel plots of a mild steel sample in 1 M HCl containing inhibitors **6**, **7** and **8** at different temperature

Sample	Temp (°C)	Concentrations		Tafel					
		ppm (by wt.)	μM	E_{corr} vs. *SCE* (mV)	β_a (mV dec^{-1})	β_c (mV dec^{-1})	I_{corr} (μA cm^{-2})	υ_{corr} (mm y^{-1})	η(%)[a]
6	60	0	0	–495	73.8	–169	2465	28.6	-
		0.36	1.00	–494	64.4	–106	1506	17.5	38.9
		0.64	1.75	–494	58.8	–117	1395	16.2	43.4
		1.77	4.85	–492	70.8	–109	1038	12.0	57.9
		3.20	8.75	–491	79.9	–113	764	8.86	69.0
		6.40	17.5	–490	99.2	–127	486	5.64	80.3
		9.59	26.2	–486	89.1	–122	365	4.23	85.2
		12.9	35.2	–484	84.5	–110	335	3.89	86.4
		25.7	70.2	–481	92.3	–103	286	3.32	88.4
		64.0	175	–476	96.7	–106	177	2.05	92.8
7	50	0	0	–483	51.2	–117	505	5.85	-
		0.37	1.00	–478	59.8	–117	217	3.14	46.3
		0.65	1.75	–472	64.6	–119	245	2.84	51.5
		1.81	4.85	–467	82.1	–124	183	2.12	63.7
		3.27	8.75	–461	80.3	–108	126	1.46	75.0
		6.54	17.5	–455	71.4	–111	88.9	1.03	82.4
	60	0	0	–495	73.8	–169	2465	28.6	-
		0.37	1.00	–494	68.2	–112	1375	16.0	44.2
		0.65	1.75	–491	63.7	–104	1171	13.6	52.5
		1.81	4.85	–489	54.2	–112	858	9.95	65.2
		3.27	8.75	–486	75.7	–103	584	6.78	76.3
		6.54	17.5	–480	75.3	–118	431	5.01	82.5
		9.80	26.2	–480	94.1	–171	261	3.03	89.4
		13.2	35.2	–478	87.8	–111	187	2.17	92.4
		26.2	70.2	–478	85.0	–108	148	1.72	94.0
		65.4	175	–475	68.9	–101	76.4	0.89	96.9
	70	0	0	–498	60.9	–102	4508	52.3	-
		0.37	1.00	–493	65.2	–117	2466	28.6	45.3
		0.65	1.75	–486	67.4	–98.2	2200	25.5	51.2
		1.81	4.85	–485	84.3	–112	1650	19.1	63.4
		3.27	8.75	–477	92.1	–114	1253	14.5	72.2
		6.54	17.5	–472	85.5	–103	888	10.3	80.3
8	60	0	0	–495	73.8	–169	2465	28.6	-
		0.68	1.75	–497	75.2	–84.4	1496	17.4	39.3
		1.89	4.85	–499	75.3	–89.9	1156	13.4	53.1
		3.41	8.75	–506	85.4	–96.6	892	10.4	63.8
		6.82	17.5	–507	91.8	–99.7	636	7.38	74.2
		10.2	26.2	–507	96.5	–108	458	5.32	81.4
		13.7	35.2	–508	92.2	–112	397	4.60	83.9
		27.4	70.2	–510	89.1	–106	145	1.69	94.1
		68.2	175	–510	84.2	–105	126	1.46	94.9

[a] Inhibition Efficiency, IE (i.e., η) = surface coverage θ.

Table 3.3 Results of LPR method in 1 M HCl containing inhibitors **6**, **7** and **8** at different temperature.

Sample	Temp (°C)	Concentrations ppm (by wt.)	Concentrations μM	LPR R'_p (Ω cm^2)	LPR θ [a]	LPR θ(%)
6	60	0	0	2.38	-	-
		0.36	1.00	3.97	0.401	40.1
		0.64	1.75	4.34	0.452	45.2
		1.77	4.85	5.63	0.577	57.7
		3.20	8.75	7.63	0.688	68.8
		6.40	17.5	12.8	0.814	81.4
		9.59	26.2	17.0	0.860	86.0
		12.9	35.2	18.2	0.869	86.9
		25.7	70.2	20.0	0.881	88.1
		64.0	175	30.9	0.923	92.3
7	50	0	0	1.89	-	-
		0.37	1.00	3.57	0.471	47.1
		0.65	1.75	4.04	0.532	53.2
		1.81	4.85	5.49	0.656	65.6
		3.27	8.75	7.50	0.748	74.8
		6.54	17.5	11.4	0.835	83.5
	60	0	0	2.38	-	-
		0.37	1.00	4.50	0.471	47.1
		0.65	1.75	5.15	0.538	53.8
		1.81	4.85	7.23	0.671	67.1
		3.27	8.75	10.0	0.762	76.2
		6.54	17.5	14.6	0.837	83.7
		9.80	26.2	28.0	0.915	91.5
		13.2	35.2	32.2	0.926	92.6
		26.2	70.2	42.5	0.944	94.4
		65.4	175	70.0	0.966	96.6
	70	0	0	9.29	-	-
		0.37	1.00	16.8	0.446	44.6
		0.65	1.75	18.8	0.505	50.5
		1.81	4.85	25.9	0.641	64.1
		3.27	8.75	34.8	0.733	73.3
		6.54	17.5	49.4	0.812	81.2
8	60	0	0	2.38	-	-
		0.68	1.75	4.20	0.434	43.4
		1.89	4.85	5.28	0.549	54.9
		3.41	8.75	6.84	0.652	65.2
		6.82	17.5	9.64	0.753	75.3
		10.2	26.2	14.1	0.831	83.1
		13.7	35.2	15.8	0.849	84.9
		27.4	70.2	37.2	0.936	93.6
		68.2	175	50.6	0.953	95.3

[a] Inhibition Efficiency, IE (i.e., η) = surface coverage θ.

3.3.4 Impedance measurements

For better understanding the corrosion inhibition performance, the EIS experiments were carried out after 30 min immersion in the test solution. The recorded impedance data (Nyquist and Bode plots) of mild steel coupon/solutions in absence or presence of different concentrations (1.75 to 175 μM) of cyclocopolymers **6-8** were fitted by the Randles equivalent electrochemical circuit (the best-fitted circuit) shown in Fig. 3.3.

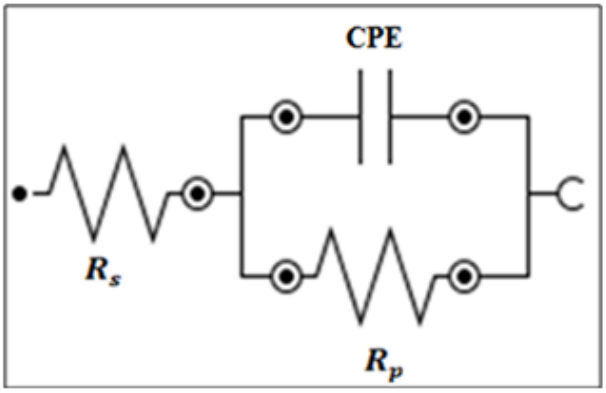

Figure 3.3 Randles Electrical-chemical equivalent circuit diagram used to modeling metal/solution interface. R_s: Solution resistance, R_p: Polarization resistance, CPE: Constant phase element

This simple circuit consists of a polarization resistance (R_p), solution resistance (R_s) and a constant phase element (*CPE*). The R_s value resulted by the potential drop between the mild steel coupon as a working electrode and the reference electrode, and its value was calculated from the meeting point of the real part (Z') axis at high frequency with the fitted semicircle. While the R_p values were obtained from intersection of the semicircle with Z' axis at low frequency, which were contributed by other resistances such as the diffusion layer resistance and charge transfer resistance and at the surface of working

electrode [123]. The net polarization resistance (R'_p) at mild steel coupon was calculated using equation (4), and its value was used later to calculate the inhibition efficiencies based on the EIS using equation (3).

$$R'_p = R_p - R_s \quad (4)$$

The *CPE* is used to express the non-ideal capacitance and non-ideal frequency response. It is commonly used in the electrochemical circuit in order to attain better fitting. The double layer capacitance (C_{dl}) relates to the *CPE* by equation (5).

$$C_{dl} = CPE(\omega)^{n-1} \quad (5)$$

where ω is the angular frequency (radian) at the maximum imaginary part of the impedance, and *n* is the surface heterogeneity.

Table 3.4 summarizes the normalized EIS data for the corrosion of a mild steel sample in 1 M HCl solutions containing different concentrations of inhibitors **6-8** at 60 °C. The EIS fitting results showed that the *n* values are lower than 1, which attributed to the poor homogeneity of surface of the mild steel. It has been found that with increasing the concentration of polymer compounds, the R'_p values were increased and the values of *CPE* were decreased as a result of increasing the thickness of the adsorbed polymer, this eventually leads to increase in the inhibition efficiency, which reached to 96.4% in case of using 175 μM of polymer compound **7**. An increase in the adsorption of cyclocopolymer compounds **6-8** at the higher concentrations on the metal surface causes the *n* values to become lower indicating an increase in the heterogeneity of the metal surface. The results obtained from EIS study inveterate the results of the gravimetric weight loss, LPR and Tafel.

Table 3.4 Impedance parameters for the corrosion of a mild steel sample in 1 M HCl solutions containing inhibitors **6**, **7** and **8** at 60 °C.

Sample	Concentration		R_s (Ω cm^2)	R_p (Ω cm^2)	CPE[a] (μF cm^{-2})	n	R'_p (Ω cm^2)	η(%)
	ppm (by wt.)	μM						
6	0	0	0.373	1.963	922	0.989	1.590	-
	0.64	1.75	0.479	3.537	566	0.905	3.058	48.0
	1.77	4.85	0.485	4.050	492	0.919	3.565	55.4
	3.20	8.75	0.447	5.837	348	0.846	5.390	70.5
	6.40	17.5	0.436	9.077	335	0.827	8.641	81.6
	9.59	26.2	0.430	15.87	301	0.793	15.44	89.7
	12.9	35.2	0.128	16.52	262	0.722	16.39	90.3
	25.7	70.2	0.292	18.57	203	0.669	18.28	91.3
	64.0	175	0.334	19.96	197	0.554	19.63	91.9
7	0	0	0.373	1.963	922	0.989	1.590	-
	0.65	1.75	0.433	3.759	465	0.941	3.326	52.2
	1.81	4.85	0.368	5.100	317	0.801	4.732	66.4
	3.27	8.75	0.362	7.157	325	0.716	6.795	76.6
	6.54	17.5	0.126	8.910	311	0.658	8.784	81.9
	9.80	26.2	0.005	15.60	366	0.646	15.59	89.8
	13.2	35.2	0.419	20.05	247	0.780	19.63	91.9
	26.2	70.2	0.303	28.19	391	0.844	27.89	94.3
	65.4	175	0.330	44.10	207	0.835	44.17	96.4
8	0	0	0.373	1.963	922	0.989	1.590	-
	0.68	1.75	0.510	3.256	546	0.896	2.746	42.1
	1.89	4.85	0.447	3.889	406	0.771	3.442	53.8
	3.41	8.75	0.474	4.878	343	0.758	4.404	63.9
	6.82	17.5	0.521	6.805	309	0.840	6.284	74.7
	10.2	26.2	0.391	9.477	312	0.815	9.086	82.5
	13.7	35.2	0.532	10.54	305	0.847	10.01	84.1
	27.4	70.2	0.462	26.96	329	0.869	26.50	94
	68.2	175	0.557	30.55	252	0.875	29.99	94.7

[a]Double layer capacitance (C_{id}) and coating capacitance (C_c) are usually modeled with a constant phase element (*CPE*) in modeling an electrochemical phenomenon.

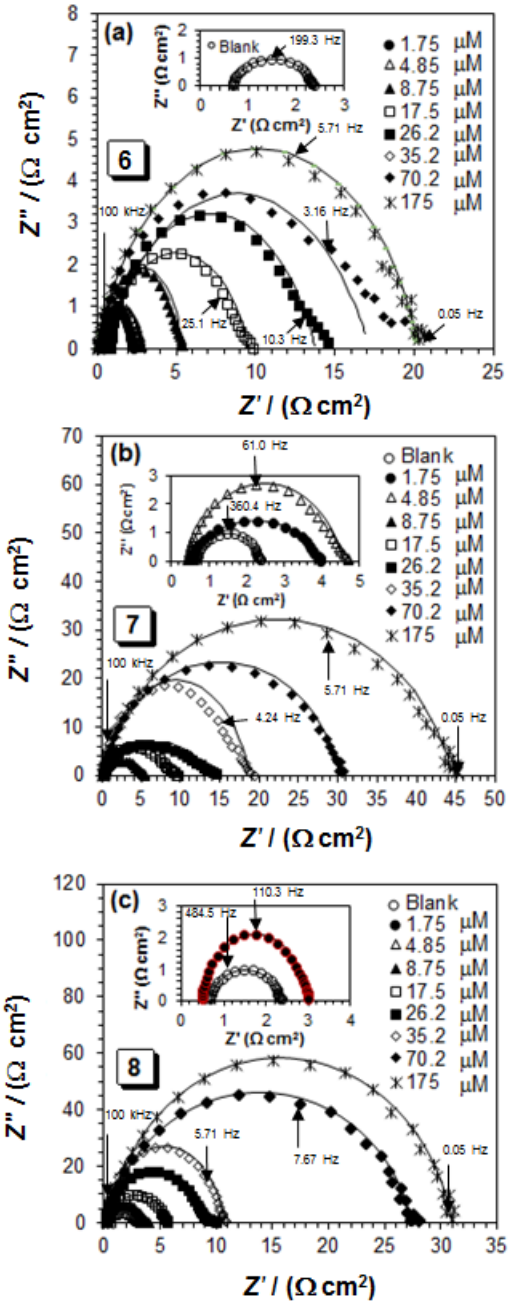

Figure 3.2 Nyquist diagram of (a) **6**, (b) **7** and (c) **8** on the mild steel at 60 °C in 1 M HCl containing various concentrations of polymers. Solid line in the Nyquist plot fitted to the equivalent circuit; solid lines represent fitted data and various symbols represent experimental data

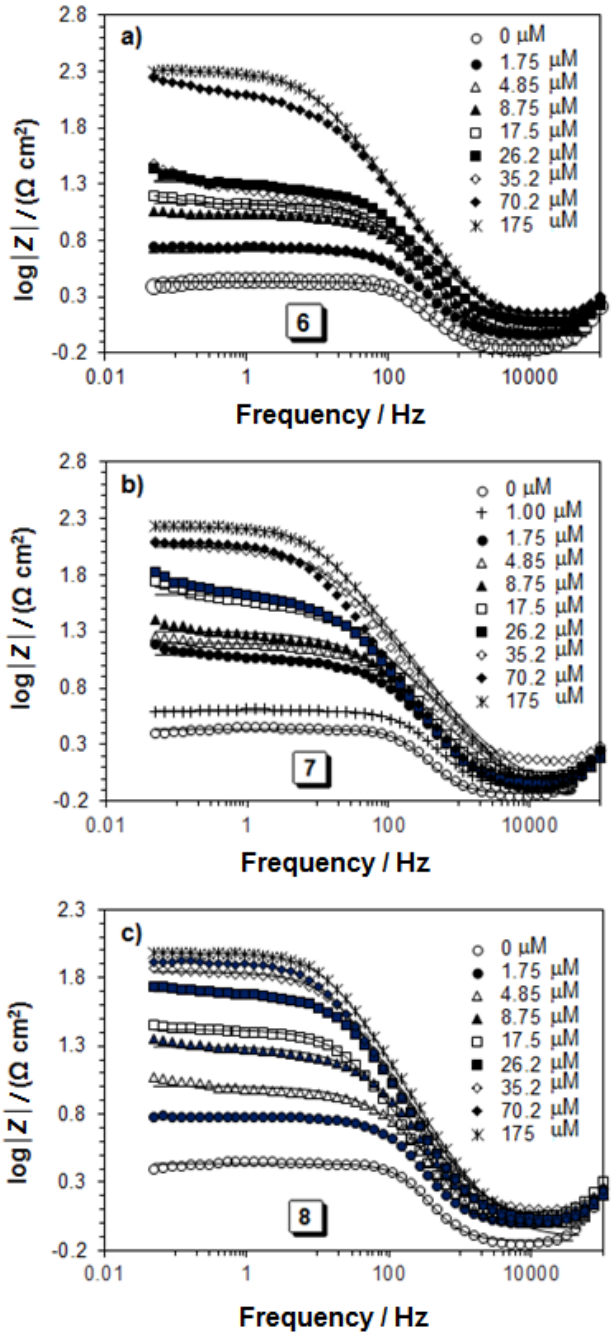

Figure 3.5 Bode phase angle plots of (a) **6**, (b) **7** and (c) **8** on the mild steel at 60 °C in 1 M HCl containing various concentrations of polymers. Solid lines represent fitted data and various symbols represent experimental data

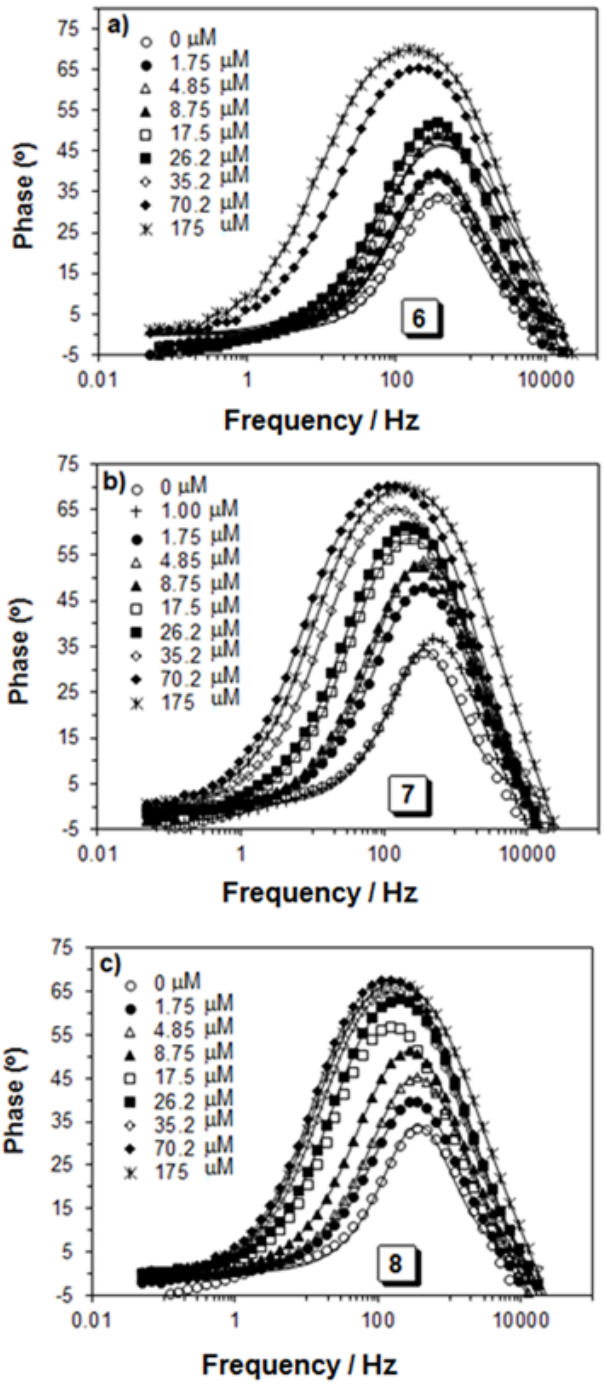

Figure 3.6 Bode magnitude plots of (a) **6**, (b) **7** and (c) **8** on the mild steel at 60 °C in 1 M HCl containing various concentrations of polymers. Solid lines represent fitted data and various symbols represent experimental data

The Nyquist and Bode plots are shown in Fig. 3.4-3.6 for different concentrations (1.75 to 175 μM) of polymer compounds **6-8**. The inset figures in Fig. 3.4 showed the magnified Nyquist plots at blank and low concentrations of polymers. The Nyquist plots shown in Fig. 3.4, clearly demonstrated that the diameter of the semicircles increases with the increasing inhibitors' concentrations, which suggest an increase in the protective layer of the inhibitor molecules on the mild steel surface. Bode magnitude plots (Fig. 3.5) for compounds **7** and **8** imply an increase in the polarization resistance (R_p) with increasing the polymer concentrations. Bode phase angle plots (Fig. 3.6) for compounds **6-8** show an increase in the angle value at intermediate frequency with increasing the inhibitor concentrations, which demonstrates decrease in the capacitance at the surface of the mild steel electrode, thereby decreasing the local dielectric constant as well as increasing the adsorbed amount of inhibitors on the mild steel coupon surface.

3.3.5 Adsorption isotherms

The adsorption ability of inhibitor molecules determines the inhibition effectiveness imparted on the mild steel surface. With a view to having an insight into the adsorption mechanism of the synthesized polymer compounds, their adsorption thermodynamic was studied, and the most common four adsorption isotherms (i.e. Freundlich, Langmuir, Frumkin and Temkin's isotherms) describing the relationship between the surface coverage (θ) and the bulk low concentration of inhibitor (C) (equations 6-9) [124] were tested using the linear least square method as shown in Fig. 3.7.

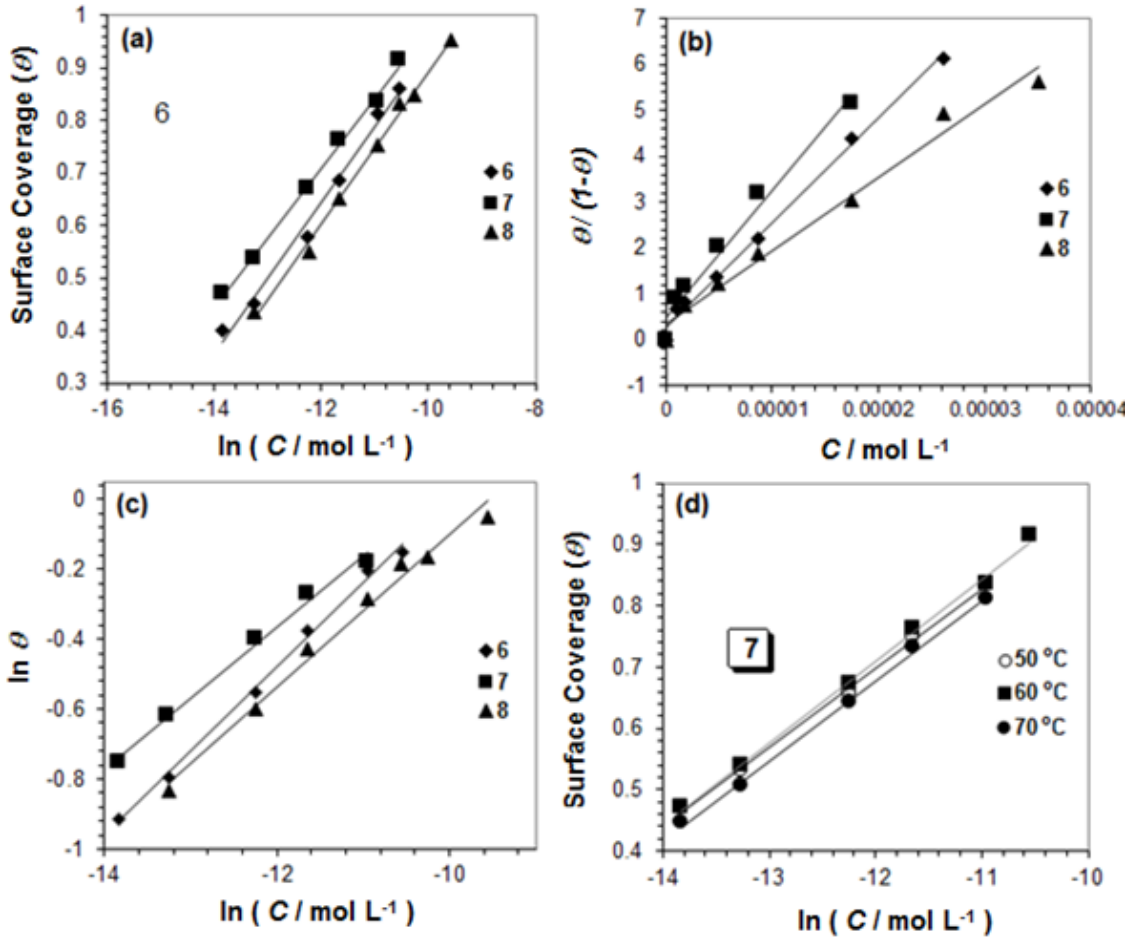

Figure 3.7 a) Temkin adsorption isotherm plots, b) Langmuir adsorption isotherm, c) Freundlich adsorption isotherm for the adsorption of inhibitors **6-8** at 60 °C, and d) Temkin adsorption isotherm for the adsorption of inhibitor **7** at various temperatures, on the surface of mild steel

Freundluich: $\theta = K_{ads} C^{n}$ (6)

Langmuir: $\theta/(1-\theta) = K_{ads} C$ (7)

Frumkin (Frumkin, 1925): $K_{ads} C = \{\theta/(1-\theta)\} e^{-2\alpha\theta}$ (8)

Temkin: $K_{ads}\, C = e^{f\,\theta}$ (9)

The square correlation coefficients (R^2) and the value of the constant in the tested isotherm models for polymer compounds **6-8** at different temperatures are tabulated in Table 3.5.

Table 3.5 Square of correlation coefficients (R^2) and values of the constants in the adsorption isotherms of Temkin, Frumkin, Langmuir and Freundlich in the presence of inhibitors **6**, **7** and **8** in 1 M HCl solution (LPR data used for the isotherm)

Sample	Temp (°C)	Temkin[1] (R^2, f)	Langmuir[2] (R^2)	Frumkin[3] (R^2, a)	Freundlich[4] (R^2, n)
6	60	0.9883, 6.9	0.9981	0.8452, -0.2	0.9966, 0.2
7	50	0.9975, 7.8	0.9992	0.9522, -0.2	0.9977, 0.2
	60	0.9973, 7.5	0.9942	0.9796, -0.2	0.9930, 0.2
	70	0.9976, 7.7	0.9926	0.9764, -0.2	0.9946, 0.2
8	60	0.9952, 6.9	0.9873	0.8655, -0.2	0.9879, 0.2

[1]Temkin: $K_{ads}C = e^{f\theta}$

[2]Langmuir: $\theta/(1-\theta) = K_{ads}C$

[3]Frumkin: $K_{ads}C = \{\theta/(1-\theta)\}\ e^{-2a\theta}$

[4]Freundluich: $\theta = K_{ads}C^{\,n}$

The higher correlation coefficient values obtained from Langmuir, Freundlich and Temkin isotherm models (Table 3.5) suggest that the adsorption of inhibition is achieved by a mixed chemisorption and physisorption mechanism, which means that electrostatic as well as chemical interaction between the metal surface and the polymer compounds contributed to the adsorption process. To further explore the adsorption mechanism, the thermodynamic parameters (adsorption equilibrium constant (K_{ads}), free energy (ΔG^o_{ads}), enthalpy (ΔH^o_{ads}) and entropy of adsorption (ΔS^o_{ads}) were calculated using equations 10 and 11, and presented in Table 3.6.

$$K_{ads} = \frac{1}{55.5} \exp\left(\frac{-\Delta G^{\circ}_{ads}}{RT}\right) \quad (10)$$

$$\Delta G^0 = \Delta H^0 - T\Delta S^0 \quad (11)$$

Table 3.6 : The values of the adsorption equilibrium constant from Langmuir adsorption isotherms and free energy, enthalpy, entropy changes of the mild steel dissolution in the presence of inhibitors **6**, **7** and **8** in 1 M HCl

Sample	Temp (°C)	$K_{ads}\times10^{-5}$ (L mol^{-1})[a]	ΔG^o_{ads} (kJ mol^{-1})	ΔH^o_{ads} (kJ mol^{-1})	ΔS^o_{ads} (J mol^{-1} K^{-1})
6	60	13601929	-44.1	-	-
7	50	37721678	-46.8		
	60	32596030	-46.5	-57.2	32.0
	70	29435181	-46.2		
8	60	10665365	-43.5	-	-

[a]K_{ads} obtained in L/mg was converted to L/mol

The negative ΔG^o_{ads} and ΔH^o_{ads} values obtained from Fig. 3.8 indicate that the adsorption process is spontaneous and exothermic, respectively. Typically, the mechanism of adsorption can be classified as a physisorption, chemisorption or mixed mechanism based on the magnitude of ΔG^o_{ads} and ΔH^o_{ads}. When the absolute value of $-\Delta G^o_{ads}$ is lower than 20 kJ mol^{-1} and the ΔH^o_{ads} is less negative than -40 kJ mol^{-1} the adsorption process is described as physisorption.

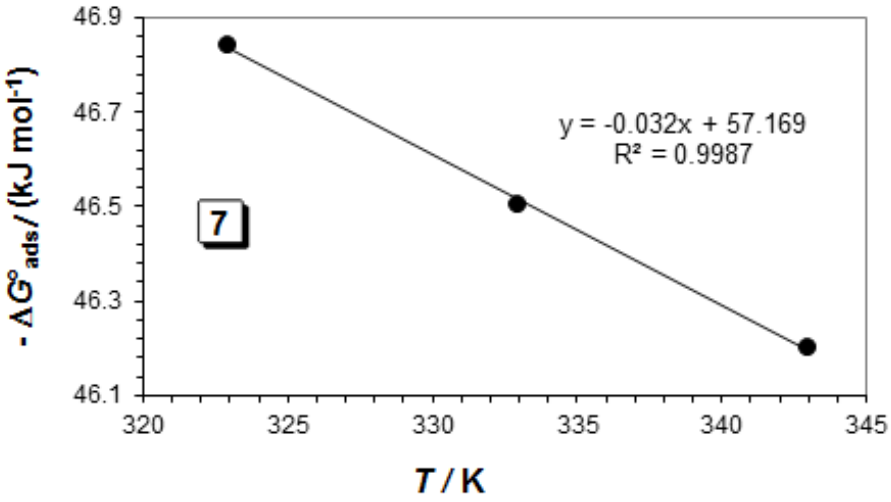

Figure 3.8 Variation of $-\Delta G^{\circ}_{ads}$ versus T on mild steel in 1 M HCl containing **7**

On the other hand, when the absolute value of $-\Delta G^{o}_{ads}$ is higher than 40 kJ mol^{-1} and the ΔH^{o}_{ads} is more negative than -100 kJ mol^{-1}, the adsorption process can be classified as chemisorption or mixed mechanism would follow if the absolute value of $-\Delta G^{o}_{ads}$ is higher than 20 kJ mol^{-1} but less than 40 kJ mol^{-1} [125–128]. The calculated values of ΔG^{o}_{ads} are ranging between -43.5 and -46.8 kJ mol^{-1}, and the ΔH^{o}_{ads} for adsorption of the synthesized polymer compound **7** was found to be -57.2 kJ mol^{-1} (Table 3.6). This suggests that the adsorption is attained through a mixed mechanism by the influence of chemisorption mechanism. The non-bonded and π electrons induce the synthesized polymer molecules in different media, and interact with the low-lying vacant *d*-orbitals of iron at the anodic sites by overlapping chemically and electrostatically. [129,130]. The positive value of ΔS^{o}_{ads} (32 J mol^{-1} K^{-1}) for polymer compound **7** adsorption on mild steel in 1 M HCl (Table 3.6, Fig. 3.8) is an indication for increasing the randomness on the solid surface/inhibitor interface where the adsorbed inhibitor molecules displaced the adsorbed water molecules on the surface of mild steel.

3.3.6 Surface analysis

The XPS and SEM-EDX were used to further confirm the adsorption of polymer compound onto the mild steel surface.

3.3.6.1 XPS analysis

The intensity (counts) versus binding energy (eV) plot for the polymer compounds adsorbed onto the metal surface was recorded by XPS, and are presented in Fig. 9a-f. Fig. 9a-c show the wide scan XPS spectra of polymer compounds **6-8**. The signals of S 2p, N 1s, C 1s, O 1s suggest that the polymer compounds which contain N, C, O and S are present onto the metal surface, and the Fe 2p signal comes from the metal substrate and its corrosion product. The high-resolution XPS spectra of O 1s, C 1s, and Fe 2p are presented in Fig 9 (b, d, f). The presence of O 1s peaks at 532.6, 532.0 and 530.2 shown in Fig. 9b can be associated with the fact that all these studied polymers of the type O=O, C-O and O^{2-} thereby implying the interaction between the polymer molecules and the oxide layer, which help forming a thin film onto the metal surface [131,132]. The XPS deconvoluted profiles of C 1s spectrum showed C-C aliphatic peak, C=O and C-N peaks near 286.6 and 285.4 eV, respectively (Fig. 9d). In high resolution XPS spectrum of Fe 2p, the intensity peaks appeared near 716.2, 712.4, 709.8 and 707.3 can be assigned to $Fe(OH)_x$, Fe^{3+} (2p), Fe^{2+} and Fe^{0} (2p) (Fig. 9f).

The XPS samples were prepared by immersing the mild steel coupons for 6 h in test solution containing 175 μM polymer at 60 °C in 250 mL of 1 M HCl. The parameters obtained from XPS analysis are depicted in Table 3.7.

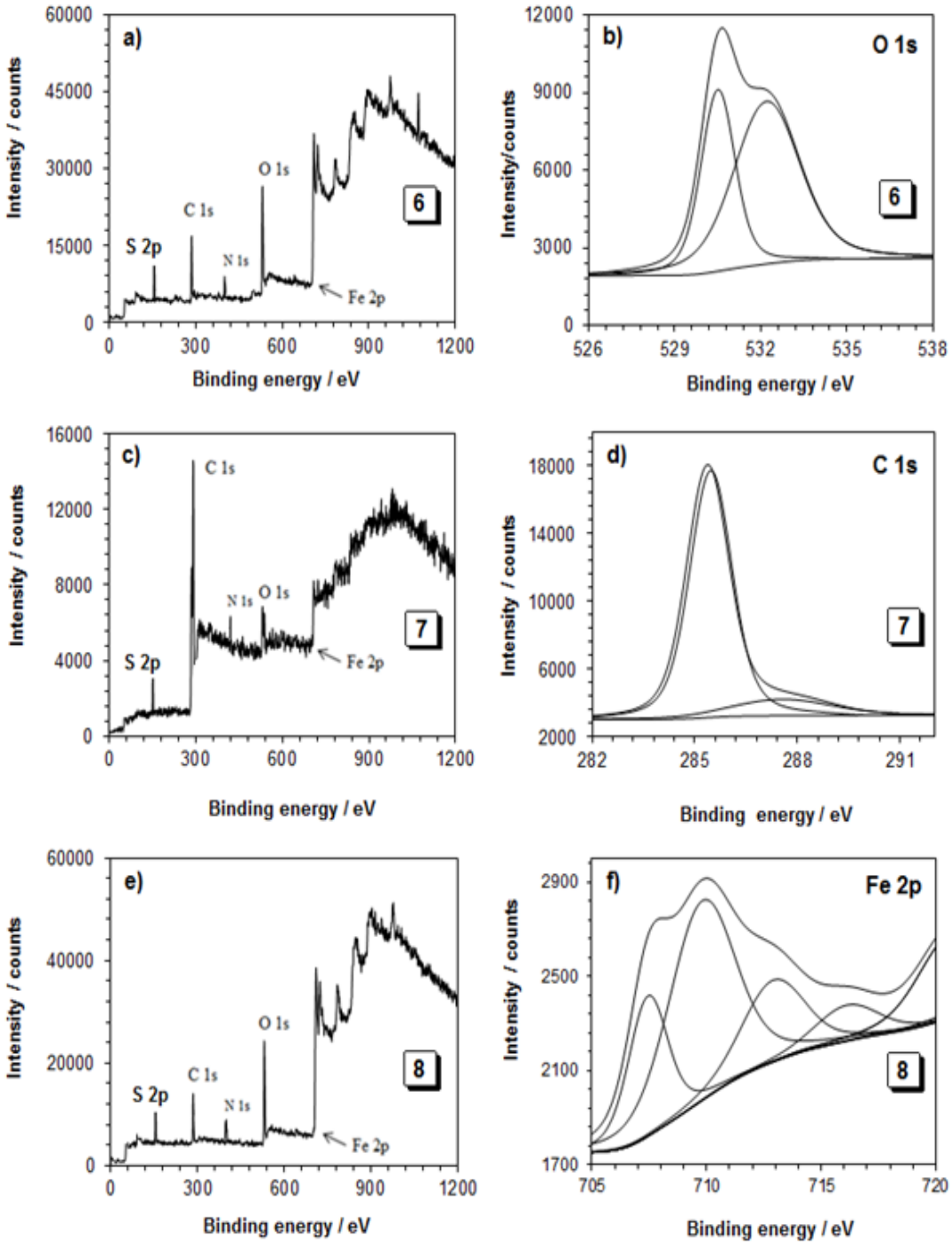

Figure 3.9 (a) XPS survey spectrum of (a) **6**, (c) **7** and (e) **8**, and the XPS deconvoluted profiles of (b) O 1s of **6**; (d) C1s of **8**, and (f) Fe 2p of **8** after immersing in 1 M HCl at 60 ºC for 6 h (175 µM)

Table 3.7 XPS scan composition of mild steel coupon in 1 M HCl containing **6**, **7** and **8** at 60 °C

Peak	Approx. binding energy (eV)	Composition (atom %)		
		6	**7**	**8**
C 1s	285.4	31.5	29.3	34.4
C 1s	286.6	19.4	18.7	13.2
O 1s	530.2	13.2	15.7	14.5
O 1s	532.0			30.6
O 1s	532.6	26.5	28.2	
N 1s	400.2	3.98	1.86	3.09
Fe 2p	707.3	1.61	2.52	1.39
Fe 2p	709.8	2.98	1.99	0.97
Fe 2p	712.4		1.30	1.27
Fe 2p	716.2			0.43
Cl 2p	199.2	0.84		

3.3.6.2 SEM- EDX analysis

SEM-EDX were used to study the surface morphology of the mild steel in absence and presence of polymer compound **7** after the immersion for 6 h in 1 M HCl, and are presented in Fig. 3.10b, c. The polished mild steel surface without exposed to 1 M HCl shown in figure 3.10a was used as reference. In absence of polymer compound **7** shown in Fig. 3.10b, the metal surface was severely damaged, surface roughness and porosity were very high, and intensely corroded by the aggressive acid medium (1 M HCl). In presence of polymer compound (175 μM), the effects of corrosion were suppressed; the smoother surface was detected (Fig. 3.10c) compared to the untreated surface (Fig. 3.10b). The mild steel surface was relatively intact and smooth, which could suggest that the inhibitor compound **7** protects the metal surface against aggressive corrosive media by the formation of thin layer onto the mild steel surface.

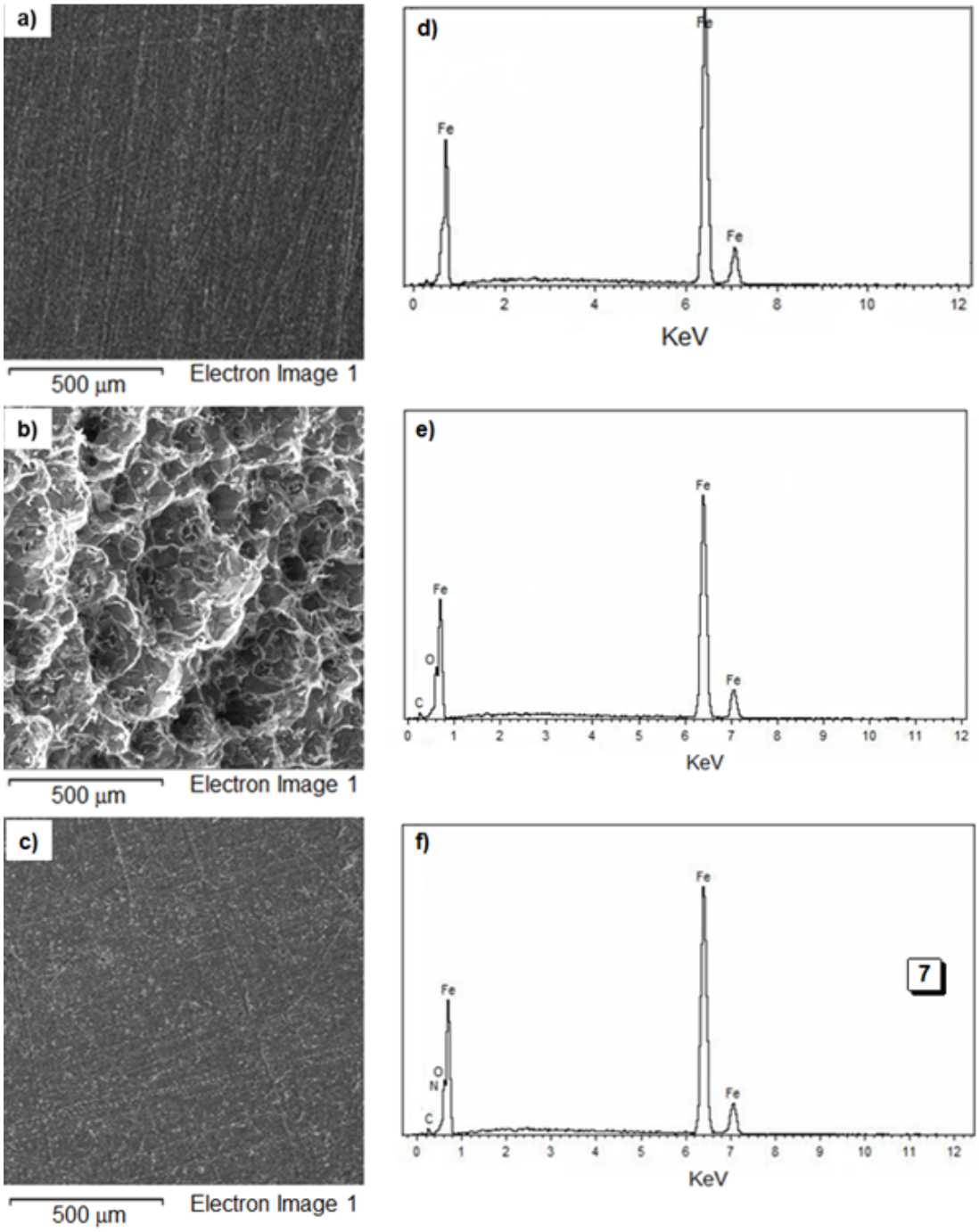

Figure 3.10 SEM micrographs on the surface of the mild steel: a) polished, after immersion of 6 h: b) untreated mild steel in 1 M HCl and c) mild steel treated in presence of 175 µM of inhibitor **7**. The corresponding EDX spectra are in d, e and f

The EDX analysis was also incorporated to further confirm the adsorption of the polymer compound **7** onto the metal surface. The strong iron signal was detected for the reference (polished) sample (Fig. 3.10d), while the iron and oxygen signal appeared in the uninhibited sample could be due to the slow atmospheric oxidation and formation of Fe_2O_3 oxide films (Fig. 3.10e). In Fig. 3.10f, the inhibited surface appeared with the signal of iron with additional signals of carbon, nitrogen and oxygen atoms implied the presence of adsorbed polymer compound that forms a protective layer onto the metal surface to resist the surface from the corrosion attack.

3.4 Conclusions

The inhibition effects of cyclocopolymers of sulfur dioxide and biogenic amino acid methionine residue containing ester functionality and sulfide, sulfoxide or sulfone motifs in each alternate repeat units have been investigated for their feasibility as a corrosion inhibitor in acid media using gravimetric weight loss and electrochemical methods. From the present study, the following conclusions can be drawn:

1. The synthesized cyclocopolymers showed excellent corrosion efficiency resisting mild steel corrosion in 1 M HCl.
2. The corrosion efficiencies increase with increasing the concentration of the polymers. In presence of 175 μM, the maximum corrosion efficiencies for the cyclocopolymer **6-8** were determined to be 92, 97 and 95%, respectively.

3. The inhibition efficiencies obtained from gravimetric weight loss, potentiodynamic polarization and electrochemical impedance spectroscopy techniques are coherent to each other.
4. The polymer compounds studied in the present study act as a mixed-type inhibitor.
5. The polymer compound **7** adsorbed onto the metal surface by chemisorption and physisorption processes, and obeys Langmuir, Temkin and Freundlich adsorption isotherms.
6. The negative values of ΔG^{o}_{ads} and ΔH^{o}_{ads} suggest that the adsorption process of polymer **7** is spontaneous and exothermic. The adsorption is attained through a mixed mechanism by the influence of chemisorption mechanism. The ΔS^{o}_{ads} values indicate increasing the randomness on the solid surface/inhibitor interface where the adsorbed inhibitor molecules displace the adsorbed water molecules on the surface of the mild steel.
7. The XPS and SEM-EDX supported the adsorption that forms a thin film onto the metal surface and protects the metal surface from corrosion attack.

CHAPTER 4

Inhibition of Mild Steel Corrosion in Hydrochloric Acid Medium by Polymeric Inhibitors Containing Residues of Essential Amino Acid Methionine

4.1 Introduction

Mild steel has low carbon content (up to 0.3%), which is readily available, cheap and found huge applications in oil and gas industries due to its notably high mechanical properties [133]. It becomes very vulnerable with continuous use of acids in various industrial processes [134]. Inhibitors' ability to protect the mild steel surface from corrosion in the acid media makes its use a highly practical method. Different types of organic and inorganic compounds are widely explored as corrosion inhibitors for the protection of metal surfaces [135]. Organic corrosion inhibitors utilize the service of lone pair of electrons in heteroatoms to cover metal surface by formation of coordinate-type bonds with the metal's vacant *d*- orbitals. The increase in inhibition efficiency in the order O < N < S < P signifies the greater polarizability of the lone pairs in the third-period elements thereby making them better inhibitors [111].

The inhibitor molecules usually interfere with anodic or cathodic reactions occurring on the metal surfaces to minimize or eliminate corrosion process [113]. However, most of the synthetic inhibitors were found to be not only expensive but also toxic and cause health problems [136]. Therefore, it is an utmost demand in these days to replace the synthetic inhibitors by a cheap, non-toxic, most effective and environmentally friendly corrosion inhibitors.

In this chapter, we will discuss the synthesis of a group of 'apparently' green cyclopolymers from non-toxic and inexpensive biogenic amino acid ester of methionine **1** (Scheme 1)**.**

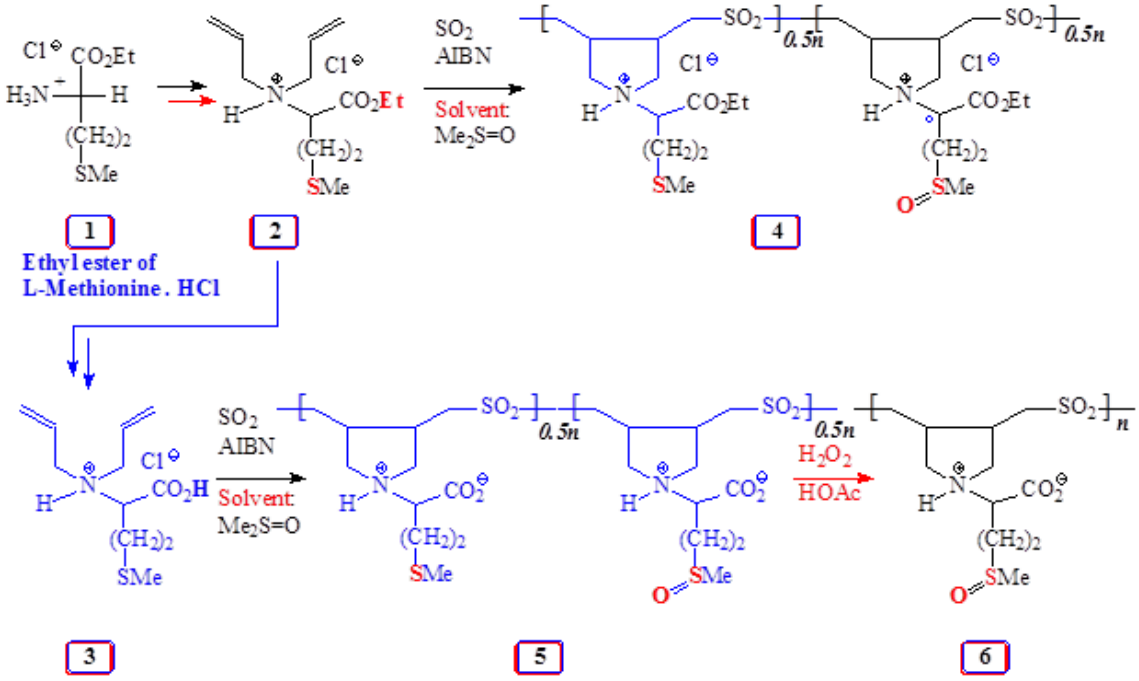

Scheme 4.1 Synthesis of methionine-based diallylamine salts-sulfur dioxide copolymers

The polymerization process led to embed the skeleton of pyrrolidine ring in the polymer chains. The immensely important Butler's cyclopolymerization protocol [77,79,80], used in the synthesis, led to polymers **4**, **5** and **6**, the repeating units of which contained the residues of amino acid methionine and/or methionine sulfoxide. The presence of pH-responsive N along with O and S as well as multiple anchoring points in a polymer chain has provided us an opportunity to examine and compare the efficacy of the functional motifs of the sulfide *versus* sulfoxide and carboxyl (CO_2H) *versus* ester (CO_2Et) in the inhibition of mild steel corrosion in 1.0 M HCl. The corrosion efficiency and adsorption

characteristics of these potentially green polymers on mild steel has been evaluated by gravimetric and various electrochemical techniques as well as by X-ray photoelectron spectroscopy (XPS), and scanning electron microscopy (SEM) and energy dispersive X-ray spectroscopy (EDX).

4.2 Experimental

4.2.1 Materials

Ethyl ester hydrochloride of L-Methionine **1,** allyl bromide and Azobisisobutyronitrile (AIBN) were purchased from Fluka Chemie AG. AIBN was recrystallized from $CHCl_3$-EtOH. Hydrogen peroxide (35 w/v %), hydrochloric acid (37% w/v), acetic acid and potassium carbonate (K_2CO_3) were purchased from BDH Chemical Ltd (Pool, England), and used as received. Dimethylsulfoxide (DMSO), dried over CaH_2 overnight, was distilled (bp $_{4\ mmHg}$ 64–65 °C). All solvents (reagent grade) obtained from Sigma Aldrich, and used as received.

4.2.2 Physical methods

FT-IR (Perkin Elmer 16F PC FTIR), and NMR (JEOL LA 500 MHz) were utilized to determine the structural composition of the compounds. The elemental composition was determined by Perkin Elmer Elemental Analyzer (Model 2400). The viscosity values of the synthesized compounds were determined by Ubbelohde viscometer (Viscometer Constant 0.005317 $mm^2\ s^{-2}$). Thermogravimetric analysis (TGA) was performed using Platinum/Platinum–Rhodium (Type R) thermocouples under N_2 (flow rate 50 mL/min) using an SDT thermogravimetric analyzer (Q600: TA Instruments, New Castle, DE, USA) by stepping up the temperature (10 °C/min) over 20–800 °C. A potentiostat-

galvanostat (Auto Lab, Model # 10A-BST707A) connected with a computer was used to measure the electrochemical properties.

4.2.3 Synthesis

L-Methionine **1** -derived monomer **2**, and its SO_2-copolymers **4** were prepared following the published literature procedure [84]. The ester functionality in L-Methionine **1** -derived monomer **2** is hydrolyzed to **3**, and its SO_2-copolymers **5** and **6** were prepared as described [121].

4.2.4 Specimens

For gravimetric measurements, rectangular shape mild steel coupon samples of size 2.5×2.0×0.1 cm^3 were used. For electrochemical polarization and impedance measurements, a flag shaped mild steel coupons (1 mm thick; exposure area: *ca.* 2 cm^2) with an approximate stem of 3 cm embedded by a Araldite (RS, Saudi Arabia) were abraded by different grades of emery papers (grade 100 to 1500), rinsed with deionized distilled water, degreased with acetone followed by another wash by deionized distilled water and dried in a hot air at room temperature, and stored in a desiccator before their use. The chemical composition of mild steel specimens used in gravimetric, electrochemical polarization and impedance measurements were as follow: C (0.089), Mn (0.34), Cr (0.037), Ni (0.022), Mo (0.007), Cu (0.005), V (0.005), P (0.010), Fe (99.47).

4.2.5 Solutions

HCl solution was prepared from concentrated HCl (37%, reagent grade) by diluting to 1.0 M, with distilled de-ionized water. The corrosion inhibitors with different concentrations

in μM were dissolved in 1.0 M HCl solution, and 1.0 M HCl solution without the presence of inhibitor was considered as blank.

4.2.6 Gravimetric measurements

The mild steel coupons (2.5 cm×2.0 cm×0.1 cm) having almost equal masses and size were used to perform the gravimetric measurements. The mild steel coupons were immersed by hanging in 250 mL of 1.0 M HCl for 6 h in the presence or absence of the synthesized inhibitors at 60 °C. After a certain period of time, the steel coupons were removed from the solution, wiped with a tissue paper, rinsed with water, and dried in a vacuum oven.

The percent inhibition efficiency (η %) was calculated using the weight loss of the mild steel coupons *via* Eq. (1):

$$\eta\ \% = \frac{W_b - W_i}{W_b} \times 100 \qquad (1)$$

where, W_i and W_b represent weight loss in the presence or absence of polymer molecule, respectively.

The average relative weight loss of the mild steel coupons was determined from the three individual measurements. The average weight losses in percentage was deviated within a range of 0.5-3.0%.

4.2.7 Electrochemical measurements

4.2.7.1 OCP versus time

The required time to reach steady OCP at the surface of mild steel coupon immersed in different concentrations (0, 1.00 and 175 μM) of inhibitors **4, 5** and **6** in 1.0 M HCl solution was measured.

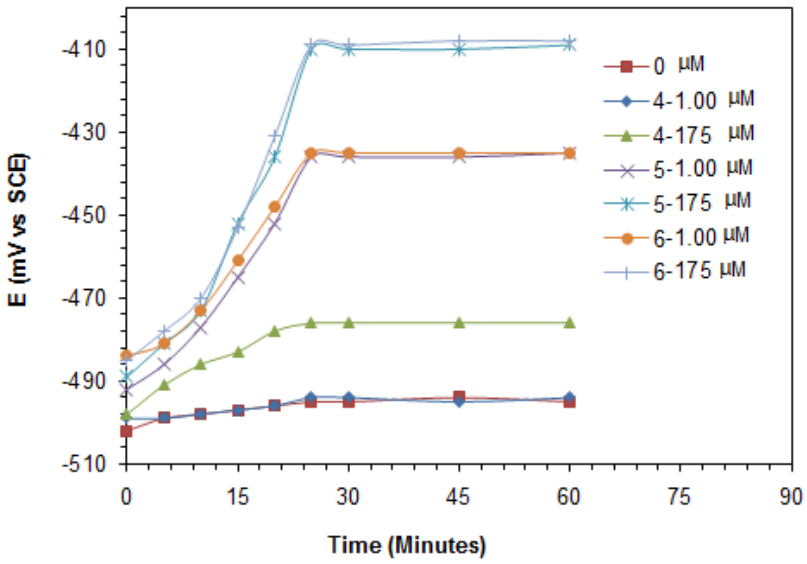

Figure 4.1 OCP variation of mild steel with immersion time in 1.0 M HCl solution containing various concentrations (1.00 and 175 μM) of **4-6** at 60 ºC

As shown in Fig. 4.1, the OCP was measured at various times (0 to 60 min.) and it has been found the steady OCP was achieved after around 30 min.

4.2.7.2 Tafel extrapolations

Three electrode type electrochemical cell and 750 mL round bottom flask were used to perform the experiments. The reference electrode is saturated calomel electrode (SCE), the auxiliary electrode is graphite rod (≈ 5 mm diameter) and the working electrode is the

mild steel coupon which was pre-corroded for 30-60 min to reach the stable OCP. All of them were immersed in the 1 M HCl (250 mL) test solution at 60 ºC. Computerized potentiostat-galvanostat (Auto Lab, Booster 10A-BST707A, Eco Chemie, Netherlands) controlled by NOVA (version 1.8) software was used to record the polarization curves with a current of 1 A. The scan was performed in potential window ± 250 mV around the corresponding OCP with a scan rate of 0.5 mV/s. The Inhibition efficiencies based on the corrosion current density were calculated using equation 2:

$$\eta(\%)=\left(\frac{I_{corr\ Blank}-I_{corr\ Inhibitor}}{I_{corr\ Blank}}\right) x\,100 \qquad (2)$$

Where $I_{corr\ Blank}$ is the current of corrosion in absence of inhibitors and $I_{corr\ Inhibitor}$ is in presence of inhibitor.

4.2.7.3 Linear Polarization Resistance (LPR) method

The same electrochemical cell and the conditions described in section 4.2.7.2 were used to measure the LPR by recording the current versus potential range of ±10 mV around E_{corr}. The obtained polarization resistances in absence (R'_p) and presence ($\overline{R'_p}$) of inhibitors were used to calculate the surface coverage (θ) which correlated to the inhibition efficiencies calculated based on LPR ($\eta\%$) using equation (3):

$$(\eta\%) = (\theta\%) = \left(\frac{\overline{R'_p}-R'_p}{\overline{R'_p}}\right) x\,100 \qquad (3)$$

4.2.7.4 Electrochemical Impedance Spectroscopy (EIS)

The electrochemical impedance measuring experiments were done in a new test solution (250 mL of 1 M HCl) at 60 ºC using the electrochemical cell which consists of three electrodes connected to the computerized potentiostat-galvanostat system described in section 4.2.7.2. Using the NOVA processing software (version 1.8), the Nyquist and Bode plots were recorded at corresponding OCP in frequency range from 100 KHz to 50 mHz with amplitude 10 mV. The obtained data were fitted with the most suitable (lowest deviation from the experimental values) electrochemical equivalent circuit.

4.2.8 Surface analysis

4.2.8.1 X-ray photoelectron microscopy

The XPS analysis was performed by a X-ray photoelectron spectrometer (Thermos Scientific, Model # Escalab 250 Xi). Avantage software was used to process the data. The C 1s peak at 285.4 eV was considered to be as reference peak. A non-linear least squares algorithm with a Gaussian-Lorentzian combination and a Shirley baseline was used to deconvolute the XPS spectra.

4.2.8.2 SEM and EDX

The surface morphology of the inhibited (presence of polymer) and corroded (blank) metal surface was performed using a field-emission scanning electron microscope (FESEM, Lyra 3, Tescan, Czech Republic) with acceleration beam was in ranges 20-30 kV. In addition, an energy dispersive X-ray (EDX) spectroscope (Oxford Inc., UK) fitted with an X-Max detector was used to determine the chemical compositions and for mapping the levels of homogeneity of these metal surfaces. The SEM images were

captured after immersing the steel samples at 60 °C for 6 h in absence (0 μM) or presence of polymer (175 μM).

4.3 Results and Discussion

4.3.1 Synthesis of the polymeric inhibitors

Cyclopolymerization [77–79] of diallylammonium salts or their alternate copolymerization [80–82] with SO_2 have etched an important place in the synthesis of a plethora of industrially significant ionic polymers. The copolymerization of monomer **2**/SO_2 in solvent dimethyl sulfoxide (DMSO) led to the formation of water-soluble polymer **4** having sulfide and sulfoxide moieties in a 1:1 as a result of oxide exchange from DMSO (Scheme 4.1) [82]. Note that the polymerization carried out in ethanol/or acetone solvent gave water-insoluble copolymer **4** (y = 0). The water-solubility of polymer **4** containing equal proportion of sulfide and sulfoxide motifs is desired since its corrosion inhibition of mild steel in 1.0 M HCl can then be studied.

In the current work, the ester functionality in monomer **2** is hydrolyzed to **3** with the anticipation that the corresponding water-soluble polymers **5** and **6** could be tested for inhibition of mild steel corrosion, thereby providing the opportunity to compare the inhibition efficiencies of ester and carboxyl groups. To study the effect of sulfoxide motifs alone, we converted hydrolyzed copolymer **5** having sulfide and sulfoxide moieties into sulfoxide motifs as in **6**. The current polymeric inhibitors **4**-**6** offer greater latitude in safeguarding the metal surface: (i) they contain three important heteroatoms: N, O and S, (ii) as polymers, they have multiple points to anchor on the metal surface [85,86], (iii) the retention of all three original motifs of methionine (i.e. amine N, thiol -S-, and CO_2^-) in the polymer chain is anticipated to provide abundant lone pairs of

electrons as well as chelating ligands to complex with Fe^{2+} on the metal surface. The corrosion efficiency and adsorption characteristics of these polymers would allow us to compare the inhibition efficiencies of the polymers using gravimetric and potentiodynamic polarization methods, and electrochemical impedance spectroscopy (EIS). The surface morphology of the polymer containing mild steel surface has been evaluated by X-ray photoelectron spectroscopy (XPS), and scanning electron microscopy (SEM) and energy dispersive X-ray spectroscopy (EDX).

The intrinsic viscosity [η] of copolymer **4**, determined from viscosities of 1-0.125% solutions in 0.1 M NaCl at 30 °C, was found to be 0.127 dL g^{-1}. The intrinsic viscosity [η] of **5** and **6**, in the presence of 1 equivalent of NaOH in 0.1 M NaCl at 30 °C were determined to be 0.055 and 0.061 dL g^{-1} , respectively. These low values of [η] indicate the low molar masses of the polymers. The thermal degradation of the synthesized copolymers were examined by TGA to realize the chemical stability of the inhibitors. The TGA curves of polymers **4-6** showed good thermal stability and no sudden weight loss has been observed up to 200 °C.

4.3.2 Gravimetric measurements

The results of gravimetric weight loss measurements, which were carried out in triplicate using mild steel coupons immersed in the presence or absence of the synthesized polymer solution in 1.0 M HCl for 6 h at 60 °C are depicted in Table 4.1.

Table 4.1 The η% [a] for inhibitors **4**, **5** and **6** obtained by gravimetric method for the inhibition of corrosion of mild steel at 60 ºC in 1.0 M HCl for 6 h.

Sample	η (%) at concentration of inhibitors (in μM)							
	1.75	4.85	8.75	17.5	26.2	35.2	70.2	175
4	50.6	57.7	74.3	82.1	90.5	90.8	92.4	93.0
5	76.9	88.6	93.5	96.2	98.0	98.7	99.3	99.5
6	60.1	72.4	78.2	87.3	90.9	93.0	93.4	93.8

[a] IE (i.e., η) = surface coverage θ.

The inhibition efficiency was found to be very excellent in all studied polymer compounds **4-6**. Table 4.1 showed that the measured inhibition efficiency values for 175 μM of polymer compounds **4-6** were determined to be 93.0, 99.5, and 93.8%, respectively, while at the polymer concentration of 35.2 μM (≈11 ± 1 ppm), the corresponding inhibition efficiency values were estimated to be 90.8, 98.7 and 93.0%, respectively. It is apparent from the gravimetric weight loss results (Table 4.1) that an increase in the concentrations of the copolymers **4-6** in 1.0M HCl increases the inhibition efficiency and reaches a maximum value suggesting the formation of a monolayer film onto the mild steel surface. In all the concentrations of studied polymer molecules, the 1: 1 ratio of sulfide and sulfoxide motifs in hydrolyzed copolymer **5** gave the best protection. At a concentration of 175 μM, the inhibition efficiency value of the copolymer **5** was determined to be 99.5%. The excellent inhibition efficiency obtained by the hydrolyzed copolymers confirm the presence of surface active functional motifs containing –S-, -S=O, -N- that resist the corrosion onto the mild steel surface.

4.3.3 Polarization measurements

The steady open circuit potential (OCP) values were obtained from the experiment measuring the OCP values versus immersion time for a mild steel coupon in the presence or absence (blank) of various copolymers **4-6** at a concentration of 1.00 μM and 175 μM in 1.0 M HCl solution. The results presented in Fig. 4.1 showed that the OCP in absence of the inhibitors slightly shifted towards positive direction and became stable very fast, resulting in the free corrosion potential E_{corr} of the mild steel coupon. In the presence of inhibitors, the OCP values had a slower rate of changing with higher magnitude towards a positive direction and reached the steady state after ≈30 min. The magnitude of the E_{corr} shifts towards a positive direction increased with increase in the inhibitor concentration. Shifting of E_{corr} towards the positive direction suggests the inhibitors are preferentially getting adsorbed on the anodic sites of mild steel surface.

Fig. 4.2 shows the Tafel potentiodynamic polarization curves for the mild steel in absence and presence of different concentrations (1.00 to 175 μM) of inhibitors **4-6** in 1.0 M HCl solution at 60 ºC. The extrapolation of linear segments of anodic and cathodic sides in Tafel plots was used to obtain various electrochemical parameters such as the produced current density of corrosion (i_{corr}) and corrosion potential (E_{corr}) of mild steel coupons which are summarized in Table 4.2. As shown in Table 4.2, the significant decrease in the i_{corr} is an evidence of the inhibitive nature of the synthesized compounds. The shifting of E_{corr} values to positive direction with a magnitude higher than 85 mV in case of using hydrolyzed copolymer compounds **5** and **6** suggested that they are anodic type inhibitors, which mainly block the anodic sites and suppresses the anodic reaction [122].

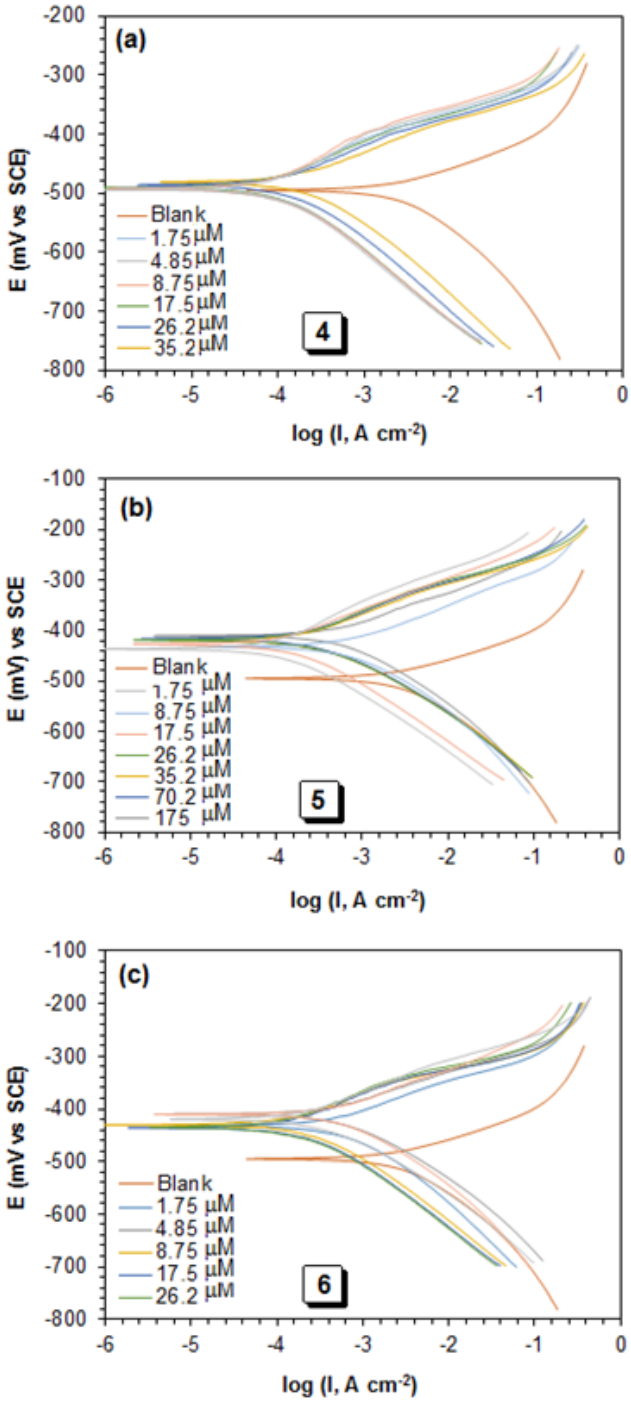

Figure 4.1 Potentiodynamic polarization curves at 60 °C for mild steel in 1.0 M HCl containing various concentrations of (a) **4**, (b) **5** and (c) **6**

Table 4.2 Results of Tafel plots of a mild steel sample in 1.0 M HCl containing inhibitors **4**, **5** and **6** at different temperature

Sample	Temp (°C)	Concentrations		Tafel					
		ppm (by wt.)	μM	E_{corr} vs. SCE (mV)	β_a (mV dec^{-1})	β_c (mV dec^{-1})	I_{corr} (μA cm^{-2})	υ_{corr} (mm y^{-1})	η (%)[a]
4	60	0	0	–495	73.8	–169	2465	28.6	-
		0.36	1.00	–494	64.4	–106	1506	17.5	38.9
		0.64	1.75	–494	58.8	–117	1395	16.2	43.4
		1.77	4.85	–492	70.8	–109	1038	12.0	57.9
		3.20	8.75	–491	79.9	–113	764	8.86	69.0
		6.40	17.5	–490	99.2	–127	486	5.64	80.3
		9.59	26.2	–486	89.1	–122	365	4.23	85.2
		12.9	35.2	–484	84.5	–110	335	3.89	86.4
		25.7	70.2	–481	92.3	–103	286	3.32	88.4
		64.0	175	–476	96.7	–106	177	2.05	92.8
5	50	0	0	–483	51.2	–117	505	5.85	-
		0.30	1.00	–479	73.7	–127	170	2.03	66.3
		0.53	1.75	–477	87.8	–134	134	1.55	73.5
		1.46	4.85	–461	76.5	–137	86.9	1.01	82.8
		2.64	8.75	–458	70.8	–159	52.5	0.61	89.6
		5.27	17.5	–456	69.8	–134	30.8	0.36	93.9
	60	0	0	–495	73.8	–169	2465	28.6	-
		0.30	1.00	–455	93.6	–144	784	9.09	68.2
		0.53	1.75	–436	79.4	–142	454	5.27	81.6
		1.46	4.85	–436	81.6	–112	209	2.15	91.5
		2.64	8.75	–432	82.3	–103	140	1.35	94.3
		5.27	17.5	–427	85.3	–124	71.5	0.83	97.1
		7.90	26.2	–419	91.0	–137	51.8	0.60	97.9
		10.6	35.2	–419	97.5	–103	44.4	0.52	98.2
		21.2	70.2	–416	92.5	–112	22.2	0.26	99.1
		52.8	175	–410	91.0	–115	14.8	0.17	99.4
	70	0	0	–498	60.9	–102	4508	52.3	-
		0.30	1.00	–490	87.1	–104	2376	23.6	47.3
		0.53	1.75	–487	79.1	–93.4	2087	20.0	53.7
		1.46	4.85	–485	96.4	–113	1434	13.5	68.2
		2.64	8.75	–481	98.1	–106	983	10.7	78.2
		5.27	17.5	–476	66.0	–98.7	618	7.17	86.3
6	60	0	0	–495	73.8	–169	2465	28.6	-
		0.54	1.75	–435	110	–90.0	1055	12.2	57.2
		1.50	4.85	–434	84.6	–6 8.7	848	9.84	65.6
		2.71	8.75	–434	108	–121	628	7.28	74.5
		5.42	17.5	–432	86.0	–96.2	380	4.41	84.6
		8.11	26.2	–430	74.3	–80.4	288	3.34	88.3
		10.9	35.2	–419	90.0	–84.1	202	2.34	91.8
		21.8	70.2	–410	81.2	–89.3	187	2.17	92.4
		54.1	175	–409	93.2	–87.7	175	2.03	92.9

[a] Inhibition Efficiency, IE (i.e., η) = surface coverage θ.

In case of the coester polymer compound **4** the shifting was less than 20 mV, therefore it could be classified as a mixed type inhibitor. However, the higher reduction in the anodic current densities in comparison to the one in the cathodic current densities is indicative of the greater decrease in the anodic oxidation rate. The inhibitors thwarted the corrosion reactions by forming a barrier film on the metal surface under the major influence of anodic control. It was also observed that there is no significant change or clear trends in cathodic (β_c) and anodic (β_a) slopes, which suggests no change in the inhibition mechanism with increasing concentrations of the inhibitors.

The corrosion inhibition efficiencies of the synthesized inhibitor compounds for mild steel coupon in 1.0 M HCl solution at 60 ºC, obtained from Tafel and LPR experiments are summarized in Tables 4.2 and 4.3, respectively. To our great satisfaction, the hydrolyzed copolymer compound **5** showed excellent inhibition efficiencies. In addition, it has been found that they are in good agreement with the inhibition efficiencies calculated based on the weight loss method (Table 4.1).

Table 4.3 Results of LPR method in 1.0 M HCl containing inhibitors **4**, **5** and **6** at different temperature

Sample	Temp (°C)	Concentrations		LPR		
		ppm (by wt.)	μM	R'_p (Ω cm^2)	θ [a]	θ (%)
4	60	0	0	2.38	-	-
		0.36	1.00	3.97	0.401	40.1
		0.64	1.75	4.34	0.452	45.2
		1.77	4.85	5.63	0.577	57.7
		3.20	8.75	7.63	0.688	68.8
		6.40	17.5	12.8	0.814	81.4
		9.59	26.2	17.0	0.860	86.0
		12.9	35.2	18.2	0.869	86.9
		25.7	70.2	20.0	0.881	88.1
		64.0	175	30.9	0.923	92.3
5	50	0	0	1.89	-	-
		0.30	1.00	5.46	0.654	65.4
		0.53	1.75	7.30	0.741	74.1
		1.46	4.85	11.4	0.835	83.5
		2.64	8.75	18.5	0.898	89.8
		5.27	17.5	32.0	0.941	94.1
	60	0	0	2.38	-	-
		0.30	1.00	7.19	0.669	66.9
		0.53	1.75	12.1	0.804	80.4
		1.46	4.85	29.8	0.920	92.0
		2.64	8.75	44.9	0.947	94.7
		5.27	17.5	149	0.984	98.4
		7.90	26.2	170	0.986	98.6
		10.6	35.2	238	0.990	99.0
		21.2	70.2	340	0.993	99.3
		52.8	175	595	0.996	99.6
	70	0	0	9.29	-	-
		0.30	1.00	18.0	0.484	48.4
		0.53	1.75	20.2	0.539	53.9
		1.46	4.85	30.1	0.691	69.1
		2.64	8.75	46.0	0.798	79.8
		5.27	17.5	70.4	0.868	86.8
6	60	0	0	2.38	-	-
		0.54	1.75	5.68	0.581	58.1
		1.50	4.85	6.76	0.648	64.8
		2.71	8.75	9.02	0.736	73.6
		5.42	17.5	14.9	0.840	84.0
		8.11	26.2	21.1	0.887	88.7
		10.9	35.2	29.8	0.920	92.0
		21.8	70.2	32.6	0.927	92.7
		54.1	175	35.0	0.932	93.2

[a] Inhibition Efficiency, IE (i.e., η) = surface coverage θ.

4.3.4 Impedance measurements

For better understanding the corrosion inhibition performance, the EIS experiments were carried out after immersing the mild steel for 30 min in the test solution. The recorded impedance data (Nyquist and Bode plots) of mild steel coupon/solutions with and without the corrosion inhibitors **4-6** at different concentrations (1.75 to 175 μM) were fitted by the Randles equivalent electrochemical circuit (the best fitted circuit) shown in Fig. 4.3.

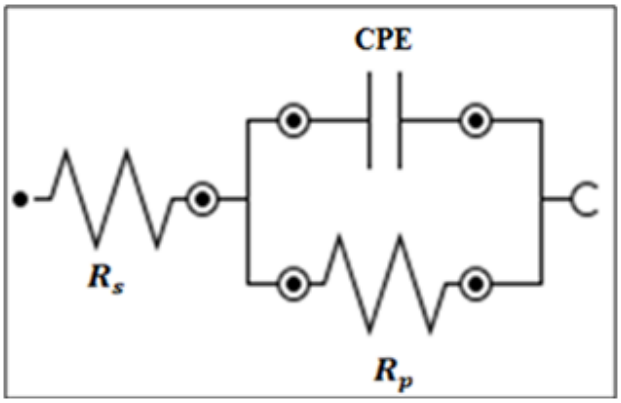

Figure 4.3 Randles electrical-chemical equivalent circuit diagram used to modeling metal/solution interface. Rs: Solution resistance, Rp: Polarization resistance, CPE: Constant phase element

The simple circuit consists of a polarization resistance (R_p), solution resistance (R_s) and a constant phase element (CPE). The R_s value resulted by the potential drop between the mild steel coupon as a working electrode and the reference electrode, and its value was calculated from intersection of the real part (Z′) axis at high frequency with the fitted semicircle. While the R_p values were achieved from the intersection of semicircle with Z′ axis at low frequency, which were contributed by other resistances such as the diffusion layer resistance and charge transfer resistance at the surface of working electrode (mild

steel) [123]. The net polarization resistance or charge transfer resistance (R'_p) at mild steel coupon was calculated using the equation (4), and its value was used later to calculate the inhibition efficiencies based on the EIS using equation (3).

$$R'_p = R_p - R_s \quad (4)$$

The CPE is used to express the non-ideal capacitance and non-ideal frequency response. It is commonly used in the electrochemical circuit in order to attain better fitting. The double layer capacitance (C_{dl}) relates to the CPE by equation (5).

$$C_{dl} = CPE(\omega)^{n-1} \quad (5)$$

where ω is the angular frequency (radian) at the maximum imaginary part of the impedance, and *n* is the surface heterogeneity.

The EIS fitting results showed that the *n* values are lower than 1, which attributed to the poor homogeneity of surface of the mild steel coupon. Table 4.4 summarizes the normalized EIS results for the corrosion of a mild steel sample in 1.0 M HCl solutions containing different concentrations of inhibitors **4-6** at 60 °C.

It has been found that with increase in the concentration of inhibitors the R'_p were increased and the values of CPE were decreased as a result of increasing the thickness of the adsorbed inhibitor, this eventually leads to increase the inhibition efficiency of 99.2% in case of using 175 μM of compound **5**. An increase in the heterogeneity of the mild steel surface caused by the increase in the adsorption of **4-6** inhibitors at higher concentrations results in the lower *n* values. The results obtained from EIS study confirmed the findings of the LPR, Tafel and gravimetric methods.

Table 4.4 Impedance parameters for the corrosion of a mild steel sample in 1.0 M HCl solutions containing inhibitors **4**, **5** and **6** at 60 °C

Sample	Concentration ppm (by wt.)	Concentration μM	R_s (Ω cm^2)	R_p (Ω cm^2)	CPE[a] (μF cm^{-2})	n	R'_p (Ω cm^2)	η (%)
4	0	0	0.373	1.963	922	0.989	1.590	-
	0.64	1.75	0.479	3.537	566	0.905	3.058	48.0
	1.77	4.85	0.485	4.050	492	0.919	3.565	55.4
	3.20	8.75	0.447	5.837	348	0.846	5.390	7 0.5
	6.40	17.5	0.436	9.077	335	0.827	8.641	81.6
	9.59	26.2	0.430	15.87	301	0.793	15.44	89.7
	12.9	35.2	0.128	16.52	262	0.722	16.39	90.3
	25.7	70.2	0.292	18.57	203	0.669	18.28	91.3
	64.0	175	0.334	19.96	197	0.554	19.63	91.9
5	0	0	0.373	1.963	922	0.989	1.590	-
	0.53	1.75	0.720	7.106	138	0.816	6.386	75.1
	1.46	4.85	0.748	14.58	113	0.947	13.83	88.5
	2.64	8.75	0.378	21.03	71.8	0.916	20.65	92.3
	5.27	17.5	0.496	36.64	91.2	0.891	36.14	95.6
	7.90	26.2	0.501	47.26	60.5	0.865	46.76	96.6
	10.6	35.2	0.930	89.26	21.8	0.884	88.33	98.2
	21.2	70.2	0.480	145.0	38.3	0.847	144.5	98.9
	52.8	175	0.851	199.7	33.9	0.867	198.8	99.2
6	0	0	0.373	1.963	922	0.989	1.590	-
	0.54	1.75	0.577	4.336	463	0.883	3.759	57.7
	1.50	4.85	0.343	5.902	416	0.888	5.559	71.4
	2.71	8.75	0.393	7.074	401	0.822	6.681	76.2
	5.43	17.5	0.400	11.68	357	0.857	11.28	85.9
	8.12	26.2	0.484	17.22	285	0.873	16.74	90.5
	10.9	35.2	0.630	21.55	105	0.856	20.92	92.4
	21.8	70.2	0.539	23.58	79.6	0.845	23.04	93.1
	54.1	175	0.781	25.24	53.8	0.812	24.46	93.5

[a]Double layer capacitance (C_{id}) and coating capacitance (C_c) are usually modeled with a constant phase element (CPE) in modeling an electrochemical phenomenon.

The Nyquist and Bode plots are shown in Fig. 4.4(a-f) for different concentrations (1.75 to 175 μM) of inhibitors **4-6**. The inset figures in Fig. 4.4(a, b) show the magnified Nyquist plots at blank (0 μM). In the Nyquist plots (Fig. 4.4(a-c), it is clearly evident that increasing the copolymers concentration increases the diameter of the semicircle suggesting an increase in the formed protective layer on the surface of the mild steel electrode due to the adsorption of the inhibitor compounds. Bode phase angle plots (Fig. 4.4d) for compound **6** show an increase in the angle value at intermediate frequency with increasing the inhibitor concentrations. It shows decreasing in the capacitance at the surface of the mild steel electrode which is attributed to the decreasing in the local dielectric constant as well as increase in the adsorbed amount of inhibitors on the coupon surface. Bode magnitude plots (Fig. 4.4(e,f)) for compounds **5** and **6** implied an increase in the polarization resistance (R_p) with increasing the inhibitor concentrations. However, those R_p can be obtained from intersection of the horizontal plateau region at low frequency with the Y-axis of log|Z|.

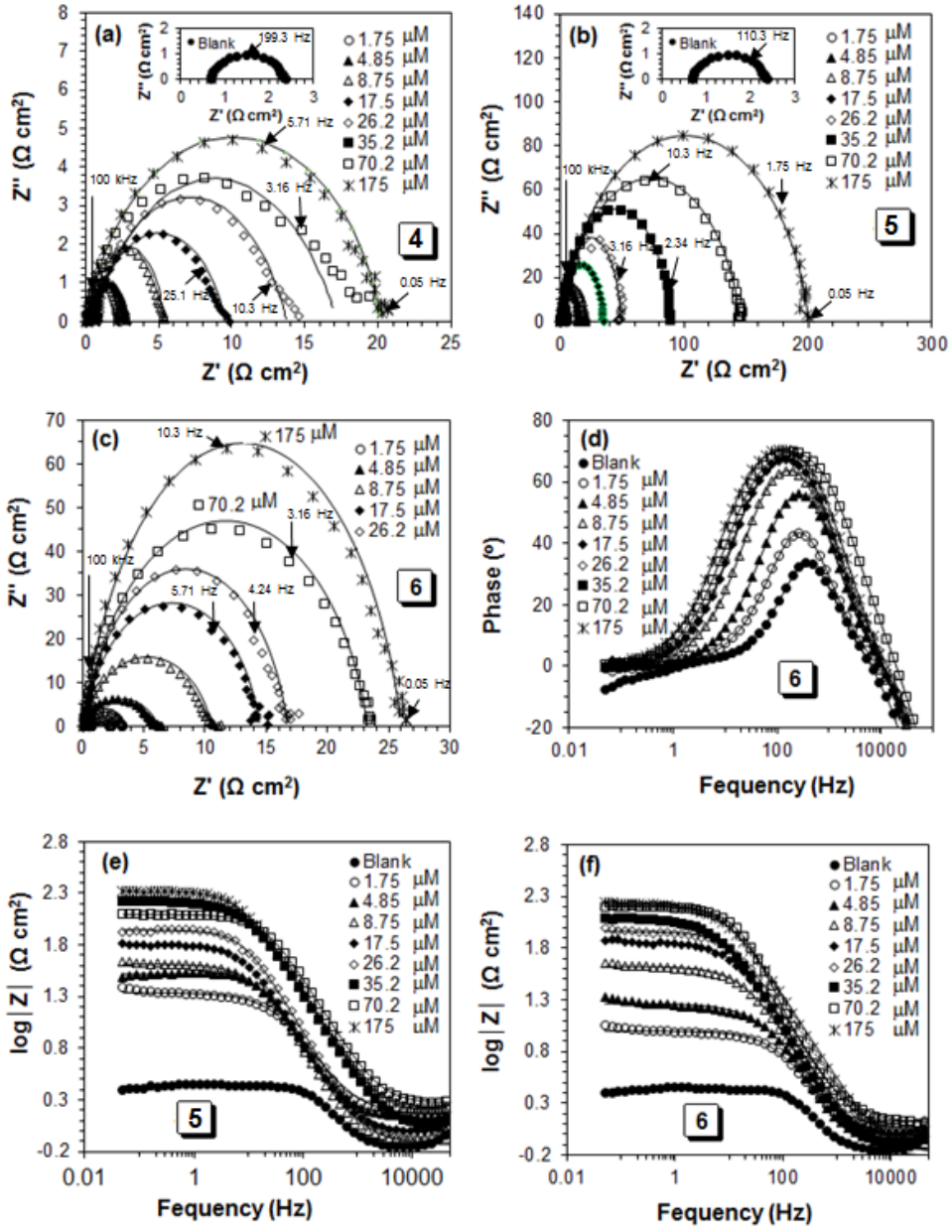

Figure 4.2 Nyquist diagram of (a) **4**, (b) **5** and (c) **6**, Bode phase angle plots of (d) **6** and impedance plots (e) **5** and (f) **6** of mild steel at 60 °C in 1.0 M HCl containing different concentrations of inhibitors. Solid line in the Nyquist plot fitted to the equivalent circuit ; solid lines represent fitted data and various symbols represent experimental data

4.3.5 Adsorption isotherms

The effectiveness (i.e., inhibition efficiency) of inhibitor molecules mainly depends on their adsorption ability onto the surface of mild steel. The synthesized copolymers **4-6** employed to study the inhibition efficiency ($\eta\%$) persuaded to have the understanding of the surface coverage (θ) are presented in Tables 4.1-4.4.

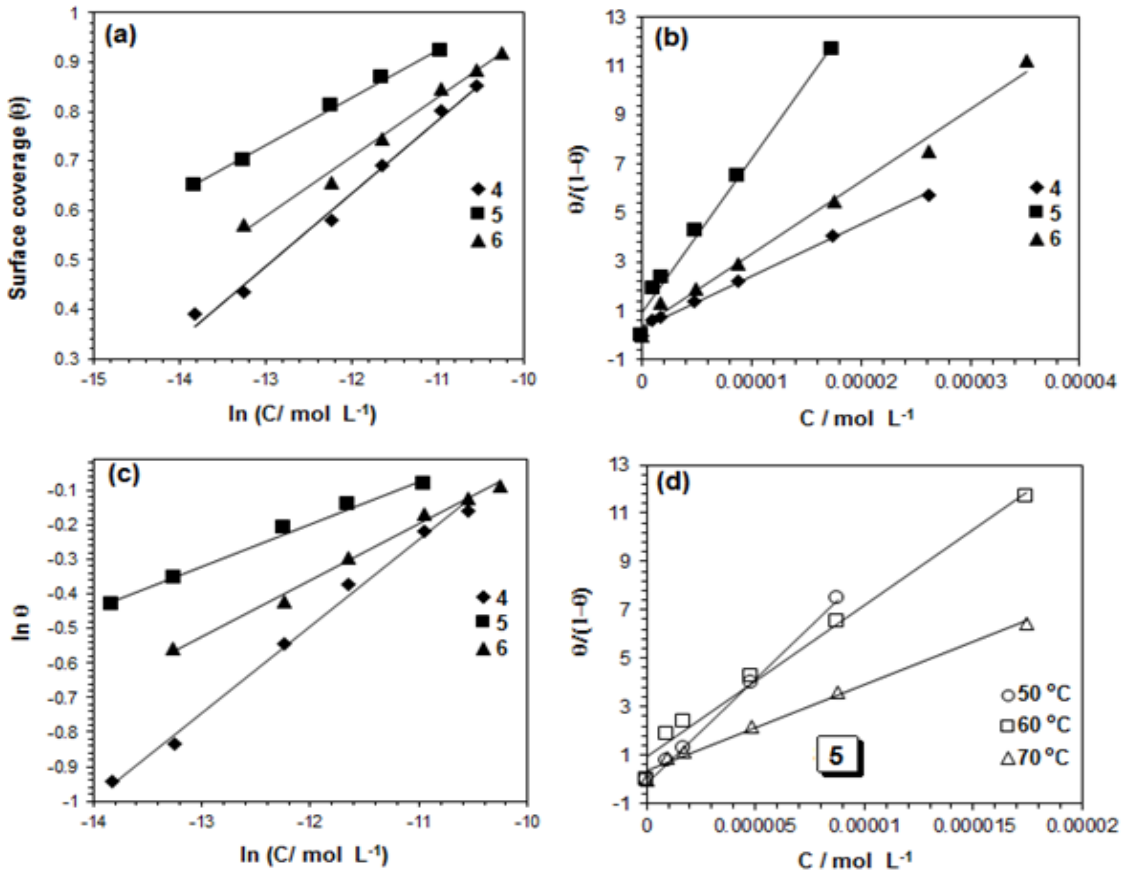

Figure 4.5 a) Temkin's adsorption isotherm plots, b) Langmuir adsorption isotherm, c) Freundlich adsorption isotherm for the adsorption of inhibitors **4-6** at 60 °C, and d) Langmuir adsorption isotherm for the adsorption of inhibitor 5 at various temperatures, on the surface of mild steel

With a view to understanding the adsorption mechanism of the synthesized copolymers, their adsorption thermodynamics were studied. The most commonly used four adsorption isotherms (i.e. Freundlich, Langmuir, Frumkin and Temkin's isotherms) describing the relationship between the surface coverage (θ) and the bulk low concentration of inhibitor (C) (Eqs. 6-9) [124] were applied using the linear least square method as shown in Fig. 4.5(a-d).

Freundluich: $\theta = K_{ads}C^{n}$ (6)

Langmuir: $\theta/(1-\theta) = K_{ads}C$ (7)

Frumkin (Frumkin, 1925): $K_{ads}C = \{\theta/(1-\theta)\} e^{-2\alpha\theta}$ (8)

Temkin: $K_{ads}C = e^{f\theta}$ (9)

Table 4.5 Square of coefficient of correlation (R^2) and values of the constants in the adsorption isotherms of Temkin, Frumkin, Langmuir and Freundlich in the presence of inhibitors **4**, **5** and **6** in 1.0 M HCl solution (Tafel data used for the isotherm)

Sample	Temp (°C)	Temkin[1] (R^2, f)	Langmuir[2] (R^2)	Frumkin[3] (R^2, a)	Freundlich[4] (R^2)
4	60	0.9912, 7.0	0.9947	0.8965, -1.1	0.9942, 0.3
5	50	0.9923, 4.7	0.9992	0.9969, -0.3	0.9799, 0.3
	60	0.9973, 10	0.9999	0.9808, -2.1	0.9926, 0.1
	70	0.9975, 7.1	0.9998	0.9238, -1.1	0.9946, 0.2
6	60	0.9897, 8.3	0.9910	0.7348, -1.1	0.9929, 0.2

[1]Temkin: $K_{ads}C = e^{f\theta}$

[2]Langmuir: $\theta/(1-\theta) = K_{ads}C$

[3]Frumkin: $K_{ads}C = \{\theta/(1-\theta)\} e^{-2a\theta}$

[4]Freundluich: $\theta = K_{ads}C^{n}$

As an evident from the higher R^2 values of straight lines obtained by employing the Langmuir isotherm model, it was the best to explain the adsorption mechanism of the synthesized inhibitors. This indicates the adsorption of inhibition is achieved predominantly by chemisorption. However, the synthesized inhibitors also showed good fit for the Freundlich and Temkin adsorption isotherms, which implies physisorption through an electrostatic interaction between the surface of mild steel and inhibitors also contributed to the adsorption process. For further investigation of the adsorption mechanism, the thermodynamic parameters (adsorption equilibrium constant (K_{ads}), free energy (ΔG^o_{ads}), enthalpy (ΔH^o_{ads}) and entropy of adsorption (ΔS^o_{ads}) were calculated using equations 10 and 11, and presented in Table 4.6.

$$K_{ads} = \frac{1}{55.5} \exp\left(\frac{-\Delta G^{\circ}}{RT}\right) \quad (10)$$

$$\Delta G^0 = \Delta H^0 - T\Delta S^0 \quad (11)$$

Table 4.6 The values of the adsorption equilibrium constant from Langmuir adsorption isotherms and free energy, enthalpy, entropy changes of the mild steel dissolution in the presence of inhibitors **4**, **5** and **6** in 1.0 M HCl

Sample	Temp (°C)	$K_{ads}\times10^{-5}$ (L mol^{-1})[a]	ΔG^o_{ads} (kJ mol^{-1})	ΔH^o_{ads} (kJ mol^{-1})	ΔS^o_{ads} (J mol^{-1} K^{-1})
4	60	211355	-42.4	-	-
5	50	874490	-46.1		
	60	592127	-45.0	-86.5	125
	70	338445	-43.6		
6	60	296004	-43.2	-	-

[a]K_{ads} obtained in L/mg was converted to L/mol

The negative values of ΔG^{o}_{ads} and ΔH^{o}_{ads} obtained from Figure 4.6 indicate the spontaneous and exothermic adsorption process, respectively. Generally, the mechanism of adsorption can be classified as physisorption or chemisorption or mixed mechanism based on the magnitude of ΔG^{o}_{ads} and ΔH^{o}_{ads}. When the absolute value of ΔG^{o}_{ads} is lower than 20 kJ mol^{-1} and the ΔH^{o}_{ads} is less negative than -40 kJ mol^{-1} the adsorption process is termed as physisorption. While the absolute value of ΔG^{o}_{ads} is higher than 40 kJ mol^{-1} and the ΔH^{o}_{ads} is more negative than -100 kJ mol^{-1} the adsorption can be classified to be chemisorption; the mixed adsorption mechanism follow if the absolute value of ΔG^{o}_{ads} is higher than 20 kJ mol^{-1} but less than 40 kJ mol^{-1} [126,127,137,138].

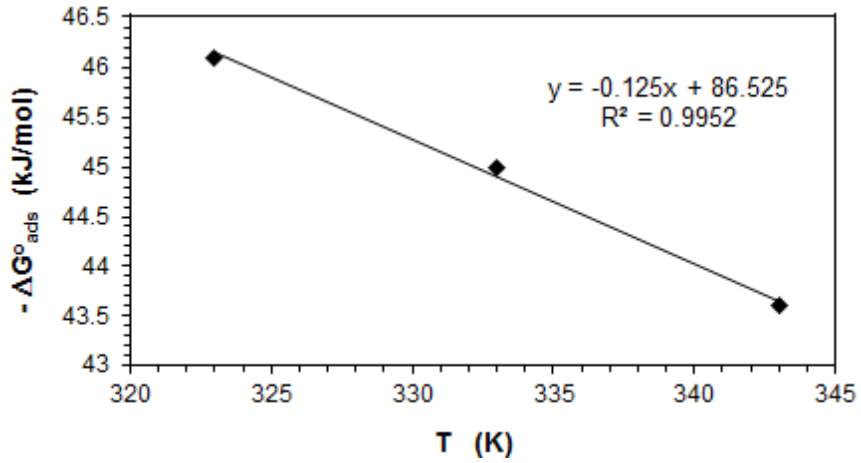

Figure 4.6 Variation of $-\Delta G^{\circ}_{ads}$ versus T on mild steel in 1.0 M HCl containing **5**.

The calculated values of ΔG^{o}_{ads} were found in between -42.4 and -46.1 kJ mol^{-1} and the ΔH^{o}_{ads} for adsorption of inhibitor compound **5** is -86.5 kJ mol^{-1} (Table 4.6), indicates the adsorption is attained through a mixed mechanism by predominance of chemisorption. The inhibitor molecules induced by the non-bonded and π electrons interact with the anodic sites of iron *via* overlapping with the low-lying vacant *d*-orbitals chemically and electrostatically [129,130]. The positive value of ΔS^{o}_{ads} (125 J mol^{-1} K^{-1}) for compound **5**

on mild steel in 1.0 M HCl obtained from Fig. 4.6 is an indication for increasing the randomness on the solid surface/inhibitor interface where the adsorbed inhibitor molecules displaced the adsorbed water molecules on the surface of mild steel.

4.3.6 Surface analysis

The corrosion studies using different methods showed that the inhibitor compounds were able to protect mild steel coupons with a formation of thin films onto the metal surface. To further confirm the inhibitive effects of the synthesized polymeric materials, the surface of the mild steel in absence and presence of inhibitor compounds were explored by XPS, SEM and EDX.

4.3.6.1 XPS analysis

The XPS was used to obtain the intensity (counts) versus binding energy (eV) plot for the thin film formed by the immersion of mild steel coupons in 175 μM of polymer compounds **4-6** in 1.0 M HCl for 6 h, and are presented in Fig. 4.7. The XPS survey spectrum of polymer compounds **5** and **6** covered in the mild steel (Fig. 4.7 a, b) have shown the representative signals for S 2p, N 1s, C 1s, O 1s, which confirms the presence of polymer compounds consists of N, C, O and S as a form of thin layer onto the mild steel surface. The S 2p signals obtained from sulfide and sulfoxide functionalities of polymer compounds appear close to 162.2 eV and 168.2 eV [139] (Fig. 4.7 a,b), respectively, and Fe 2p signals appears from the mild steel (Fig. 4.7 a,b, f).

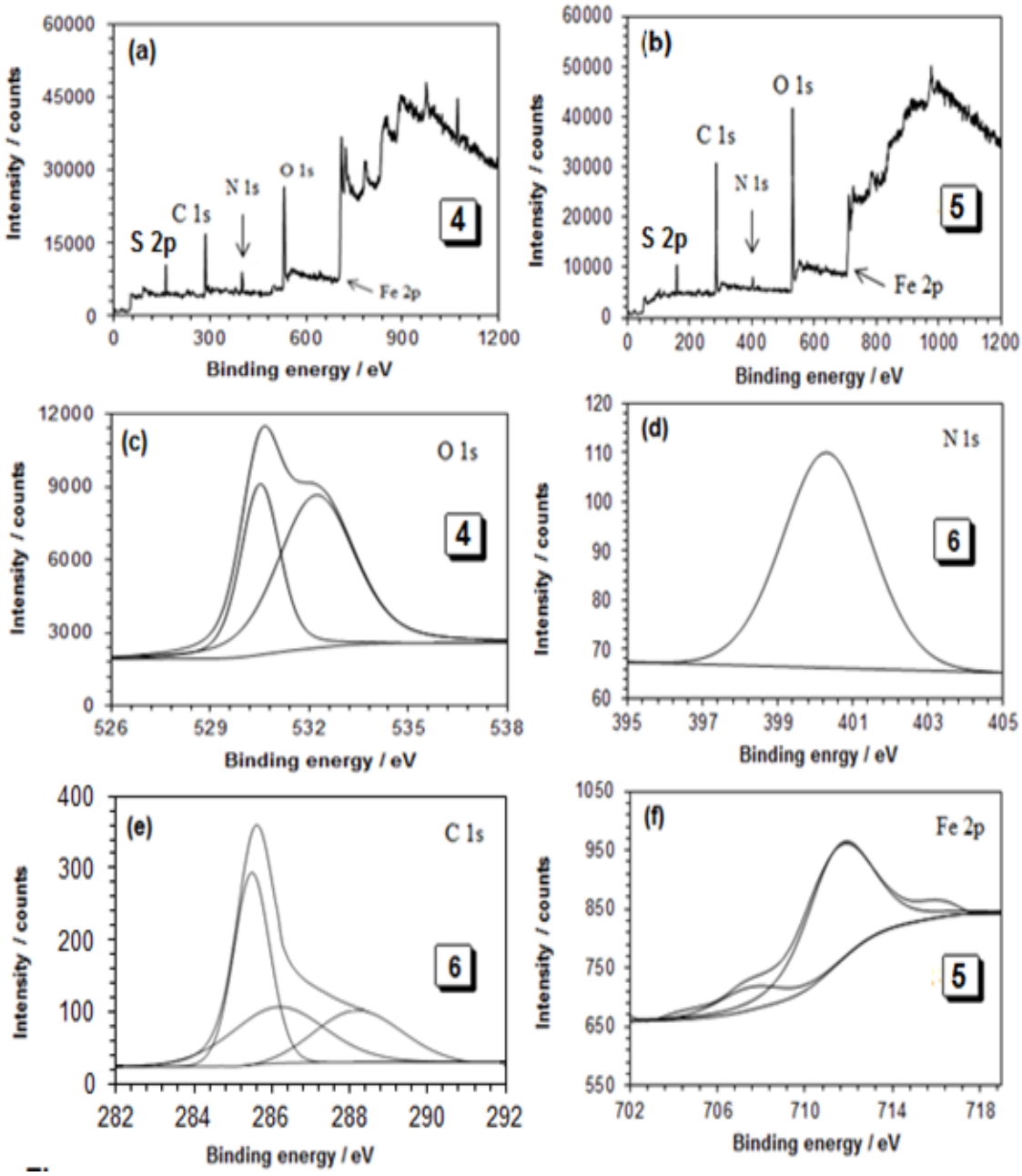

Figure 4.7 (a) XPS survey spectrum of **5** and (b) **6**, and the XPS deconvoluted profiles of (c) O 1s of **4**; (d) N 1s of **6**, (e) C 1s of **6**, and (f) Fe 2p of **5** after immersing in 1.0 M HCl at 60 ºC for 6 h in the presence of **4-6** (175 μM).

The deconvoluted XPS spectra for O 1s, N 1s, C 1s and Fe 2p are shown in Fig. 4.7 (c-f). The intensity peaks appears at 530.2 and 532.0 eV indicating the presence of O 1s which could be attributed to O^{2-} and O=O, thereby implying the formation of a thin film by the interaction between the polymer molecules and the oxide layer onto the metal surface (Fig. 4.7c) [131,132]. The deconvoluted peak appeared at 400 eV confirms the presence of nitrogen, thereby indicating the presence of polymer onto the metal surface (Fig. 4.7d). The XPS deconvoluted profiles of C 1s spectrum showed three peaks (Fig. 4.7e). The C-C aliphatic peak, the C=O, and C-N bond and COO- peaks appeared at 285.4, 286.6 and 288.9 eV, respectively. The intensity signals appeared at 707.3 and 713.8 can be assigned to Fe^{3+} (2p) and Fe^{0} (2p) (Fig. 4.7f). The surface parameters from XPS analysis are depicted in Table 4.7.

Table 4.7 XPS scan composition of mild steel coupon in 1.0 M HCl containing 175 μM of **4**, **5** and **6** at 60 °C

Peak	Approx. binding energy (eV)	Composition (atom %)		
		4	**5**	**6**
C1s	285.4	31.5	31.7	30.8
C1s	286.6	19.4	5.19	4.72
C1s	288.9		11.2	8.31
O1s	530.2	13.2	13.6	10.1
O1s	532.0		32.1	33.6
O1s	532.7	26.5		
N1s	400.2	3.98	2.95	4.12
Fe2p	707.3	1.61	0.83	0.87
Fe2p	711.4	2.98		2.13
Fe2p	713.8		2.44	1.89
Cl2p	199.2	0.84		

4.3.6.2 SEM- EDX analysis

To further understand the inhibition process, the SEM-EDX was used to study the surface morphology of the polished, untreated and polymer treated mild steel surface, and are presented in Fig. 4.8a-c.

The mild steel coupons were dipped in absence or presence of polymer compound **5** in 1.0 M HCl solution for 6 h. The surface morphology of the polished sample was used as reference (Fig. 4.8a). It can be clearly seen from the Fig. 4.8b that the surface of the mild steel is seriously damaged and become porous after the immersion in comparison to the polished surface shown in Fig. 4.8a. However, in presence of 175 μM of polymer compound **5**, the surface was found to be relatively smooth (Fig. 4.8c), and can be comparable to the polished surface (Fig. 4.8a).

This findings demonstrated that the polymer compound form a protective thin film layer by adsorption and reduce the accessibility between the metal surface and acid solution. In order to confirm the composition of the thin films formed onto the metal surfaces, the EDX analysis was carried out, and results are shown in Fig 4.8d-f. The polished metal surface appear with strong iron signal (Fig. 4.8d), while the oxygen and iron signals are found to be in 1.0 M HCl exposed mild steel samples. This could be due to the atmospheric oxidation and/or formation of Fe_2O_3 films (Fig. 4.8e). The polymer treated mild steel surface appeared with signals of carbon, nitrogen, oxygen atoms and decreased iron signal (Fig. 4.8f), thereby suggested the adsorption of polymer compound onto the mild steel surface and protect the metal from corrosion.

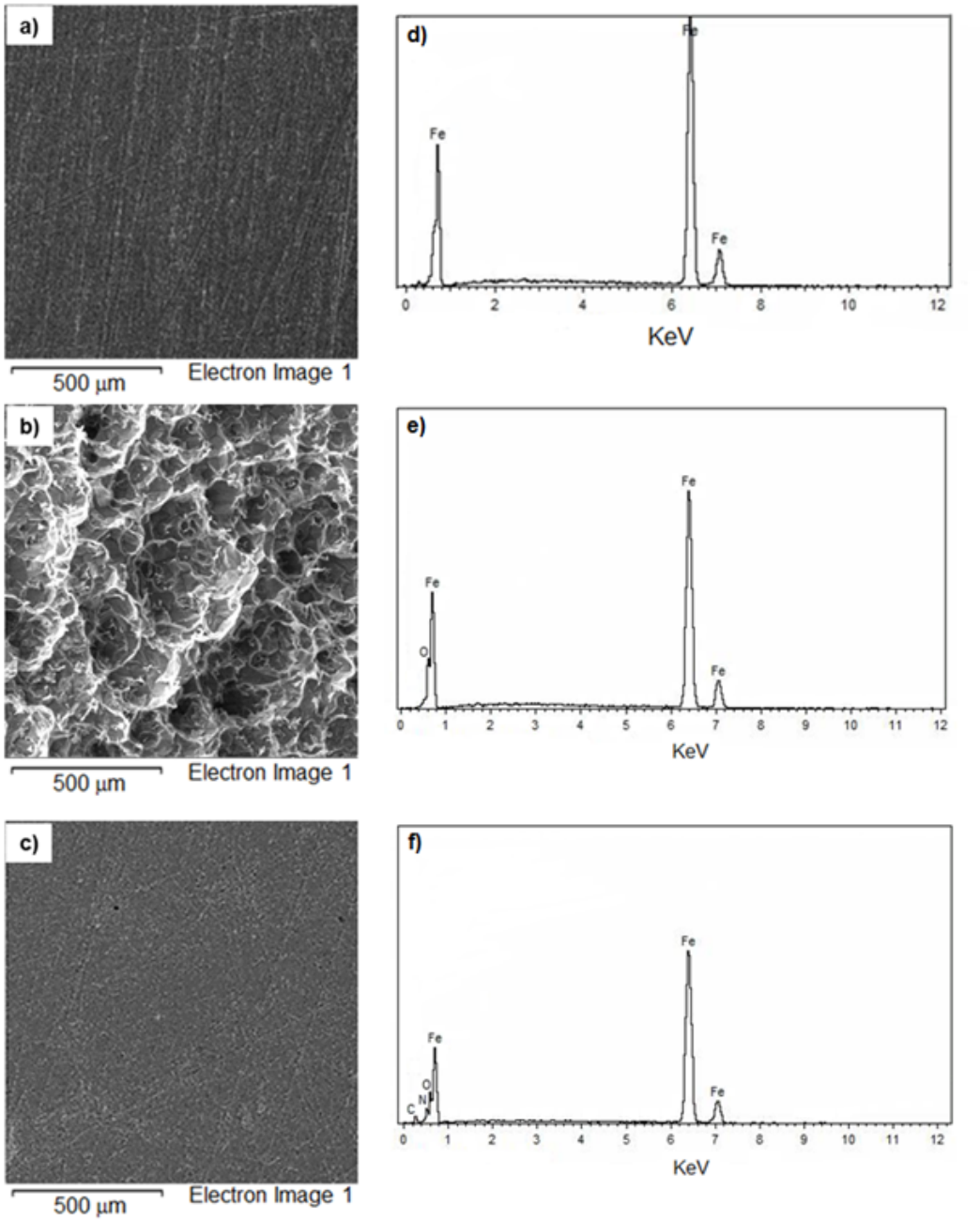

Figure 4.8 SEM micrographs on the surface of the mild steel: a) polished, after immersion of 6 h: b) untreated mild steel in 1.0 M HCl and c) mild steel treated in presence of 175 µM of inhibitor **5**

4.4 Conclusions

The inhibition effects of amino acid methionine based three cyclocopolymers have been studied by potentiodynamic polarization, electrochemical impedance spectroscopy and gravimetric weight loss techniques. From the data obtained from this study, the following conclusions can be drawn:

1. The synthesized polymer compounds inhibited corrosion very well in 1.0 M HCl.
2. The corrosion efficiencies increase with increasing the concentration of the inhibitor compounds. The copolymer compound **5** appeared with maximum inhibition efficiencies of >99% at a concentration as low as 20 ppm (70 μM).
3. The inhibition efficiencies obtained from gravimetric weight loss, potentiodynamic polarization and electrochemical impedance spectroscopy techniques are in well agreement.
4. The coester polymer compound **4** acts as a mixed inhibitor, while hydrolyzed copolymer compounds **5** and **6** suggested to be anodic type inhibitors.
5. Adsorption of polymer compounds onto the mild surface follow chemisorption and physisorption processes, and obeyed three different adsorption mechanisms such as Langmuir, Temkin and Freundlich adsorption isotherms.
6. The negative values of ΔG^{o}_{ads} suggest the spontaneous adsorption. The ΔH^{o}_{ads} of inhibitor compound **5** indicates the formation of chemisorbed film on the mild steel surface, while ΔS^{o}_{ads} indicated increasing the randomness on the solid surface/inhibitor interface where the adsorbed inhibitor molecules displace the adsorbed water molecules on the surface of mild steel.

7. The XPS, SEM and EDX measurements have shown that the synthesized compounds form a protective film on the surface of the mild steel and resist from further corrosion attack.

CHAPTER 5

CONCLUSION AND FUTURE WORKS

5.1 Conclusions

Cationic **4-7** (Scheme 2.1) and zwitterionic polymers **10-12** (Scheme 2.2) based on amino acid methionine and its derivative methionine sulfoxide and sulfone have been synthesized *via* cyclopolymerization of diallylamine salts. The TGA indicated that the synthesized polyelectrolytes were stable up to 200 ^{o}C. The solubility of the polymers is greatly influenced by the oxidation state of the sulfur; while the sulfide pendant imparts water-insolubility, polymers bearing polar sulfoxide and sulfone pendants were found to be water-soluble. The synthesized polymers containing unquenched nitrogen and sulfur valences acted superbly in mitigating mild steel corrosion in 1 M HCl. The presence of nonbonding electrons in nitrogen as well as in the more polarizable sulfur motifs, leads to the formation of coordinate type of bond with the vacant d-orbitals of iron or accumulated Fe^{2+} especially on anodic sites of the metal surface thereby imparting corrosion inhibition. The synthesized cyclocopolymers **6-8** (Scheme 3.1) of sulfur dioxide and biogenic amino acid methionine residue containing ester functionality and sulfide, sulfoxide or sulfone motifs in each alternate repeat units showed excellent corrosion efficiency resisting mild steel corrosion in 1 M HCl. The corrosion efficiencies increase with increasing the concentration of the polymers. In presence of 175 μM, the maximum corrosion efficiencies for the cyclocopolymer **6-8** (Scheme 3.1) were determined to be 92, 97 and 95%, respectively. The polymer compounds **6-8** (Scheme 3.1) act as a mixed-type inhibitor. The polymer compound **7** (Scheme 3.1) adsorbed onto the metal surface by chemisorption and physisorption processes, and obeys Langmuir,

Temkin and Freundlich adsorption isotherms. The negative values of ΔG^{o}_{ads} and ΔH^{o}_{ads} suggest that the adsorption process of polymer **7** (Scheme 3.1) is spontaneous and exothermic. The adsorption is attained through a mixed mechanism by the influence of chemisorption mechanism. The ΔS^{o}_{ads} values indicate increasing the randomness on the solid surface/inhibitor interface where the adsorbed inhibitor molecules displace the adsorbed water molecules on the surface of the mild steel.

The synthesized cyclocopolymers **4-6** (Scheme 4.1) imparted maximum corrosion inhibition efficiencies of 92, 99 and 93%, respectively at a concentration of 175 μM. The coester polymer compound **4** (Scheme 4.1) acts as a mixed inhibitor, while the hydrolyzed copolymer compounds **5** and **6** (Scheme 4.1) suggested to be anodic type inhibitors. Adsorption of polymer compounds onto the mild surface follow chemisorption and physisorption processes, and obeyed three different adsorption mechanisms such as Langmuir, Temkin and Freundlich adsorption isotherms. The negative values of ΔG^{o}_{ads} suggest the spontaneous adsorption. The ΔH^{o}_{ads} of inhibitor compound **5** (Scheme 4.1) indicate the formation of chemisorbed film on the mild steel surface, while ΔS^{o}_{ads} indicated increasing the randomness on the solid surface/inhibitor interface where the adsorbed inhibitor molecules displace the adsorbed water molecules on the surface of mild steel.

The inhibition efficiencies obtained from gravimetric weight loss, potentiodynamic polarization and electrochemical impedance spectroscopy techniques are coherent to each other. The XPS, SEM and EDX measurements have shown that the synthesized compounds form a protective film on the surface of the mild steel and resists from further corrosion attack.

5.2 Future Works

All of the synthesized copolymers showed excellent corrosion inhibition efficiencies in 1 M HCl acidic medium at 60 ^{o}C. However, there are some scopes for the future study that have been outlined below:

- The synthesized polymeric corrosion inhibitors can undergo cytotoxicity screening test for the measurement of toxicity
- Comparative production cost should be analyzed with commercially available inhibitors
- These excellent inhibitors can be tested in other electrolytic corrosive medium such as NaCl, H_2SO_4, H_3PO_4 etc. to see if they perform in those media as well
- Exploitation of other new and emerging electrochemical evaluation techniques such as electrochemical frequency modulation (EFM), electrochemical noise (EN)
- Employing other surface characterization techniques to gain more insight into the complex corrosion phenomena that occurs on the metal surface.
- Performance of quantum chemical studies to have an understanding of the theoretical parameters such as the highest occupied molecular orbital energy ($E_{HOMO)}$, the lowest unoccupied molecular orbital energy (E_{LUMO}), energy gap (ΔE), fraction of electrons transferred (ΔN) that could support the experimental findings

References

[1] P.R. Roberge, Handbook of Corrosion Engineering, second ed., McGraw-Hill, New York, 2000.

[2] L. Popoola, A. Grema, G. Latinwo, B. Gutti, A. Balogun, Corrosion problems during oil and gas production and its mitigation, Int. J. Ind. Chem. 4 (2013) 35–50.

[3] P. Marcus, Corrosion Mechanisms in Theory and Practice, second ed., Marcel Dekker, New York, 2011.

[4] B.D.B. Tiu, R.C. Advincula, Polymeric corrosion inhibitors for the oil and gas industry: Design principles and mechanism, React. Funct. Polym. 95 (2015) 25–45.

[5] P.B. Raja, M. Ismail, S. Ghoreishiamiri, J. Mirza, M.C. Ismail, S. Kakooei, et al., Reviews on Corrosion Inhibitors: A Short View, Chem. Eng. Commun. 203 (2016) 1145–1156.

[6] J. Davis, Corrosion: understanding the basics, first ed., ASM International, Ohio, 2000.

[7] A.G. Lichtenstein, The Silver Bridge collapse recounted, J. Perform. Constr. Facil. 7 (1994) 249–261.

[8] B. Bowonder, The Bhopal Accident, Technol. Forecast. Soc. Chanage. 32 (1987) 169–182.

[9] T. Maurath, Stress corrosion cracking caused a swimming-pool disaster, (1989) E120–E121.

[10] C.H. Cho, Legitimation strategies used in response to environmental disaster: A french case study of total SA's *Erika* and AZF incidents, Eur. Account. Rev. 18 (2009) 33–62.

[11] Natural gas explosion rocks Westmoreland County and U.S. gas markets |PittsburghPost-Gazette.http://www.post-gazette.com/local/westmoreland/2016/04/29/Emergency-crews-respond-to-gas-well-explosion-in-Westmoreland-County-pennsylvania/stories/201604290161 (accessed July 9, 2018).

[12] Ohio State Fair Accident Caused By "Excessive Corrosion," Ride Manufacturer Says | HuffPost. https://www.huffingtonpost.com/entry/ohio-state-fair-accident-cause_us_5987d5c6e4b08b75dcc7b8d3 (accessed July 9, 2018).

[13] L. Zhao, H.K. Teng, Y.S. Yang, X. Tan, Corrosion inhibition approach of oil production systems in offshore oilfields, Mater. Corros. 55 (2004) 684–688.

[14] R. Javaherdashti, How corrosion affects industry and life, Anti-Corrosion Methods

Mater. 47 (2000) 30–34.

[15] G. Koch, J. Varney, N. Thompson, O. Moghissi, M. Gould, J. Payer, International Measures of Prevention , Application , and Economics of Corrosion Technologies Study, NACE International, Houton, 2016.

[16] H.L. Lim, Assessing level and effectiveness of corrosion education in the UAE, Int. J. Corros. 2012 (2012) 1-10.

[17] H. Baker, H. Okamoto, ASM Handbook, Volume 3., ASM International, Ohio, 1992.

[18] M. Finšgar, J. Jackson, Application of corrosion inhibitors for steels in acidic media for the oil and gas industry: A review, Corros. Sci. 86 (2014) 17–41.

[19] D. Brondel, R. Edwards, A. Hayman, D. Hill, T. Semerad, Corrosion in the Oil Industry, Oilf. Rev. 6 (1994) 4–18.

[20] G.H. Koch, M.P.H. Brongers, N.G. Thompson, Y.P. Virmani, J.H. Payer, Corrosion costs and preventive strategies in the United States, Federal Highway Administration. FHWA-RD-01-156 (2002) 1–12.

[21] S. Nešić, Key issues related to modelling of internal corrosion of oil and gas pipelines – a review, Corros. Sci. 49 (2007) 4308–4338.

[22] W.A. Hamilton, Sulphate-reducing bacteria and anaerobic corrosion, Annu. Rev. Microbiol. 39 (1985) 195–217.

[23] B. Nimmo, G. Hinds, Beginners Guide to Corrosion, National Physical Laboratory, London, 2003.

[24] T. Richardson, B. Cottis, D. Scantlebury, R. Lindsay, S. Lyon, M. Graham, Shreir's Corrosion, 4th ed., Elsevier, Oxford, 2010.

[25] J. A. Beavers, N. G. Thompson, CC Technologies, External Corrosion of Oil and Natural Gas Pipelines, ASM Handbook, vol. 13C, Corrosion: Environment and Industries, ASM International, Ohio, 2006, 1015–1026.

[26] T.E. Perez, Corrosion in the oil and gas industry: An increasing challenge for materials, Jom. 65 (2013) 1033–1042.

[27] J. Sun, L. Yang, W. Liu, M. Lu, Electrochemical behavior and localized corrosion of X65 steel in high salt concentration brines with CO_2 saturated, Mater. Res. Express. 5 (2018) 1-9.

[28] D. Brondel, R. Edwards, A. Hayman, D. Hill, T. Semerad, Corrosion in the Oil Industry, Oilf. Rev. 6 (1994) 4–18.

[29] What is Sulfide Stress Cracking (SSC)? - Definition from Corrosionpedia, (2018). https://www.corrosionpedia.com/definition/1225/sulfide-stress-cracking-ssc (accessed January 21, 2018).

[30] What is Chloride Stress Corrosion Cracking (CSCC)? - Definition from Corrosionpedia, (2018). https://www.corrosionpedia.com/definition/1505/chloride-stress-corrosion-cracking-cscc (accessed January 21, 2018).

[31] M.N. Rahuma, B.K. M, Corrosion in Oil and Gas Industry : A Perspective on Corrosion Inhibitors, J. Mater. Sci. Eng. 3 (2014) 4172.

[32] B.M. Miksic, A.Y. Furman, M.A. Kharshan, Effectiveness of the corrosion inhibitors for the petroleum industry under various flow conditions, NACE Int. Corr. Conf. Expo. 09573 (2009) 1–9.

[33] M.N. Rahuma, M.B. El-sabbah, I.M. Hamad, Effect of serine and methionine on electrochemical behavior of the corrosion of mild steel in aqueous solutions, ISRN Corros. 2013 (2013) 1-7.

[34] I.B. Obot, N.O. Obi-egbedi, S.A. Umoren, Antifungal drugs as corrosion inhibitors for aluminium in 0.1 M HCl, Corros. Sci. 51 (2009) 1868–1875.

[35] Z. Hasan, S.H. Jhung, Removal of hazardous organics from water using metal-organic frameworks (MOFs): Plausible mechanisms for selective adsorptions, J. Hazard. Mater. 283 (2015) 329–339.

[36] S.A. Umoren, U.F. Ekanem, Inhibition of mild steel corrosion in h2so4 using exudate gum from pachylobus edulis and synergistic potassium halide additives, Chem. Eng. Commun. 197 (2010) 1339–1356.

[37] L. Garverick, Corrosion in the petrochemical industry, ASM international, Ohio, 1994.

[38] M.B. Kermani, A. Morshed, Carbon dioxide corrosion in oil and gas production—a Compendium, Corrosion. 59 (2003) 659–683.

[39] W.A. Derungs, Naphthenic acid corrosion—an old enemy of the petroleum industry, Corrosion. 12 (1956) 41–46.

[40] A.L. Larsen, Film Forming Hydrazine-containing Corrosion Inhibitor, US3770055 A, 1973.

[41] M.A. Kelland, Production Chemicals for the Oil and Gas Industry, second ed., CRC Press, Florida, 2010.

[42] D.E. Arthur, A. Jonathan, P.O. Ameh, C. Anya, A review on the assessment of polymeric materials used as corrosion inhibitor of metals and alloys, Int. J. Ind. Chem. 4 (2013) 2-11.

[43] A.A. Fathima Sabirneeza, R. Geethanjali, S. Subhashini, Polymeric Corrosion Inhibitors for Iron and Its Alloys: A Review, Chem. Eng. Commun. 202 (2015) 232–244.

[44] S.L. Granese, B.M. Rosales, C. Oviedo, J.O. Zerbino, The inhibition action of

heterocyclic nitrogen organic compounds on Fe and steel in HCl media, Corros. Sci. 33 (1992) 1439–1453.

[45] N.O. Eddy, E.E. Ebenso, U.J. Ibok, Adsorption, synergistic inhibitive effect and quantum chemical studies of ampicillin (AMP) and halides for the corrosion of mild steel in H_2SO_4, J. Appl. Electrochem. 40 (2010) 445-456.

[46] S. Papavinasam, Corrosion inhibitors, in: R.W. Revie (Eds.), Uhlig's Corrosion Handbook, John Wiley & Sons, Inc., New York, 2011, pp. 1021–1032.

[47] C.G. Dariva, A.F. Galio, Corrosion Inhibitors–Principles, Mechanisms and Applications, in: M. Aliofkhazraei (Eds.), Developments in Corrosion Protection, InTech, Rijeka, 2014, pp. 365–379.

[48] E. Bardal, Corrosion and Protection, Springer, London, 2004.

[49] S.A. Umoren, M.M. Solomon, I.I. Udosoro, A.P. Udoh, Synergistic and antagonistic effects between halide ions and carboxymethyl cellulose for the corrosion inhibition of mild steel in sulphuric acid solution, Cellulose. 17 (2010) 635–648.

[50] Chemisorption. https://www.corrosionpedia.com/definition/260/chemisorption (accessed April 30, 2018).

[51] L. Cecchetto, D. Delabouglise, J.P. Petit, On the mechanism of the anodic protection of aluminium alloy AA5182 by emeraldine base coatings. Evidences of a galvanic coupling, Electrochim. Acta. 52 (2007) 3485–3492.

[52] D.-K. Kim, S. Muralidharan, T.-H. Ha, J.-H. Bae, Y.-C. Ha, H.-G. Lee, et al., Electrochemical studies on the alternating current corrosion of mild steel under cathodic protection condition in marine environments, Electrochim. Acta. 51 (2006) 5259–5267.

[53] R. Subasri, T. Shinohara, K. Mori, Modified TiO_2 coatings for cathodic protection applications, Sci. Technol. Adv. Mater. 6 (2005) 501–507.

[54] B.M. Praveen, T. V. Venkatesha, Y. Arthoba Naik, K. Prashantha, Corrosion studies of carbon nanotubes-Zn composite coating, Surf. Coatings Technol. 201 (2007) 5836–5842.

[55] A.S. Fouda, M. Abdallah, A. Attia, Inhibition of carbon steel corrosion by some cyanoacetohydrazide derivatives in hcl solution, Chem. Eng. Commun. 197 (2010) 1091–1108.

[56] N. Saxena, S. Kumar, Anisalidine derivatives as corrosion inhibitors of copper in acidic media, Prot. Met. Phys. Chem. Surfaces. 51 (2015) 701–709.

[57] G. Gece, Drugs: A review of promising novel corrosion inhibitors, Corros. Sci. 53 (2011) 3873–3898.

[58] B. Sanyal, Organic compounds as corrosion inhibitors in different environments - A review, Prog. Org. Coatings. 9 (1981) 165–236.

[59] S.A.A. El -Maksoud, The Effect of Organic Compounds on the Electrochemical Behaviour of Steel in Acidic Media. A Review, Int. J. Electrochem. Sci. (2008).

[60] M. Bethencourt, F.J. Botana, J.J. Calvino, M. Marcos, M. a. Rodriguez-Chacon, Lanthanide compounds as environmentally friendly corrosion inhibitors of aluminium alloys] a review, Corros. Sci. 40 (1998) 1803.

[61] B.R.W. Hinton, Corrosion inhibition with rare earth metal salts, J. Alloys Compd. 180 (1992) 15–25.

[62] S.N. Tiwari, S. Prakash, Literature review Magnesiumoxide as inhibitor of hot oil ash corrosion, Mater. Sci. Technol. 14 (1998) 467–472.

[63] P.B. Raja, M.G. Sethuraman, Natural products as corrosion inhibitor for metals in corrosive media - A review, Mater. Lett. 62 (2008) 113–116.

[64] S. Hooshmand Zaferani, M. Sharifi, D. Zaarei, M.R. Shishesaz, Application of eco-friendly products as corrosion inhibitors for metals in acid pickling processes - A review, J. Environ. Chem. Eng. 1 (2013) 652–657.

[65] R. Rajalakshmi, A. Prithiba, S. Leelavathi, An overview of emerging scenario in the frontiers of eco-friendly corrosion inhibitors of plant origin for Mild Steel, J. Chem. Acta. 1 (2012) 6-13.

[66] B.A. Abd-El-Nabey, N. Khalil, A. Mohamed, Inhibition by amino acids of the corrosion of steel in acid, Surf. Technol. 24 (1985) 383–389.

[67] M.A. Amin, K.F. Khaled, Q. Mohsen, H.A. Arida, A study of the inhibition of iron corrosion in HCl solutions by some amino acids, Corros. Sci. 52 (2010) 1684–1695.

[68] K. Barouni, L. Bazzi, R. Salghi, M. Mihit, B. Hammouti, A. Albourine, et al., Some amino acids as corrosion inhibitors for copper in nitric acid solution, Mater. Lett. 62 (2008) 3325–3327.

[69] M.S.S. Morad, A.E.H.A. Hermas, M.S.A. Aal, Effect of amino acids containing sulfur on the corrosion of mild steel in phosphoric acid solutions polluted with Cl-, F- and Fe3+ ions-behaviour near and at the corrosion potential, J. Chem. Technol. Biotechnol. 77 (2002) 486–494.

[70] K.M. Ismail, Evaluation of cysteine as environmentally friendly corrosion inhibitor for copper in neutral and acidic chloride solutions, Electrochim. Acta. 52 (2007) 7811–7819.

[71] M.S. El-Deab, Interaction of cysteine and copper ions on the surface of iron: EIS, polarization and XPS study, Mater. Chem. Phys. 129 (2011) 223–227.

[72] G.M. Abd El-Hafeza, W.A. Badawy, The use of cysteine, N-acetyl cysteine and methionine asenvironmentally friendly corrosion inhibitors for Cu-10Al-5Ni alloyin neutral chloride solutions, Electrochim. Acta. 108 (2013) 860–866.

[73] N.H. Helal, M.M. El-Rabiee, G.M.A. El-Hafez, W.A. Badawy, Environmentally safe corrosion inhibition of Pb in aqueous solutions, J. Alloys Compd. 456 (2008) 372–378.

[74] H. Saifi, M.C. Bernard, S. Joiret, K. Rahmouni, H. Takenouti, B. Talhi, Corrosion inhibitive action of cysteine on Cu-30Ni alloy in aerated 0.5 M H2SO4, Mater. Chem. Phys. 120 (2010) 661–669.

[75] W.A. Badawy, K.M. Ismail, A.M. Fathi, Corrosion control of Cu-Ni alloys in neutral chloride solutions by amino acids, Electrochim. Acta. 51 (2006) 4182–4189.

[76] N.H. Helal, W.A. Badawy, Environmentally safe corrosion inhibition of Mg-Al-Zn alloy in chloride free neutral solutions by amino acids, Electrochim. Acta. 56 (2011) 6581–6587.

[77] P.K. Singh, V.K. Singh, M. Singh, Zwitterionic polyelectrolytes: a reviw. e, Polymer 7 (2007) 1–34.

[78] S.A. Ali, S.A. Haladu, A.M.Z. El-Sharif, Synthesis and application of a cyclopolymer bearing a propylphosphonic acid and a propylcarboxylic acid pendants in the same repeating unit, J. Polym. Res. 23 (2016) 167-177.

[79] G.B. Butler, Cyclopolymerization and cyclocopolymerization, Marcel Dekker, New York, 1992.

[80] W. Jaeger, J. Bohrisch, A. Laschewsky, Synthetic polymers with quaternary nitrogen atoms-Synthesis and structure of the most used type of cationic polyelectrolytes, Prog. Polym. Sci. 35 (2010) 511–577.

[81] S.A. Ali, O.C.S. Al-Hamouz, Comparative solution properties of cyclocopolymers having cationic, anionic, zwitterionic and zwitterionic/anionic backbones of similar degree of polymerization, Polym. 53 (2012) 3368–3377.

[82] N.Y. Abu-Thabit, I.W. Kazi, H.A. Al-Muallem, S.A. Ali, Phosphonobetaine/sulfur dioxide copolymer by Butler's cyclopolymerization process, Eur. Polym. J. 47 (2011) 1113–1123.

[83] S.A. Ali, Y. Umar, B.F. Abu-Sharkh, H.A. Al-Muallem, Synthesis and comparative solution properties of single-, twin-, and triple-tailed associating ionic polymers based on diallylammonium salts, J. Polym. Sci. Part A Polym. Chem. 44 (2006) 5480–5494.

[84] H.A. Al-Muallem, M.A.J. Mazumder, M.K. Estaitie, S.A. Ali, A novel cyclopolymer containing residues of essential amino acid methionine: synthesis and application, Iran. Polym. J. 24 (2015) 541–547.

[85] R.R. Annand, R.M. Hurd, N. Hackerman, Adsorption of Monomeric and Polymeric Amino Corrosion Inhibitors on Steel, J. Electrochem. Soc. 112 (1965) 138-144.

[86] R. Bacskai, A.H. Schroeder, D.C. Young, Hydrocarbon-soluble alkylaniline/formaldehyde oligomers as corrosion inhibitors, J. Appl. Polym. Sci. 42 (1991) 2435–2441.

[87] R. Ulman, In: H.F. Mark, N.G. Gaylord, N.M. Bikales (Eds.), Encyclopedia of Polymer Science and Technology, vol. 1, Interscience, New York, 1964.

[88] H. Golchoubian, F. Hosseinpoor, Effective oxidation of sulfides to sulfoxides with hydrogen peroxide under transition-metal-free conditions, Molecules. 12 (2007) 304–311.

[89] S.A. Ali, N.Y. Abu-Thabit, H.A. Al-Muallem, Synthesis and solution properties of a pH-responsive cyclopolymer of zwitterionic ethyl 3-(N,N-diallylammonio)propanephosphonate, J. Polym. Sci. Part A Polym. Chem. 48 (2010) 5693–5703.

[90] S.A. Ali, S.A. Haladu, H.A. Al-Muallem, Bis[3-(diethoxyphosphoryl)propyl]diallylammonium chloride: Synthesis and use of its cyclopolymer as an antiscalant, J. Appl. Polym. Sci. 131 (2014) 1–11.

[91] M.A.J. Mazumder, H.A. Al-Muallem, S.A. Ali, The effects of N-pendants and electron-rich amidine motifs in 2-(p-alkoxyphenyl)-2-imidazolines on mild steel corrosion in CO_2-saturated 0.5M NaCl, Corros. Sci. 90 (2015) 54–68.

[92] H.-J. Butt, K. Graf, M. Kappl, Physics and Chemistry of Interfaces, Wiley-VCH Verlag GmbH Co. KGaA, Weinheim, 2003.

[93] Y. Shechter, Selective oxidation and reduction of methionine residues in peptides and proteins by oxygen exchange between sulfoxide and sulfide, J. Biol. Chem. 261 (1986) 66–70.

[94] G.B. Butler, R.J. Angelo, Preparation and Polymerization of Unsaturated Quaternary Ammonium Compounds. VIII. A Proposed Alternating Intramolecular-Intermolecular Chain Propagation, J. Am. Chem. Soc. 79 (1957) 3128–3131.

[95] M. Yoshizawa, H. Ohno, Molecular Brush Having Molten Salt Domain for Fast Ion Conduction, Chem. Lett. 28 (1999) 889–890.

[96] T.A. Wielema, J.B. Engberts, Zwitterionic polymers–I. Synthesis of a novel series of poly(vinylsulphobetaines). Effect of structure of polymer on solubility in water, Eur. Polym. J. 23 (1987) 947–950.

[97] J.C. Salamone, W. Volksen, A.P. Olson, S.C. Israel, Aqueous solution properties of a poly(vinyl imidazolium sulphobetaine), Polymer. 19 (1978) 1157–1162.

[98] S. Kudaibergenov, W. Jaeger, A. Laschewsky, Polymeric betaines: synthesis, characterization, and application, Adv. Polym. Sci. 201 (2006) 157–224.

[99] F. Rullens, M. Devillers, A. Laschewsky, New regular, amphiphilic poly(ampholyte)s: Synthesis and characterization, Macromol. Chem. Phys. 205 (2004) 1155–1166.

[100] S.A. Ali, M.A.J. Mazumder, H.A. Al-muallem, Synthesis and Solution Properties of a New pH-Responsive Polymer Containing Amino Propanesulfonic Acid Residues, 43 (2002) 172–184.

[101] C. Liu, X. Gu, M. Cui, Q. Xu, R. Li, A novel ternary copolymerized polyzwitterionic of poly (AM/DMAM/MAEDAPS): synthesis and solution properties, J. Polym. Res. 21 (2014) 620-632.

[102] P.G. Higgs, J. Joanny, Theory of polyampholyte solutions, J. Chem. Phys. 94 (1991) 1543–1554.

[103] K. Nishida, K. Kaji, T. Kanaya, N. Fanjat, Determination of intrinsic viscosity of polyelectrolyte solutions, Polymer. 43 (2001) 1295–1300.

[104] Z.A. Jamiu, S.A. Ali, Alternate cyclopolymer of diallylglutamic acid and sulfur dioxide, RSC Adv. 6 (2016) 31019–31030.

[105] R. Barbucci, M. Casolaro, N. Danzo, V. Barone, P. Ferruti, A. Angeloni, Effect of Different Shielding Groups on the Polyelectrolyte Behavior of Polyamines, Macromolecules. 16 (1983) 456–462.

[106] R. Barbucci, M. Casolaro, M. Nocentini, P. Ferruti, Spectroscopic and Calorimetric Studies on the Protonation of Polymeric Amino Acids, Macromolecules. 19 (1986) 1856–1861.

[107] S.A. Ali, H.A. Al-Muallem, M.T. Saeed, S.U. Rahman, Hydrophobic-tailed bicycloisoxazolidines: A comparative study of the newly synthesized compounds on the inhibition of mild steel corrosion in hydrochloric and sulfuric acid media, Corros. Sci. 50 (2008) 664–675.

[108] D. Daoud, T. Douadi, H. Hamani, S. Chafaa, M. Al-Noaimi, Corrosion inhibition of mild steel by two new S-heterocyclic compounds in 1 M HCl: Experimental and computational study, Corros. Sci. 94 (2015) 21–37.

[109] H. Ju, Z.P. Kai, Y. Li, Aminic nitrogen-bearing polydentate Schiff base compounds as corrosion inhibitors for iron in acidic media: A quantum chemical calculation, Corros. Sci. 50 (2008) 865–871.

[110] J. Fang, J. Li, Quantum chemistry study on the relationship between molecular structure and corrosion inhibition efficiency of amides, J. Mol. Struct. 593 (2002) 179–185.

[111] M.A. Kiani, M.F. Mousavi, S. Ghasemi, M. Shamsipur, S.H. Kazemi, Inhibitory

effect of some amino acids on corrosion of Pb-Ca-Sn alloy in sulfuric acid solution, Corros. Sci. 50 (2008) 1035–1045.

[112] N. Hackerman, R.M. Hurd, Proceedings of the International Congress on Metallic Corrosion, Butterworths, London, 1962.

[113] R.W. Revie, H.H. Uhlig, Corrosion and Corrosion Control: An Introduction to Corrosion Science and Engineering, Wile-Inter Science, New York, 2008.

[114] V.S. Sastri, Corrosion Inhibitors, Principles and Application, Wiley, New York, 1998.

[115] P. Shanmugasundaram, T. Sumathi, G. Chandramohan, G.N.K. Ramesh-Bapu, Corrosion inhibition study of Is:1062 grade a-low carbon steel in 1 M HCl by L-methionine- weight loss, ICP-OES and SEM-EDX studies, Int. J. Curr. Res. 5 (2013) 2183-2191.

[116] E.E. Oguzie, Y. Li, F.H. Wang, Corrosion inhibition and adsorption behavior of methionine on mild steel in sulfuric acid and synergistic effect of iodide ion, J. Colloid Interface Sci. 310 (2007) 90–98.

[117] B. Hammouti, A. Aouniti, M. Taleb, M. Brighli, S. Kertit, L-Methionine Methyl Ester Hydrochloride as a Corrosion Inhibitor of Iron in Acid Chloride Solution, Corrosion. 51 (1995) 411–416.

[118] K.F. Khaled, Corrosion control of copper in nitric acid solutions using some amino acids - A combined experimental and theoretical study, Corros. Sci. 52 (2010) 3225–3234.

[119] G.B. Butler, Cyclopolymerization, J. Polym. Sci. Part A Polym. Chem. 38 (2000) 3451–3461.

[120] F.C. Mcgrew, Structure of synthetic high polymer, J. Chem. Educ. 35 (1958) 178–186.

[121] S.A. Ali, L.K.M.O. Goni, M.A.J. Mazumder, Butler's cyclopolymerizaton protocol in the synthesis of diallylamine salts/sulfur dioxide alternate polymers containing amino acid residues, J. Polym. Res. 24 (2017) 184-196.

[122] S.Z. Duan, Y.L. Tao. Interface Chemistry, Higher Education Press, Beijing, 1990.

[123] M. Erbil, The determination of corrosion rates by analysis of AC impedance diagrams, Chim. Acta. Turc. 1 (1988) 59-70.

[124] P.C. Okafor, X. Liu, Y.G. Zheng, Corrosion inhibition of mild steel by ethylamino imidazoline derivative in CO_2-saturated solution, Corros. Sci. 51 (2009) 761–768.

[125] G.Y. El-Awady, I.A. El-Said, A.S. Fouda, Anionic surfactants as corrosion inhibitors for aluminium dissolution in HCl solutions, Int. J. Electrochem. Sci. 3 (2008) 174-190.

[126] L. Larabi, Y. Harek, M. Traisnel, A. Mansri, Synergistic influence of poly(4-vinylpyridine) and potassium iodide on inhibition of corrosion of mild steel in 1M HCl, J. Appl. Electrochem. 34 (2004) 833–839.

[127] T. Arslan, F. Kandemirli, E.E. Ebenso, I. Love, H. Alemu, Quantum chemical studies on the corrosion inhibition of some sulphonamides on mild steel in acidic medium, Corros. Sci. 51 (2009) 35–47.

[128] G.E. Badr, The role of some thiosemicarbazide derivatives as corrosion inhibitors for C-steel in acidic media, Corros. Sci. 51 (2009) 2529–2536.

[129] I.L. Rozenfeld, Corrosion Inhibitors, McGraw-Hill, New York, 1981.

[130] L. Afia, R. Salghi, L. Bammou, E. Bazzi, B. Hammouti, L. Bazzi, et al., Anti-corrosive properties of Argan oil on C38 steel in molar HCl solution, J. Saudi Chem. Soc. 18 (2014) 19–25.

[131] O. Olivares-Xometl, N. V. Likhanova, M.A. Domínguez-Aguilar, J.M. Hallen, L.S. Zamudio, E. Arce, Surface analysis of inhibitor films formed by imidazolines and amides on mild steel in an acidic environment, Appl. Surf. Sci. 252 (2006) 2139–2152.

[132] M. Tourabi, K. Nohair, M. Traisnel, C. Jama, F. Bentiss, Electrochemical and XPS studies of the corrosion inhibition of carbon steel in hydrochloric acid pickling solutions by 3,5-bis(2-thienylmethyl)-4-amino-1,2,4-triazole, Corros. Sci. 75 (2013) 123–133.

[133] J. Mosa, N.C. Rosero-Navarro, M. Aparicio, Active corrosion inhibition of mild steel by environmentally-friendly Ce-doped organic-inorganic sol-gel coatings, RSC Adv. 6 (2016) 39577–39586.

[134] P. Mourya, S. Banerjee, R.B. Rastogi, M.M. Singh, Inhibition of Mild Steel Corrosion in Hydrochloric and Sulfuric Acid Media Using a Thiosemicarbazone Derivative, Ind. Eng. Chem. Res. 52 (2013) 12733–12747.

[135] G. Trabanelli, V. Carassiti, Mechanism and Phenomenology of Organic Inhibitors, in: M.G. Fontana, R.W. Staehle (Eds.), Advances in Corrosion Science and Technology, Springer, Massachusetts, 1970, pp. 147–228.

[136] Y. Tang, X. Yang, W. Yang, Y. Chen, R. Wan, Experimental and molecular dynamics studies on corrosion inhibition of mild steel by 2-amino-5-phenyl-1,3,4-thiadiazole, Corros. Sci. 52 (2010) 242–249.

[137] R.M. El-Sherif, W.A. Badawy, Mechanism of corrosion and corrosion inhibition of tin in aqueous solutions containing tartaric acid, Int. J. Electrochem. Sci. 6 (2011) 6469–6482.

[138] C. Verma, P. Singh, M.A. Quraishi, A thermodynamical, electrochemical and surface investigation of Bis (indolyl) methanes as Green corrosion inhibitors for mild steel in 1 M hydrochloric acid solution, J. Assoc. Arab Univ. Basic Appl. Sci.

21 (2016) 24–30.

[139] G.W. Nelson, M. Perry, S.M. He, D.L. Zechel, J.H. Horton, Characterization of covalently bonded proteins on poly(methyl methacrylate) by X-ray photoelectron spectroscopy, Colloids Surfaces B Biointerfaces. 78 (2010) 61–68.

Vitae

Name	Lipiar Khan Mohammad Osman Goni
Nationality	Bangladeshi
Date of Birth	29 February 1988
Email	lipiar-osb@hotmail.com
Address	House No. 722/1, Ward No. 02, Mehar Khaa road, Bancha-nagar, Lakshmipur 3700, Bangladesh
Academic Background	**MS in Chemistry (Polymer)**, August 2015 – April 2018 Chemistry Department, KFUPM Dhahran, KSA **MS in Chemistry (Organic)**, June 2012 – April 2014 Department of Chemistry, Jahangirnagar University Dhaka, Bangladesh **BSc (Hons.) in Chemistry**, March 2008 – May 2012 Department of Chemistry, Jahangirnagar University Dhaka, Bangladesh

Publications

Peer-Reviewed Publications

[J1] Ali, S. A., **Goni, L. K. M. O.,** & Mazumder, M. A. J. (2017). Butler's cyclopolymerization protocol in the synthesis of diallylamine salts/sulfur dioxide alternate polymers containing amino acid residues. *Journal of Polymer Research*, *24*(11), 184-195.

Conference Presentations

[C1] Mazumder, M. A. J., & **Goni, L. K. M. O.** (2017, November). *Health and safety management in the chemical laboratory: A classical approach*. Paper presented at LABTECH 2017, The 4th international conference and exhibition on Laboratory Technology, Manama, The Kingdom of Bahrain.

[C2] Mazumder, M. A. J., **Goni**, **L. K. M. O.,** & Ali, S. A. (2017, September). *Diallylammonium salts containing nitrogen, ethyl ester and sulfide, sulfoxide or sulfone motifs of amino acid residues of methionine polymer as green corrosion inhibitors.* Paper presented at EUROCORR 2017, 20th International corrosion congress and process safety congress 2017, Prague, Czech Republic.

Submitted for Publication

[S1] Goni, L. K. M. O., Mazumder, M. A. J., Ali, S. A., Nazal, M. K., & Al-Muallem, H. A. (2018). Biogenic amino acid methionine-based new corrosion inhibitors of mild steel in acidic media. (Submitted to *International Journal of Minerals, Metallurgy and Materials*, Submission-ID: IJM-06-2018-0523)

[S2] Mazumder, M. A. J., **Goni, L. K. M. O.,** Ali, S. A., & Nazal, M. K. (2017). Inhibition of mild steel corrosion in hydrochloric acid medium by polymeric inhibitors containing residues of essential amino acid methionine. (Submitted to *Iranian Polymer Journal*, Manuscript Number: IPOL-D-18-00185)

Honors, Awards, & Distinctions

- Graduate Scholarship for distinguished graduate applicants, *Aug 2015 – present*
  King Fahd University of Petroleum & Minerals, Saudi Arabia
- University Merit Scholarship (one-time) for being in the top 5% in B.Sc. (Hons.) final, *May 2012*
  Jahangirnagar University, Bangladesh
- Bachelor of Science with Honours, *Dec 2011*
  Jahangirnagar University, Bangladesh
- JUCAF Scholarship (one-time) for being in the top 2% sophomores, *Jan 2010*
  Jahangirnagar University, Bangladesh
- Won several prizes for excellence in sports in the school and college level

Extracurricular Activities

- Volunteer, KFUPM Volunteer Day, *Feb 2017 - present*
  Passed an entire day eating and playing with some orphans in the last event
- Participant, KFUPM Cultural Day, *March 2017 – present*
  Anchored the program last time on behalf of Bangladeshi students at KFUPM and gave a power-point presentation on Bangladesh to the culturally diverse community at KFUPM

- Engaged in different sports activities including swimming, football, cricket, table tennis, etc.

Languages

- Bengali (Native/Bilingual Proficiency)
- English (Full Professional Proficiency)
- Urdu and Hindi (Fluent in Speaking)
- Arabic (Limited Working Proficiency)